SORLA/SORL1 AS GENETIC RISK FACTOR IN ALZHEIMER DISEASE

Inaugural-Dissertation

to obtain the academic degree

Doctor rerum naturalium (Dr. rer. nat.)

submitted to the Department of Biology, Chemistry and Pharmacy

of Freie Universität Berlin

by

Safak Caglayan

2013

Diese Arbeit wurde von September 2008 bis Februar 2013 unter der Leitung von Prof. Dr. Thomas E. Willnow am Max-Delbrück-Centrum für Molekulare Medizin durchgeführt.

1. Gutachter: Herr Prof. Dr. Fritz G. Rathjen

2. Gutachter: Herr Prof. Dr. Thomas E. Willnow

Disputation am 14.10.2013

Contents

List of figures

List of tables

List of abbreviations

Aβ	Amyloid-β
AD	Alzheimer disease
AICD	Amyloid precursor protein intracellular domain
AP	Adaptor protein
APOE	Apolipoprotein E
APP	Amyloid precursor protein
β2M	Beta-2 microglobulin
BBB	Blood-brain barrier
BCA	Bicinchoninic acid
BIN1	Bridging integrator 1
CAG	Cytomegalovirus early enhancer/chicken β-actin promoter
CHO cells	Chinese hamster ovary cells
CMV	Cytomegalovirus
CTF	Carboxy terminal fragment
E	Embryonic day
ELISA	Enzyme-linked immunosorbent assay
EOAD	Early-onset Alzheimer disease
ES cell	Embryonic stem cell
FAD	Familial Alzheimer disease
GGA	Golgi localizing, γ-adaptin ear homology domain, ARF-interacting protein
GFAP	Glial fibrillary acidic protein
IDE	Insulin degrading enzyme
LBB	London Brain Bank
LD	Linkage disequilibrium
LDLR	Low-density lipoprotein receptor
LOAD	Late-onset Alzheimer disease
LRP	Low-density lipoprotein receptor-related protein

LTP	Long term potentiation
NBB	Netherlands Brain Bank
Neo-R	Neomycin phosphotransferase gene
NeuN	Neuronal nuclei
P	Postnatal day
PACS1	Phosphofurin acidic cluster sorting protein 1
PBS	Phosphate-buffered saline
PCR	Polymerase chain reaction
PDAPP	Platelet-derived growth factor-β promoter driven human APP
PFA	Parafolmaldehyde
PSEN	Presenilin
RT-PCR	Reverse transcriptase-polymerase chain reaction
sAPP	Soluble amyloid precursor protein
SNP	Single nucleotide polymorphism
SORL1	Sortilin-related receptor
SORLA	Sorting protein-related receptor with A-type repeats
TBS	Tris-buffered saline
TGN	Trans-Golgi network
TMD	Transmembrane domain
VPS10P	Vacuolar protein sorting 10 protein

Summary

SORLA (sorting protein-related receptor with A-type repeats) is a type-I transmembrane receptor and a member of VPS10P (vacuolar protein sorting 10 protein)-domain receptor family. The receptor is expressed in neurons of the cortex, hippocampus and cerebellum of the brain. SORLA is strongly implicated in Alzheimer disease (AD) as shown in transgenic mouse models and cell culture experiments. Studies in cell culture uncovered a mechanism how SORLA is protective in AD; SORLA acts as a retention factor for amyloid precursor protein (APP) and prevents its localization to the compartments where its proteolytic processing occurs. A role for SORLA in AD is supported by a substantial amount of data from human studies. Thus, expression profiling studies showed that levels of SORLA are selectively reduced in disease-vulnerable regions of the brain in the patients with sporadic AD compared to the control individuals. Genetic association studies confirmed the casual role for SORLA in AD, as multiple single nucleotide polymorphisms (SNPs) in *SORL1* (the gene encoding SORLA) are associated with the disease.

Although some SNPs in *SORL1* were previously correlated with certain AD biomarkers, the molecular mechanism how they confer the risk for the disease was not known. I hypothesized that these genetic variants may control expression levels of SORLA. To test my hypothesis, I collected a sample set consisting of 88 brain autopsy specimens. Next, I genotyped the selected risk SNPs and determined SORLA concentrations in the sample set using a specific and reliable ELISA developed by me. In line with reduced expression of SORLA as a disease causing factor, association analyses of the genetic data and protein levels revealed that two SNPs in *SORL1*, rs2070045 and rs1699102, are associated with reduced SORLA expression levels in the brain. Interestingly, measurements of the RNA levels in the brain samples didn't show any effects of the SNPs on transcript levels. Rather, analyses of protein and RNA expression levels in the cells showed that these risk variants are affecting SORLA expression post-transcriptionally.

Ineffective codon usage due to the silent mutations might be the reason causing lower expression of SORLA in the patients carrying the risk variants.

Consistent with reduced expression of SORLA in the patients with AD, deficiency of the receptor in the mouse brain results in increased amyloidogenic processing and accumulation of Aβ, hallmarks of AD. Conceptually, increasing SORLA expression may thus represent a therapeutic approach in AD. To test this hypothesis, I carried out a second project whereby I generated a transgenic mouse line overexpressing SORLA (*Rosa26*$^{Tg/+}$) by inserting human SORLA cDNA into the murine *Rosa26* locus. I showed using ELISA that SORLA concentration is increased 4-5-fold in the brain of *Rosa26*$^{Tg/+}$ mice compared to control (*Rosa26*$^{+/+}$) animals expressing only the murine receptor. Further characterization of *Rosa26*$^{Tg/+}$ mice by immunostainings revealed neuronal localization of SORLA expressed by the transgene. These results demonstrated that *Rosa26*$^{Tg/+}$ mice represent a valid and efficient model to study effects of overexpression of SORLA *in vivo*. Next, I analyzed processing products of murine APP in the brain. I also evaluated human APP processing by breeding the mouse line with a rodent model of AD expressing the human *APP* transgene. In line with protective role of SORLA, neuronal overexpression of the receptor in the brain resulted in 2-3-fold decrease in Aβ accumulation both for the murine and human models. Surprisingly, other processing products of APP remained unaltered in *Rosa26*$^{Tg/+}$ mice. To exclude that the known catabolic pathways of Aβ weren't changed in *Rosa26*$^{Tg/+}$ mice, I showed major Aβ degrading enzymes and clearance receptors were similar in *Rosa26*$^{Tg/+}$ and *Rosa26*$^{+/+}$ mice. As a consequence, I reasoned a novel and previously unrecognized function for SORLA in clearance of Aβ. In support of this model, I showed that non-neuronal cells as well as primary neuronal cells overexpressing SORLA internalized more Aβ as compared to control cells. Additionally, I showed that the internalized Aβ is transported to lysosomes for degradation. Hence, my studies suggest a novel function of SORLA supporting the protective role of

the receptor in AD; addition to inhibiting processing of APP, SORLA might be involved in cellular catabolism of Aβ.

Taken together, my studies have identified a unique genetic mechanism whereby two SNPs control levels of SORLA expression in the human brain. Moreover, I have uncovered a novel role for SORLA in clearance of Aβ that may underlie the protective effect on AD seen in individuals with high receptor activity in the brain.

Parts of this thesis were published:

Identification of Alzheimer Disease Risk Genotype That Predicts Efficiency of *SORL1* Expression in the Brain.

Safak Caglayan, Anja Bauerfeind, Vanessa Schmidt, Anne-Sophie Carlo, Thaneas Prabarakan, Norbert Hübner, Thomas E. Willnow.

Arch. Neurol. 69 (3): 373-9, Mar 2012

Zusammenfassung

SORLA („sorting protein-related receptor with A-type repeats“) ist ein Typ-I-Transmembranrezeptor, welcher zur Familie der Rezeptoren mit VPS10P („vacuolar protein-sorting 10 protein“)-Domäne gehört. Im Gehirn ist der Rezeptor in Neuronen des Cortex, Hippocampus und des Cerebellums exprimiert. SORLA steht im Zusammenhang mit der Alzheimer-Krankheit, wie transgene Mausmodelle und Zellkulturexperimente gezeigt haben. Studien mittels Zellkulturen fanden einen zellulären Mechanismus, in dem sich SORLA protektiv auf die Alzheimer-Krankheit auswirkt; dabei fungiert SORLA als Retentionsfaktor, der APP („amyloid precursor protein“) im trans-Golgi Netzwerk der Zelle zurück hält und somit verhindert, dass das Protein in entferntere Zellkompartimente gelangt, in denen es proteolytisch prozessiert werden kann. Die Rolle von SORLA in der Alzheimer-Krankheit wird durch eine profunde Anzahl an Patientendaten belegt. Expressionsprofile dieser Patienten haben gezeigt, dass die Menge an SORLA bei Patienten mit sporadischer Alzheimer-Krankheit in Regionen des Gehirns reduziert ist, in denen sich Symptome der Alzheimer-Krankheit als erstes manifestieren. Studien, die eine genetische Assoziation von SORLA und der Alzheimer-Krankheit untersucht haben, ergaben, dass mehrere Einzelnukleotid-Polymorphismen (SNPs, „single nucleotide polymorphisms“) in *SORL1*, dem SORLA kodierendem Gen, mit der Erkrankung assoziiert sind.

Obwohl bereits gezeigt werden konnte, dass einige dieser SNPs in *SORL1* mit bestimmten Biomarkern für die Alzheimer-Krankheit korrelieren, war der molekulare Mechanismus, wie diese SNPs zu einem höheren Risiko der Erkrankung beitragen, nicht bekannt. Anhand meiner Doktorarbeit konnte ich zeigen, dass diese genetischen Varianten die Expressionsmenge von SORLA beeinflussen können. Dabei wurden 88 Patientenproben aus Gehirnautopsien gesammelt und auf auserwählte Risiko-SNPs genotypisiert, sowie die Menge an SORLA in diesen Gehirnproben bestimmt. Dazu hatte ich im Vorfeld einen spezifischen und verlässlichen ELISA für SORLA entwickelt. Die Assoziationsanalyse der genetischen SNP-Daten und der Proteinmengen

ergaben, dass zwei SNPs in *SORL1*, rs2070045 und rs1699102, mit reduzierten Expressionsmengen von SORLA im Gehirn assoziiert sind. Interessanterweise hatten diese SNPs jedoch keinerlei Effekt auf die Transkriptionsaktivität des SORLA-Gens in den Gehirnautopsien. Vielmehr stellte sich heraus, dass bei genauer Untersuchung der Protein- und RNA-Mengenim Zellkultursystem die SNPs die Expression von SORLA posttranskriptionell beeinflussen. Denkbar ist, dass die durch stille Mutationen veränderten Aminosäure-Codons nur ineffektiv translatiert werden können und somit ursächlich für die verminderte Expression von SORLA in Alzheimer-Patienten mit diesen Risikovarianten sind.

Analog zu Alzheimer-Patienten mit verminderter SORLA-Expression, führt eine SORLA-Defizienz im Mausgehirn zu einer erhöhten amyloiden Prozessierung und somit zu einer Akkumulation von Aβ-Peptiden, einem Kennzeichen der Alzheimer-Krankheit. Konzeptionell sollte eine erhöhte Expression von SORLA somit eine therapeutische Wirkung auf die Alzheimer-Krankheit haben. Um diese Hypothese zu untersuchen, generierte ich im zweiten Teil meiner Doktorarbeit eine transgene Mauslinie, welche SORLA (*Rosa26*$^{Tg/+}$) überexprimiert., Anhand dieser Tiere konnte gezeigt werden, dass die Konzentration von SORLA in Gehirnen von *Rosa26*$^{Tg/+}$-Tieren vier- bis fünffach erhöht war im Vergleich zu Kontrolltieren (*Rosa26*$^{+/+}$), welche nur den murinen Rezeptor exprimieren. Zur weiteren Charakterisierung der *Rosa26*$^{Tg/+}$-Tiere konnte ich in Immunfärbungen zeigen, dass das SORLA-Transgen in Neuronen exprimiert wird und sich somit die *Rosa26*$^{Tg/+}$-Mäuse als valides und effizientes Tiermodell eignet, um die Effekte einer Überexpression von SORLA *in vivo* genauer zu untersuchen. Als nächstes habe ich sowohl die Prozessierungsprodukte von murinem und humanem APP im Gehirn analysiert,indem ich meine transgene Mauslinie in ein Mausmodel der Alzheimer-Krankheit eingekreuzt habe. Übereinstimmend mit der protektiven Rolle von SORLA, war die murine und humane Aβ-Akkumulation in den Gehirnen um zwei- bis dreifach verringert, während . die anderen Prozessierungsprodukte von APP in den *Rosa26*$^{Tg/+}$-Tieren unverändert blieben. Um auszuschließen, dass die bekannten katabolen

Abbauwege von Aβ-Peptide in den *Rosa26*$^{Tg/+}$-Tieren verändert waren, untersuchte ich verschiedene Enzyme und Rezeptoren, die hauptsächlich für den Abbau von Aβ-Peptide verantwortlich sind, und konnte keinerlei Unterschiede zwischen *Rosa26*$^{Tg/+}$ und *Rosa26*$^{+/+}$-Tieren feststellen. Diese Resultate ließen mich zu der Schlussfolgerung kommen, dass SORLA eine neue und bisher unbekannte Funktion in der Beseitigung von Aβ-Peptide haben muss. Daten, die dieses Modell stützen, zeigten, dass sowohl nicht-neuronale Zellen als auch primäre Neuronen bei einer Überexpression von SORLA mehr Aβ-Peptide internalisieren als Kontrollzellen. Weiterhin wurde deutlich, dass internalisiertes Aβ in Lysosomen zur Degradation transportiert wird. Basierend auf meinen Resultaten schlage ich eine neuartige Funktion für SORLA vor, die eine protektive Rolle des Rezeptors bezüglich der Alzheimer-Krankheit einnimmt; zusätzlich zur Inhibierung der APP-Prozessierung könnte SORLA am zellulären Katabolismus von Aβ-Peptiden beteiligt sein.

Zusammenfassend haben meine Untersuchungen einen einzigartigen genetischen Mechanismus identifiziert, in welchem zwei SNPs die Expression von SORLA im menschlichen Gehirn kontrollieren. Des Weiteren habe ich eine neuartige Rolle für SORLA in der Beseitigung von Aβ-Peptiden gefunden, welche der Grund für den protektiven Effekt auf die Alzheimer-Krankheit in Individuen mit hoher Rezeptoraktivität im Gehirn darstellen könnte.

1. Introduction

1.1. Alzheimer disease

Dementia is a condition characterized by progressive decline in cognitive functions. World-wide there are 24.3 million people estimated to have dementia (Ballard, Gauthier et al. 2011), making it one of the most important public health problems of our aging population. The incidence of people afflicted with dementia is expected to double every 20 years due to an increase in life expectancy. Particularly, disability weight of dementia is higher than with any other disease as dementia causes disability in 11.2% of years in people above 60 years of age as compared to stroke (9.5%), musculoskeletal disorders (8.9%), heart diseases (5.0%), and all forms of cancer (%2.4) (Ferri, Prince et al. 2005).

Alzheimer disease (AD) is the most common cause of dementia, representing almost 60% of cases (Ballard, Gauthier et al. 2011). Auguste D., was the first patient diagnosed by the German psychiatrist, Alois Alzheimer. His clinical findings showed an extraordinary dementia together with a progressive cognitive decline, hallucinations, and impaired social behavior (Ferri, Prince et al. 2005). After 5 years, when Auguste D. had died at the age 55, Dr. Alzheimer performed a brain autopsy and identified the distinct neuropathological hallmarks of AD. Pathological abnormalities included miliary bodies (plaques) and dense bundles of fibrils (tangles) (Ferri, Prince et al. 2005; Blennow, de Leon et al. 2006; Holtzman, Morris et al. 2011).

1.2. Clinical features and pathology of Alzheimer disease

The most important clinical feature of AD is progressive decline in intellectual abilities of the affected individual. Since the progression of decline is slow and difficult to identify in the initial stage, it is impossible to determine the onset of the disease accurately. Other signs of the disease include aphasia (disturbance of linguistic processing) (Damasio 1992), apraxia (inability to perform learned, skilled movements) (Gross and Grossman 2008), and agnosia (impairment in recognizing objects or other stimulus that is not due

to loss of perception) (Greene 2005) along with general cognitive symptoms such as impaired judgment, decision-making, and orientation. Seven to 10 years after diagnosis, the disease results in death (Blennow, de Leon et al. 2006).

Pathologically, the AD brain can be distinguished by a gross atrophy compared to control individuals. Radiological imaging is widely used to detect the degeneration in the brain. According to the measurements obtained from postmortem tissues and live patients, the degeneration starts in the medial temporal lobe, displaying shrinkage in volume of the hippocampus and entorhinal cortex, and enlargement of the ventricles (Blennow, de Leon et al. 2006). It was also shown that the progressive decline in cortical thickness measured by magnetic resonance imaging correlates with the progression in cognitive dysfunctions (Frisoni, Fox et al. 2010; Putcha, Brickhouse et al. 2011). AD doesn't affect all of the brain regions similarly. Selective neuronal populations in the layer II of the entorhinal cortex, in the CA1 region of the hippocampus, and in certain regions of the temporal, parietal and frontal neocortex are the most vulnerable cells. However, the most important reason for the brain atrophy and cognitive decline is shrinkage and loss of the neuronal processes (Huang and Mucke 2012).

At the microscopic level, AD can be defined as a protein aggregation disorder. The pathological hallmarks of the disease are senile or neuritic plaques as well as neurofibrillary tangles in the medial temporal lobe and cortex of the brain (Ferri, Prince et al. 2005; Holtzman, Morris et al. 2011). The underlying causes of this pathology are aggregation and accumulation of extracellular amyloid plaques with dystrophic neurites and intracellular accumulation of hyperphosphorylated tau with tangle formation. Neurovascular pathology, oxidative stress, and perturbations in mitochondrial metabolism are other mechanisms implicated in the pathological alterations seen in the AD brain (Blennow, de Leon et al. 2006).

Amyloid-β (Aβ) peptide is the fundamental toxic component of the plaques. It has a size of 37-43 amino acids (Kayed, Head et al. 2003) and is processed from the amyloid precursor protein (APP) (Hardy and Selkoe 2002). Aβ peptides aggregate into insoluble forms like fibrils or can be found as oligomers in the plaques (Kayed, Head et al. 2003; Holtzman, Morris et al. 2011). Swollen, degenerating neuronal processes (axons and dendrites) along with inflammatory gliosis due to hypertrophy and proliferation of astrocytes and microglia are other features of the amyloid plaques (Lucin and Wyss-Coray 2009).

The basic component of the second pathological feature, neurofibrillary tangles, is tau protein (Goedert, Wischik et al. 1988). It is expressed in neurons as well as in glial cells and its physiological function is to stabilize microtubules together with tubulin. Hyperphosphorylated forms of tau as in AD dissociate from tubulin and aggregate to form tangles in neuronal cell bodies and dystrophic neurites. It was also shown that the severity of tau pathology correlates with neuronal dysfunction and clinical progression of AD (Holtzman, Morris et al. 2011).

The other important pathological signs of AD include degeneration of the neurons and synapses, reduction in levels of certain neurotransmitters, and vascular pathology (Blennow, de Leon et al. 2006). Most of the cells in the regions vulnerable to neurodegeneration are glutamergic neurons. Additionally, there are cholinergic and noradrenergic neurons affected by the disease. Loss of these neurons also results in decrease in neurotransmitter levels. Additionally, disruption of neuronal network connections between different brain regions causes cognitive dysfunction in AD (Palop and Mucke 2010). Brain regions affected by AD have normally highest baseline activities in the resting conditions and particularly the hippocampus is hyperactivated in learning and memory functions. Since Aβ levels are regulated by neuronal activity, this observation may explain selective Aβ deposition in certain brain regions (Palop, Chin et al. 2006; Holtzman, Morris et al. 2011; Huang and Mucke 2012).

Genetic, biochemical and neurobiological studies suggest that conformational changes, aggregation, and buildup of different forms of Aβ are the key factors initiating AD pathogenesis causing damage to the brain (Holtzman, Morris et al. 2011). These Aβ plaques (but also neurofibrillary tangles) start to accumulate an estimated 10 to 20 years before the clinical symptoms of dementia become apparent (Jack, Knopman et al. 2010).

1.3. Genetics and epidemiology of Alzheimer disease

AD is a complex and heterogeneous disorder meaning that there are multiple genes that interact with environmental factors leading to the development of AD in humans.

Genetically, AD can be divided into two forms. Most of the cases beginning after age 65 are referred as sporadic or late onset AD (LOAD). This form constitute >99% of cases. The second form, familial or early onset AD (EOAD), which appears before the age of 60, represents only a small percentage (<1%) of cases. However, this form of AD was very helpful in understanding the molecular mechanisms of this disorder (Table 1; modified from (Ballard, Gauthier et al. 2011).

1.3.1. Familial Alzheimer disease

There are four genes identified causing familial EOAD. Additionally, one locus on chromosome 10 was linked to the disease but the gene in this locus hasn't been identified yet (Bertram, Blacker et al. 2000). Mutations in three of these genes, namely amyloid-precursor protein (*APP*), presenilin 1 (*PSEN1*), and *PSEN2*, were confirmed across several studies (Goate, Chartier-Harlin et al. 1991; Schellenberg, Bird et al. 1992; Levy-Lahad, Wasco et al. 1995; Rogaev, Sherrington et al. 1995; Sherrington, Rogaev et al. 1995). These identified mutations are rare, autosomal dominant mutations showing a high degree of penetrance. They cause early onset form of AD by promoting production of Aβ peptides and by enhancing its aggregation (Selkoe and Podlisny 2002; Mayeux and Stern 2012).

Table 1. Alzheimer disease risk genes

Alzheimer disease genes		**Risk size on AD***
Familial genes		
APP	Amyloid precursor protein is a transmembrane protein expressed in neurons. It can be cleaved through non-amyloidogenic or amyloidogenic pathways. Familial AD mutations favor amyloidogenic processing yielding increased production of Aβ.	not applicable
PSEN1	PSEN1 is the active subunit of the γ-secretase enzyme. Familial AD mutations result in predisposition to produce more Aβ42, which is more prone to aggregation than Aβ40.	not applicable
PSEN2	PSEN2 is another component of the γ-secretase complex. Familial AD mutations result in predisposition to produce more Aβ42, which is more prone to aggregation than Aβ40.	not applicable
SORL1	SORLA (SORL1) interacts with APP and prevents its processing by α- and β-secretases. Familial AD mutations were identified recently, but the underlying molecular mechanisms are currently not known.	not applicable
Risk genes		
APOE	APOE is involved in clearance of Aβ. There are three isoforms of APOE with different binding and transport efficiencies. *APOE4* allele is associated with increased amyloid burden and decreased age at onset.	3.67
BIN1	BIN1 is implicated in dynamin-mediated synaptic endocytosis processes.	1.17
CLU	Clusterin interacts with soluble Aβ and can alter its toxic profile.	0.88

APP, amyloid precursor protein, *PSEN1*, presenilin 1, *APOE*, Apolipoprotein E, *BIN*, bridging integrator 1; *CLU*, clusterin; *SORL1*, Sortilin-related receptor; SORLA, Sorting protein-related receptor with A-type repeats. *Risk size estimates are based on meta-analysis results published in Alzgene database (www.alzgene.org) (Bertram, McQueen et al. 2007). Risk size estimates are not available for the familial mutations due to the full penetrance of the genetic alteration.

There is a wide spectrum of mutations in the *APP* gene (AD Mutation Database, http://www.molgen.vib-ua.be/ADMutations/). The identified missense mutations are mostly lying in or close to the Aβ-coding exons (16 and 17) of APP (Figure 1) (Mayeux and Stern 2012). Hence, these mutations alter proteolytic processing of APP by β- and γ-secretases and yield more Aβ production. Mutations near the γ-secretase cleavage site do not affect total Aβ production but increase levels of the Aβ42 form, which is more prone to aggregate and to form plaques than the Aβ40 variant. There are also mutations close to the α-secretase cleavage site within the Aβ sequence. These mutations change the structure of the peptide to a variant that forms oligomers more easily and that is cleared less efficiently (Nilsberth, Westlind-Danielsson et al. 2001; Holtzman, Morris et al. 2011). The other mutation that can cause AD is the microduplication of the entire APP gene as in patients with trisomy 21, resulting in more Aβ production (Rovelet-Lecrux, Hannequin et al. 2006).

PSEN1 and *PSEN2* are the other two genes that were identified in EOAD (Levy-Lahad, Wasco et al. 1995; Sherrington, Rogaev et al. 1995). These genes encode presenilins, which are homologous components of the γ-secretase complex along with APH-1 (anterior pharynx-defective 1), PEN-2 (presenilin-enhancer 2), and nicastrin. Presenilins are active sites of the γ -secretase complex. Mutations in these genes alter cleavage of APP and lead to an increase in plaque-prone Aβ42 levels or Aβ42/Aβ40 ratio (Scheuner, Eckman et al. 1996).

Recently, there were autosomal dominant mutations identified in *SORL1* in some EOAD cases. These mutations, which are distributed along the entire coding sequence, have potential pathogenic effects, but no mechanisms have been reported yet (Pottier, Hannequin et al. 2012).

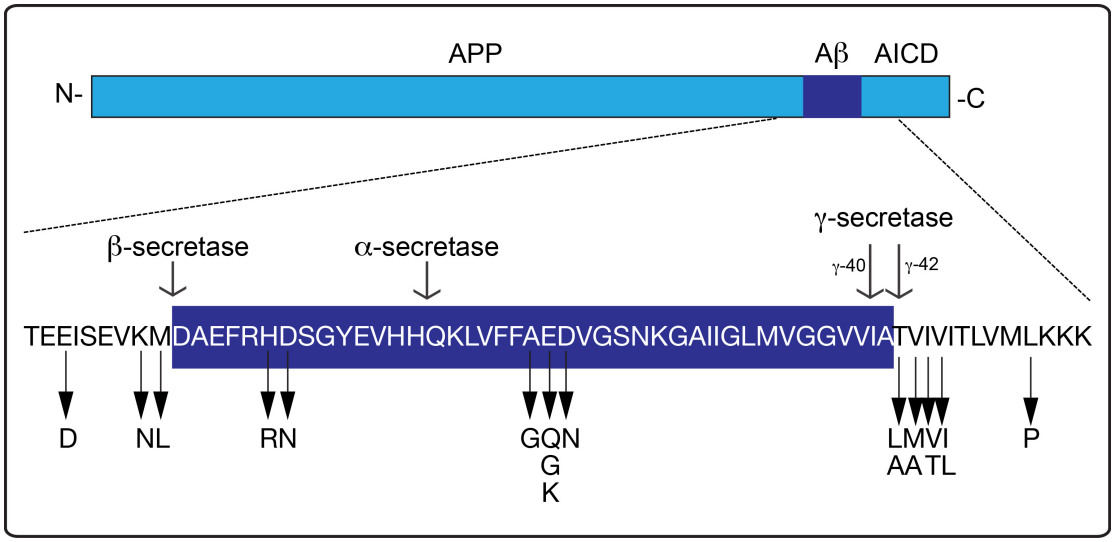

Figure 1. Missense mutations in the *APP* gene cause familial Alzheimer disease. The structural organization of the APP polypeptide sequence is shown. The amino acid sequence for Aβ (purple colored) is enlarged below. The single-letter codes for amino acids were used to depict this sequence. FAD mutations in APP are indicated by arrowheads below the normal sequence of the protein. Aβ is derived from APP by successive cleavages by β- and γ- secretases (cleavage sites indicated by arrows above the sequence). α-cleavage occurs within the Aβ domain, thereby preventing Aβ production. Rare autosomal dominant mutations causing familial early onset Alzheimer disease are clustered around the secretase cleavage sites. Typically, these mutations change cleavage efficiencies of secretases and yield more Aβ production. Alternatively, mutations within the Aβ sequence lead to a structurally different Aβ, which is more prone to aggregation or cleared less efficiently. AICD is amyloid precursor protein intracellular domain. The figure is modified from (Holtzman, Morris et al. 2011).

1.3.2. Sporadic Alzheimer disease

Sporadic late onset Alzheimer disease (LOAD) has both an environmental and a strong genetic component. It was shown in a large population based twin study that genetic factors make up almost 80% of the sporadic disease (Gatz, Reynolds et al. 2006). However, it is difficult to identify the genes predisposing to the AD and to confirm the results in different populations, as the risk size caused by individual genes is usually small (Hardy, Myers et al.

2004). The genes, which were identified as top 3 risk genes for LOAD by the Alzgene website (Bertram, McQueen et al. 2007), are listed in Table 1.

Apolipoprotein E (*APOE*) is the most significant gene associated with LOAD. Humans have three isoforms of *APOE* (*E2*, *E3*, and *E4*) that are distinguished by single amino acid changes at either position 112 or position 158 of the protein. The risk for AD is allele specific; *E4* allele increases the risk for LOAD whereas *E2* is protective (Corder, Saunders et al. 1993; Strittmatter, Saunders et al. 1993). Risk conferred by the *E4* allele is also dose-dependent. Meta-analysis showed that a single copy of *E4* increases the risk 3-fold but two copies of *E4* increase the risk of AD 15 times (Farrer, Cupples et al. 1997). Additionally, the *APOE4* allele was associated with a decreased age at disease onset (Corder, Saunders et al. 1993; Farrer, Cupples et al. 1997), as well as with the rate of age-related cognitive decline in humans (De Jager, Shulman et al. 2012).

APOE is highly expressed in the brain and involved in different functions in the brain including cholesterol metabolism, neuronal plasticity, and inflammation. There are several mechanisms that may explain the role of APOE in AD pathology. Since APOE can bind to Aβ peptide, it may be involved in the catabolism of Aβ. Thus, it was shown by *in vitro* and *in vivo* studies that APOE alters the clearance efficiency of soluble Aβ (Kim, Basak et al. 2009). Oligomerization and aggregation properties of Aβ can also be modified by APOE. Studies in *APP* transgenic mice (Bales, Verina et al. 1997) and in humans (Morris, Roe et al. 2010) showed that *APOE* has isoform-specific influences on Aβ deposition (Holtzman, Morris et al. 2011).

The other genes that were associated with LOAD have relatively smaller risk effects with size around 1.05 - 1.30 according to the Alzgene website (Table 1) (Ballard, Gauthier et al. 2011) .The most probable explanation how these genes are involved in the development of AD is that several of them are acting at the same time along with environmental factors to develop the condition (Blennow, de Leon et al. 2006).

SORL1 is also one of the genes that were associated with sporadic AD (Rogaeva, Meng et al. 2007). There are multiple single nucleotide polymorphims (SNPs) throughout the *SORL1* locus conferring risk to LOAD in different human populations (see below for further details).

1.3.3. Age and other risk factors

Aging is the most important non-genetic risk factor for sporadic AD (Huang and Mucke 2012). According to published estimates only 5% of individuals have AD at age of 65 whereas this ratio sharply increases to 50% at age 80 (Hebert, Scherr et al. 2003).

Other risk factors predisposing to AD are cardiovascular disease, hypertension, head injury, type II diabetes, obesity, low educational levels, and smoking (Mayeux and Stern 2012). Interactions of some of these factors with *APOE* can further increase the risk to acquire sporadic AD or display cognitive decline (Huang and Mucke 2012).

On the other hand, systematic studies suggest certain protective factors against AD, which mostly include lifestyle changes such as cognitive reserve (combination of education, occupation, and mental activities of the individual), diet, physical activity, and cognitive enhancement (Ballard, Gauthier et al. 2011; Huang and Mucke 2012).

1.4. Amyloid cascade hypothesis

Today, the amyloid cascade hypothesis is widely accepted to explain the molecular origin of cognitive deficits in the patients with AD. This hypothesis states that an imbalance between Aβ production and Aβ clearance results in Aβ deposits, which in turn causes neuronal dysfunction and death in the brain (Ballard, Gauthier et al. 2011; Mayeux and Stern 2012). Degeneration of neurons and synapses then leads to cognitive impairments and dementia (Blennow, de Leon et al. 2006).

In familial AD cases, the pathology results from increased production and/or aggregation of Aβ due to mutations within *APP*, *PSEN1* or *PSEN2*. Whereas

in sporadic cases, studies suggest that impairments in Aβ clearance pathways are causing the disease (Mawuenyega, Sigurdson et al. 2010). Since there are multiple genes identified as risk genes for LOAD, it is likely that these genes are altering clearance and aggregation properties of Aβ and thereby yielding in Aβ oligomers and deposits.

It is also suggested that Aβ regulates neuronal and synaptic activities (Palop, Chin et al. 2006). When soluble Aβ peptides start to form oligomers and insoluble fibrils, a vicious cycle is induced in the brain (Huang and Mucke 2012). Initially Aβ stimulates an aberrant network activity with impaired neurotransmitter receptors and synaptic transmission along with exocitotoxicity of neurons. Aberrant network activity, in turn, partially promotes Aβ production. These downstream events ultimately result in neurodegeneration and dementia (Holtzman, Morris et al. 2011).

In spite of many genetic and pathological data supporting the role of Aβ in AD pathology, the number of Aβ plaques doesn't correlate well with the cognitive decline in patients. In fact, deposition of Aβ lesions can even be detected in some individuals without dementia (Crystal, Dickson et al. 1988; Perrin, Fagan et al. 2009). Similarly, the number of plaques in transgenic AD mouse models doesn't correlate with cognitive impairment or neurodegeneration.

This apparent discrepancy leads to an alternative hypothesis that soluble Aβ oligomers (rather than insoluble plaques) are the toxic assemblies causing synaptic dysfunction and neuronal death in the brain of patients with AD. This hypothesis may explain the lack of correlation between amyloid plaques and functional impairments as it was shown that compared to plaque pathology, concentration of oligomers extracted from the brain tissue of patients with AD correlated better with the disease symptoms (McLean, Cherny et al. 1999; Mc Donald, Savva et al. 2010).

Oligomers might interfere with cellular function by blocking the essential proteins with their flexible hydrophobic surfaces. Oligomers may penetrate the cell membrane and may lead to cell death by aberrant Ca^{++} influx (Campioni, Mannini et al. 2010). Additionally, oligomeric assemblies isolated from patients with AD were shown to promote tau aggregation and neurodegeneration in the neurons (Jin, Shepardson et al. 2011).

Taken together equilibrium may exist between soluble Aβ monomers, oligomers and insoluble Aβ plaques. In this equilibrium, the oligomers might be intermediates between the monomers and fibrils, which in turn might be reservoirs for the oligomer formations. Although it is not very clear how the different Aβ structures cause synaptotoxicity, recent studies suggest that oligomers may inhibit synaptic function by blocking neurotransmitter receptors (Benilova, Karran et al. 2012). Formation of long-term potentiation (LTP) in the synapses might be inhibited with alteration of glutamate receptor activation by the secreted oligomers (Walsh, Klyubin et al. 2002). Hyperactivation and subsequent inhibition of acetylcholine receptors by these oligomers may alter neuronal gene expression profiles and interfere with the gene-expression-dependent phase of LTP (Dineley, Westerman et al. 2001). Finally, the oligomers may lead to spine loss and long-term depression by activating the calcineurin cascade (Benilova, Karran et al. 2012).

It is also possible that oligomers don't target specific receptors and cells, but that their toxicity is due to nonspecific interaction of a mixture of various hydrophobic oligomers and aggregates with the cell membranes, proteins, and lipids. These complex interactions, in turn, result in oxidative stress, in alterations in membrane electric potential, and in efflux of ions (Campioni, Mannini et al. 2010). The latter hypothesis is supported by the presence of more than 20 different Aβ variants in oligomeric assemblies. These different variants, which have different solubility, stability and activity, are generated by alternative γ-secretase cleavage steps in combination with enzymatic modification such as phosphorylation of the respective Aβ species (De

Strooper 2010; Benilova, Karran et al. 2012).

1.5. Processing and trafficking of APP

The amyloid precursor protein (APP) can be processed through two different pathways: the amyloidogenic pathway that yields Aβ, and the non-amyloidogenic pathway that prevents Aβ production (Figure 2).

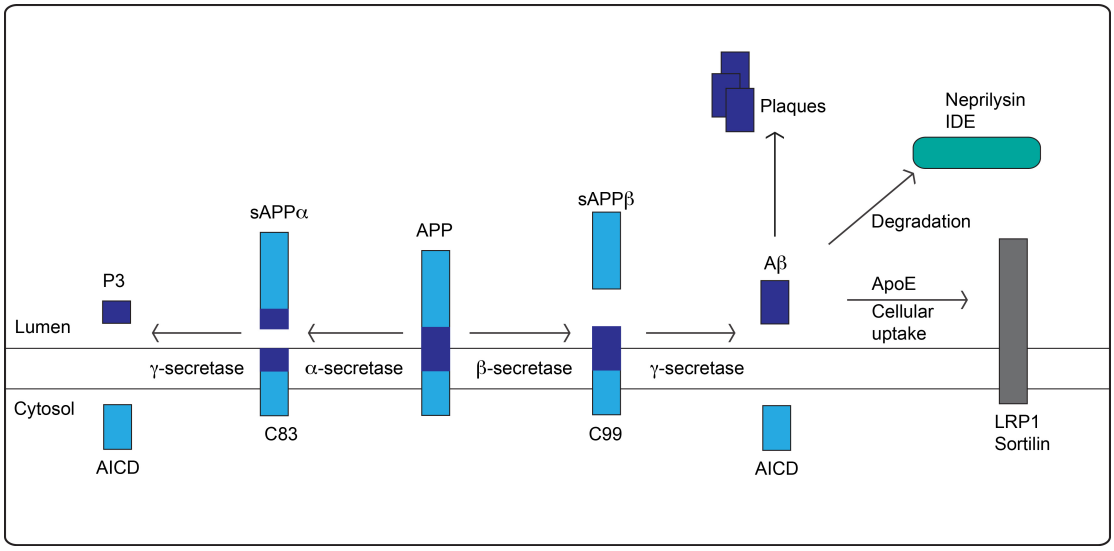

Figure 2. Cellular processing of APP and clearance of Aβ. There are two processing pathways for APP. APP can be cleaved by α-secretases to release soluble (s) APPα. Membrane-bound α-carboxy terminal fragment (αCTF or C83) of APP is then processed by γ-secretase to produce the P3 fragment and the APP intracellular domain (AICD). Amyloidogenic processing is initiated by β-secretase releasing sAPPβ. Aβ is produced by γ-cleavage of the remaining βCTF (C99). Under normal conditions, secreted soluble Aβ can interact with apolipoprotein E (APOE) and be cleared from the brain interstitial fluid. The low-density lipoprotein receptor -related protein (LRP1) and sortilin are two receptors involved in APOE-mediated Aβ clearance. Alternatively, Aβ can be catabolized in the extracellular space by proteases such as neprilysin and insulin degrading enzymes (IDE). In case of an imbalance between production and clearance pathways, Aβ peptides start to accumulate into neurotoxic oligomers and to form extracellular plaques.

Amyloidogenic processing is initiated by the β-secretase enzyme, BACE1 (β-site APP cleaving enzyme-1). It cleaves APP at the amino terminal site of the Aβ sequence and releases soluble (s) APPβ. The remaining membrane-bound carboxyl terminal fragment (CTF) of APP is βCTF or C99. It is the substrate of the γ-secretase. Cleavage of C99 by γ-secretase takes place within the transmembrane domain (TMD) and releases Aβ. Since γ-secretase cleaves the TMD of APP at several sites, different Aβ species are generated by this protease. Thus, the size of the Aβ peptide can vary between 37 and 43 amino acids length.

Aβ is a peptide also produced under normal physiological conditions (Haass, Schlossmacher et al. 1992). Secreted soluble Aβ molecules are degraded by proteinases such as insulin degrading enzyme or neprilysin (Carson and Turner 2002). They can also be cleared from interstitial fluid of the brain by low-density lipoprotein receptor related protein (LRP1) (Bell, Sagare et al. 2007; Sagare, Deane et al. 2007), or by sortilin following binding to APOE (Carlo, Gustafsen et al. 2013).

Non-amyloidogenic processing is performed by successive cleavages of APP by α- and γ-secretases. Cleavage of APP by α-secretase takes place within the Aβ sequence, liberating sAPPα fragment. The remaining CTF, αCTF or C83, is then cleaved by γ-secretease to release soluble P3 fragment and the APP intracellular domain (Figure 2).

Amyloidogenic and non-amyloidogenic processing take place in different compartments of the cell (Haass, Kaether et al. 2012). Because of this, regulation of intracellular trafficking of APP is an important factor to modulate different processing pathways. After APP molecules are synthesized in the endoplasmic reticulum, they are transported through the biosynthetic pathway to the cell surface. On their way, they are maturated by N- and O-linked glycosylation, cytoplasmic phosphorylation, and tyrosine sulphation (Walter, Capell et al. 1997; Walter and Haass 2000). When APP molecules reach the plasma membrane they can be cleaved by α-secrease for non-

amyloidogenic processing. If they are not processed there, they are rapidly internalized from the cell surface by clathrin-mediated endocytosis and delivered to endosomal compartments for amyloidogenic processing by β- and γ-secretases (Haass, Kaether et al. 2012).

1.6. Role of SORLA in Alzheimer disease

1.6.1. SORLA is an endocytosis and sorting receptor

Sorting protein-related receptor with A-type-repeats (SORLA) is a transmembrane protein and a member of vacuolar protein sorting 10 protein (VPS10P)-domain receptor family (Jacobsen, Madsen et al. 1996; Yamazaki, Bujo et al. 1996). The other members of this gene family are sortilin (Petersen, Nielsen et al. 1997), sortilin-related receptor central nervous system expressed (SORCS)-1 (Hermey, Riedel et al. 1999), SORCS-2 (Rezgaoui, Hermey et al. 2001), and SORCS-3 (Hampe, Rezgaoui et al. 2001). Their common structural motif is the VPS10P domain, which is a ligand-binding domain that was first identified in VPS10P, a sorting protein in yeast (Marcusson, Horazdovsky et al. 1994). The sequences of their VPS10P domains and their expression pattern in the brain vary considerably among the family members (Westergaard, Sorensen et al. 2004) suggesting different functions for these receptors (Willnow, Petersen et al. 2008).

SORLA has a mosaic structure as it shows structural homology with the low-density lipoprotein (LDL) receptor family proteins. In addition to its VPS10P domain, the receptor contains a YWTD-domain (also called β-propeller), ligand-binding complement type-repeats, and a cytosolic domain providing interaction with adaptor proteins (Figure 3). SORLA is a multi-ligand receptor with its ligand-binding VPS10P domain and complement-type repeats. *In vitro* binding assays showed that the VPS10P domain of SORLA interacts with the pro-peptide of the receptor, with neurotensin, and with the receptor-associated protein (RAP). Other ligands include APOE and lipoprotein lipase (LpL), which bind to ectodomain of SORLA, but not to its VPS10P portion (Jacobsen, Madsen et al. 2001). Interestingly, APOE and LpL can also bind to

the VPS10P domain in sortilin, indicating structural differences among the VPS10P domains of the two receptors (Jacobsen, Madsen et al. 2001).

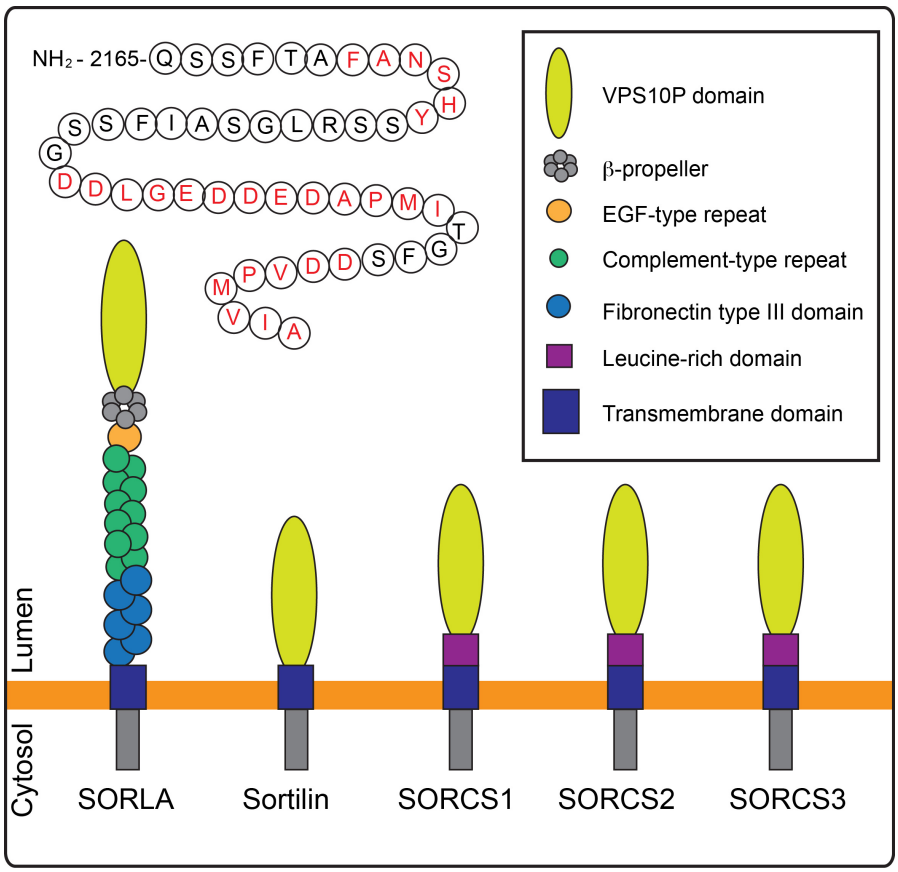

Figure 3. VPS10P domain receptors. SORLA, sortilin, SORCS1, SORCS2, and SORCS3 are members of transmembrane receptor gene family carrying a common vacuolar protein sorting 10 protein (VPS10P) domain. Additionally, the receptors have carboxyl terminal cytosolic tails that include signals for internalization and subcellular trafficking. Internalization of SORLA is mediated by adaptor protein-2, which recognizes acidic cluster (NH_2-2189-DDLGEDDEDAPMI) in the depicted cytoplasmic tail of the receptor. NH_2-791-YSVL motif is required for internalization of sortilin. GGA proteins, which mediates the transport of the receptors from the TGN to the endosomes, recognizes DXXLL type motifs in the C-terminus of SORLA and sortilin. Retrograde trafficking of the transmembrane receptors from the endosomes to the TGN is mediated by the retromer complex. VPS26 subunit of the assembly binds to the NH_2-2171-FANSHY motif in the SORLA tail. Among the members, SORLA is unique as it additionally contains a ligand binding YWTD-domain (β-propeller), EGF-type repeats, ligand-binding complement type repeats, and six fibronectin-type domain. SORCS1, sortilin-related receptor CNS (central nervous system) expressed-1. Figure is adapted from (Willnow, Petersen et al. 2008).

SORLA has a size of 250-kDa and is widely expressed including the central nervous system, blood vessels, and the kidney. In the brain, it localizes to the neurons of the entorhinal cortex, hippocampus, midbrain, brain stem, and to the Purkinje cells in the cerebellum (Kanaki, Bujo et al. 1998; Motoi, Aizawa et al. 1999). The VPS10P domain of SORLA is glycolysated with terminal GalNAc-4-SO_4 in the kidney and brain (Fiete, Mi et al. 2007). At the subcellular level, SORLA is mainly localized to endocytic vesicles, the trans-Golgi network (TGN), and the plasma membrane (Jacobsen, Madsen et al. 2001; Schmidt, Sporbert et al. 2007). An acidic cluster dileucine-like site in the cytoplasmic tail of the receptor mediates its internalization from the plasma membrane. Several cargo adaptor proteins including adaptor protein (AP)-1, AP-2, the retromer, Golgi localizing, γ-adaptin ear homology domain, ARF-interacting protein (GGA) proteins, and phosphofurin acidic cluster sorting protein 1 (PACS1) mediate shuttling of the receptor between the plasma membrane, early endosomes and the TGN. These findings suggest that SORLA acts as an endocytosis and sorting receptor between different intracellular compartments (as described in detail below) (Willnow, Petersen et al. 2008).

1.6.2. SORLA as genetic risk factor in familial and sporadic Alzheimer disease

There is substantial evidence indicating a role for SORLA in development and pathology of AD. Genetic association of *SORL1* with familial and sporadic AD was shown by several population-based studies. The single nucleotide polymorphisms (SNPs) associated with AD are distributed among the *SORL1* locus in two haplotype blocks at the 5' and 3' region. Although the overall risk size of *SORL1* risk variants as estimated by meta-analyses is small (1.10) (Reynolds, Hong et al. 2010) compared to that of *APOE*, it is still in the range of other AD risk genes. This situation can be attributed to a high allelic heterogeneity of *SORL1* locus, because usually different SNPs confer risk in different populations. The risk variants identified in *SORL1* are either intronic

or silent mutations that do not change the amino acid sequence. Moreover, one recent study showed familial autosomal dominant mutations in *SORL1 to* cause EOAD. *In silico* characterization of the mutations revealed that they are potentially pathogenic (Pottier, Hannequin et al. 2012). However, the molecular mechanism how these mutations cause AD is not known yet.

In addition to the genetic data, there are also expression data showing a causal relationship of SORLA with sporadic AD. Studies on autopsy specimens from human brains showed that SORLA expression is reduced in the disease-vulnerable regions of patients with sporadic AD compared to control subjects (Scherzer, Offe et al. 2004). The normal expression levels of SORLA in patients with familial AD (as compared to LOAD cases) indicates that loss of receptor expression is not a secondary consequence of neuronal loss, but likely a primary event in LOAD pathogenesis (Dodson, Gearing et al. 2006).

1.6.3. SORLA regulates APP trafficking and processing

The possible contributions of SORLA to onset and progression of AD have been extensively studied in the past using *in vitro* binding assays, cell culture experiments, and transgenic animal models. Intriguingly, these studies identified an unexpected role for this receptor in regulation of APP trafficking and processing.

In vitro binding assays and analytical ultracentifugation experiments showed that the complement type repeats of SORLA and the carbohydrate-linked domain of APP form a 1:1 stoichiometric complex (Andersen, Reiche et al. 2005; Andersen, Schmidt et al. 2006). Immunostainings revelead that SORLA and APP co-localize to the same intracellular compartments in neuronal and non-neuronal cell types, mainly to early endosomes and the trans-Golgi network. Moreover, deficiency of SORLA in gene-targeted mice was shown to promote APP processing and to result in accumulation of sAPPα, sAPPβ, as well as Aβ species in the brain of mice (Andersen, Schmidt et al. 2006; Offe, Dodson et al. 2006). Finally, the relevance of SORLA for amyloidogenic

processes was documented by our lab and others using different transgenic mouse models of Alzheimer disease (Dodson, Andersen et al. 2008; Rohe, Carlo et al. 2008). In these studies it was shown that lack of SORLA results in 2-3-fold increase in Aβ levels and plaque deposition.

The molecular mechanism whereby SORLA affects APP processing and why low levels of expression represent a risk for AD was uncovered in cell culture experiments. These studies demonstrated that SORLA overexpression in cells reduced the amount of APP processing products secreted into the medium (Schmidt, Sporbert et al. 2007). As SORLA harbors binding sequences for adaptor proteins in its cytoplasmic domain, it was hypothesized that the intracellular trafficking of SORLA may regulate APP routing in neurons (and thereby controls processing by secretases). In line with this hypothesis, studies in our lab showed that disruption of these binding sites in SORLA prevented appropriate trafficking of the mutant receptor and altered levels of APP processing products (Schmidt, Sporbert et al. 2007).

1.6.4. Subcellular trafficking of SORLA

One group of molecules that regulate intracellular trafficking of SORLA is GGA proteins. The GGA proteins are ubiquitously expressed clathrin adaptors involved in sorting target molecules from the TGN to the endosomes (Kirchhausen 2002). They may additionally interact with ubiquitin and mediate trafficking of ubiquitin sorting receptors in the cell (Scott, Bilodeau et al. 2004). There are three GGAs expressed in mammalian cell types; GGA1, GGA2, and GGA3. DXXLL-type (X is any amino acid) sorting sequences in the cytosolic tails of these target proteins are the main signal recognized by GGAs (Bonifacino 2004). Among the GGA adaptors, GGA3 was previously implicated in AD as it was shown that BACE1 levels and activity are regulated by GGA3-dependent lysosomal sorting of the secretase (Tesco, Koh et al. 2007). GGA1 and GGA3 proteins bind to SORLA as well. The GGA binding motif in the SORLA cytoplasmic tail includes NH_2-2206-DD residues (Uniprot reference number of the retrieved sequence is Q92673)

followed by a hydrophobic NH_2-2208-VPMVIA sequence (Jacobsen, Madsen et al. 2002). Disruption of these binding sites in SORLA results in alterations in APP processing, most probably by directing SORLA molecules to the plasma membrane (Schmidt, Sporbert et al. 2007). Additionally, mutagenesis of the cytoplasmic tail of SORLA or knockdown of GGA proteins in cells resulted in mislocalization of SORLA and APP, and induced amyloidogenic processing (Herskowitz, Offe et al. 2012). These studies suggest GGA proteins, particularly GGA1, as a sorting molecule guiding intracellular trafficking of SORLA.

Another sorting protein that interacts with SORLA is PACS1, which recognizes the acidic NH_2-2189-DDLGEDDED cluster in the cytoplasmic tail of SORLA (Jacobsen, Madsen et al. 1996). PACS1 is involved in sorting of proteins from the endosomes to the TGN (Bonifacino and Traub 2003), and it requires adaptor protein (AP)-1, and AP2 to mediate intracellular protein traffic (Crump, Xiang et al. 2001). It was shown previously that accurate intracellular localization of furin and mannose-6-phosphate receptor is depending on PACS1 interaction (Wan, Molloy et al. 1998). In addition to these targets, studies in our lab showed that also SORLA requires PACS1 to localize to the TGN and endosomal compartments. When binding of PACS1 was inhibited by mutating the acidic cluster motif in the C-terminus of SORLA, proper localization of the receptor to the late-Golgi/TGN is disrupted. As a consequence, APP trafficking was altered and amyloidogenic processing enhanced (Schmidt, Sporbert et al. 2007).

Another adaptor complex that regulate SORLA trafficking is called retromer. The complex that was first identified in yeast to mediate endosome to Golgi transport of Vps10 protein (Seaman, Marcusson et al. 1997). Mammalian retromer consists of cargo-selective trimer (VPS35, VPS26, and VPS29), and the SNX proteins (Seaman 2012). The retromer complex is implicated in several cellular functions as it mediates trafficking of a range of cargoes including the cation-independent mannose 6-phosphate receptor, the iron transporter DM1-II/Slc11a2, Wntless/MIG-14 (involved in Wnt transport),

Crumbs that is required for cell polarity, TGN38, TGN46, sortilin and SORLA (Bonifacino and Hurley 2008; Seaman 2012). Deficiency of the retromer complex leads to accumulation of aymloidogenic processing products in the brain of mice and neurodegeneration in fruit flies (Muhammad, Flores et al. 2008). The VPS26 component of the retromer complex recognizes NH_2-2171-FANSHY signal in the SORLA tail (Jacobsen, Madsen et al. 1996; Fjorback, Seaman et al. 2012). Mutation of this motif in SORLA sequence alters the localization of SORLA in neuronal cell lines and increases concentration of APP processing products (Fjorback, Seaman et al. 2012). These results suggest that association of the retromer complex with occurrence of AD may partially be explained by its role in regulation of intracellular trafficking of SORLA.

Findings in the recent years emphasized importance of the APP trafficking pathways in regulation of Aβ production. Studies on the function of SORLA provide a working model how SORLA activity contributes to the development of AD (Figure 4) (Willnow, Carlo et al. 2010). This model suggests that SORLA acts as a sorting receptor of APP. It binds to APP to regulate intracellular trafficking and thereby processing of the precursor protein. The adaptor proteins, in turn, tightly regulate subcellular trafficking of SORLA and deficiency of these sorting proteins or their inability to recognize SORLA alters processing of APP as well. Loss of receptor expression in patients with AD or in mice results in increased APP processing and Aβ deposits. Hence, an important field of investigation might be whether increasing the concentration of the receptor can prevent or delay AD development. If this hypothesis holds true, the next important question will be how to achieve this overexpression in the brain of humans.

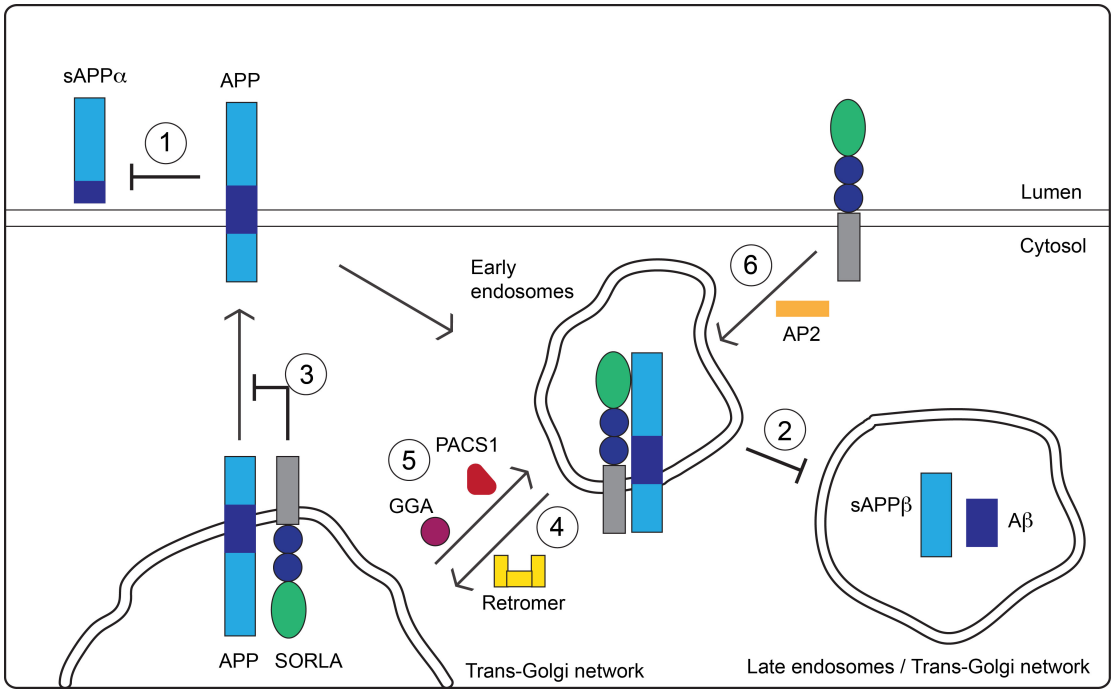

Figure 4. SORLA regulates trafficking and processing of APP. After co-translation transport into the endoplasmatic reticulum, APP molecules are transported through the Golgi and trans-Golgi network to plasma membrane where they can be cleaved by α-secretase (1). Unprocessed APP proteins are internalized via early endosomes into late endosomal vesicles for cleavage by β- and γ-secretases to liberate Aβ (2). SORLA interferes with both APP processing pathways by keeping the precursor protein in the trans-Golgi network (TGN) (3). It can also spare the APP molecules from β- and γ-secretases by transporting them from early endocytic vesicles back to the TGN (4). Subcellular trafficking of SORLA is regulated by the adaptor proteins binding to specific motifs in 54-residue cytoplasmic domain of the receptor (see the figure 3 for details). The retromer complex is involved in sorting of SORLA from the endosomal compartments to the TGN (4). GGA proteins are involved in shuttling of SORLA from the TGN to the endocytic compartments whereas PACS1 sorts the receptor either way (5). Internalization of SORLA is mediated by adaptor protein 2 (AP2) (6).

2. Aim of the thesis project

SORLA/SORL1 is an important genetic risk factor in both sporadic and familial forms of AD. Several SNPs were identified in the *SORL1* locus associated with sporadic AD. However the mechanism how these genetic risk variants are predisposing to the condition hasn't been known. Since SORLA levels are reduced in some patients with AD, my first objective was to test whether the allelic variations in *SORL1* associated with the risk of AD may act by altering the expression level of SORLA in the brain of patients.

SORLA deficiency, as in patients with AD or in knockout mouse models, accelerates amyloidogenic processing and predisposes to AD. Based on these findings, overexpression of the receptor may be beneficial by reducing amyloidogenic burden and AD progression. Still, this hypothesis had not been rigorously explored. Thus, the second major aim of my thesis was to provide a proof of concept using transgenic animal models that SORLA overexpression reduces amyloidogenic processing in the brain and may represent a novel therapeutic strategy to combat AD.

3. Materials and Methods

3.1. Primer sequences

Name	Sequence, 5'-3'
18S rRNA forward	CGC CGC TAG AGG TGA AAT TC
18S rRNA reverse	TGG GCA AAT GCT TTC GCT C
APOE forward	TAA GCT TGG CAC GGC TGT CCA AGG A
APOE reverse	ACA GAA TTC GCC CCG GCC TGG TAC ACT GCC
CAG genotyping	AGT CCC TAT TGG CGT TAC T
CAG rec forward	TAG AGT CGA GGC CGC TCT AG
CAG rec reverse	GGG TGA ATA GGA ACG GGA GTC
Deleter forward	CGC CAT CCA CGC TGT TTT GAC C
Deleter reverse	CAG CCC GGA CCG ACG ATG AAG
LoxP 1	TAA GGG ATC TGT AGG GCG CA
LoxP 2	TGT CCT CAA CCG CGA GCT GT
OIMR 316	GGA GCG GGA GAA ATG GAT ATG
OIMR 883	AAG TCG CTC TGA GTT GTT AT
PDAPP forward	GGT GGA AAT GTC TGG TCC TGG AGG G
PDAPP reverse	ATC TGG CCC TGG GGA AAA AAG
SORLA BstEII rev	CAG ATG GTG ACC ACA GCT TG
SORLA cDNA 1	TCC ATA GTC GTA AGA CAC GTA CAC
SORLA cDNA 2	AGT GAT CCT TGA GGA AGT GAG
SORLA cDNA 3	ACT TCC TGG ACC TCA CTA CTA C
SORLA cDNA 4	GTT CAT TCT GTA TGC TGT GAG GA
SORLA cDNA 5	TCC AAA TAC AGT GGG TCC CAG
SORLA cDNA 6	TGC CAG GAT GGT TCC GAT GA
SORLA cDNA 7	TGA GTT CGA ATG CCA CCA AC
SORLA cDNA 8	TGC GGT GAC TAG TCG TGG AAT A
SORLA cDNA 9	TCC TGA CCA GGA CTT GTT GTA TG
SORLA G511R fw	TGG CTC AGT GCG AAA GAA CTT
SORLA G511R rev	AAG TTC TTT CGC ACT GAG CCA
SORLA start fw	ATC CAC TAG TCC AGT GTG GTG
SORLA Y141C fw	TCT TAC GAC TGT GGA AAA TCA T
SORLA Y141C rev	ATG ATT TTC CAC AGT CGT AAG A
Rs2070045 forward	CAG GGA CTG GTC GGA TGA AG
Rs2070045 reverse	CTT CAT CCG ACC AGT CCC TG
Rs1699102 forward	CTG CCC AAA CGG CAC TTG CA
Rs1699102 reverse	TGC AAG TGC CGT TTG GGC
Zeocin forward	AGT TGA CCA GTG CCG TTC
Zeocin reverse	GAT GAA CAG GGT CAC GTC G

3.2. TaqMan Gene Expression Assays

Gene	**Assay ID, Applied Biosystems**
18S ribosomal RNA	Mm03928990_g1
Apolipoprotein E (Apoe)	Mm00437573_m1
Insulin degrading enzyme (*Ide*)	Mm00473077_m1
Lrp1	Mm00464608_m1
Neprilysin	Mm00485028_m1
Sort1	Mm00490905_m1
SORL1 (human)	Hs00983791_m1
Beta-2 microglobulin (*β2M, human*)	Hs00984230_m1

3.3. TaqMan SNP Genotyping Assays

SNP ID	**Assay ID, Applied Biosystems**
Rs2282649	15957099_10
Rs1784931	137900_10
Rs2276346	25473294_10
Rs641120	1379945_10
Rs689021	1379954_10
Rs1625828	8799428_10
Rs2101756	15810165_10
Rs726601	638413_20
Rs1699102	8799430_10
Rs2070045	25634796_10
Rs668387	638456_10
Rs1010159	1379899_1
Rs7131432	29266026_10
Rs11218313	1379942_10

3.4. Media

Medium	Composition
Dissociation medium	Dulbecco's Modified Eagle Medium (DMEM) with Glutamax (Life Technologies), 5% fetal calf serum (FCS), 100 u/ml penicillin, 0.1 mg/ml streptomycin
Enzyme medium	50 ml DMEM with GlutaMAX, 0.025 µl/ml Papain (Worthington), 10 mg L-Cysteine (Merck), 1 mM $CaCl_2$, 0.5 mM EDTA
LB medium	10 g/l bacto-tryptone, 5 g/l bacto-yeast extract, 10 g/l NaCl; pH 7.2
SOC medium	20 g/l bacto-peptone, 5 g/l bacto-yeast extract, 0.5 g/l NaCl, 0.17 g/l KCl, 0.95 g/l $MgCl_2$, 3.6 g/l glucose; pH 7.0
LB agar	LB-medium, 15 g/l agar
ES cell medium	5.58 g DMEM media powder (Life Technologies), 1.0 g $NaHCO_3$, 83.5 ml ES-FCS, 5.5 ml penicillin/streptomycin, 5.5 ml L-glutamine, 5.5 ml non essential amino acids (Millipore), 3.8 µl 2-mercaptoethanol, 55 µl murine leukemia inhibitory factor (LIF; Millipore)
ES cell freezing medium	60 ml ES cell medium, 20 ml ES-FCS, 20 ml 20% DMSO
Neuronal medium	50 ml Neurobasal-A medium (Life Technologies), 1 ml B-27 (Life Technologies), 0.5 ml Glutamax (Gibco), 50 u/ml penicillin, 0.05 mg/ml streptomycin
Stopping medium	10 ml dissociation medium, 25 mg Albumin (Sigma), 25 mg Trypsin inhibitor (Sigma)

3.5. Buffers and solutions

Buffer/Solution	Composition
Blocking buffer for immunoblotting	5% milk powder in TBS-T
Blocking buffer for immunostaining	1% bovine serum albumin (BSA), 10% normal donkey serum (Millipore), 0.5% Tween-20 in PBS
Cryoprotective buffer	25% glycerol, 25% ethylene glycol, 0.05 M phosphate buffer in PBS
Cresyl violet solution	0.1 g cresyl violet acetate in 100 ml H_2O, 0.3 ml glacial acetic acid just before use.
DNA-loading buffer (10x stock)	0.25% (w/v) bromphenol blue, 0.25% xylencyanol, 30% glycerol
Homogenization buffer	20 mM Tris, 150 mM NaCl, 5 mM EDTA, pH 7.4
Hot-shot alkaline lysis buffer	1.25 M NaOH, 1 mM EDTA
Hot-shot neutralization buffer	2 M Tris HCl; pH 5
Low TE buffer	10 mM Tris HCl, 1 mM EDTA; pH 8.0
Lysis buffer for protein extraction	50 mM Tris, 150 mM NaCl, 5 mM EDTA, 1x Triton X-100, 0.02% sodium azide (NaN_3)
Lysis buffer for mini prep	200 mM NaOH, 1% SDS
Neutralization buffer for mini prep	3 M CH_3CO_2K; pH 5.5
NuPAGE running buffer (20x stock)	50 mM MOPS, 50 mM Tris, 0.1% SDS, 1 mM EDTA, pH 7.7
NuPAGE transfer buffer (20x stock)	25 mM Bicine, 25 mM Bis-Tris, 1 mM EDTA, pH 7.2
PBS	1.5 M NaCl, 80 mM Na_2HPO_4, 20 mM NaH_2PO_4
PBS-T	0.05% Tween-20 in PBS
PFA	4% parafolmaldehyde in PBS
Ponceu S solution	0.1% Ponceu S (Sigma) in 1% Acetic acid
Prehybridization buffer	50% formamide, 5x SSC pH 4.5, 50 µg/ml heparin, 100 µg/ml tRNA, 0.1% Triton X-100
Resuspension buffer for mini prep	50 mM Tris HCl, 10 mM EDTA, 100 µg/ml RNase A; pH 8.0
Running buffer for immunoblotting (10x stock)	125 mM Tris, 960 mM Glycine, 1% SDS
SSC buffer (20x)	3 M NaCl, 0.3 M trisodium citrate ($Na_3C_6H_5O_7$), pH 4.5 or 7.0
SSC-T buffer (2x)	0.1% Tween-20 in 2x SSC, pH 7.0
SSC-T buffer (0.2x)	0.1% Tween-20 in 0.2x SSC, pH 7.0
SSC washing buffer I	0.1% SDS in 2x SSC

Buffer/Solution	**Composition**
SSC washing buffer II	0.5% SDS in 0.1x SSC
TAE buffer	40 mM Tris HCl, 1mM EDTA, 20 mM glacial acetic acid, pH 8.0
Tail buffer	10 mM Tris HCl, 0.3 M sodium acetate (NaOAc), 0.1 mM EDTA, 1% SDS, pH 7.0
TBS (10x stock)	250 mM Tris, 1.37 M NaCl, 27 mM KCl, pH 7.4
TBS-T	0.1% Tween-20 in 1x TBS
Transfer buffer for immunoblotting	15 mM Tris, 125 mM Glycine, pH 8.3

3.6. Kits

APP Human ELISA Kit, Life Technologies

BigDye Terminator v3.1 Cycle Sequencing Kit, Applied Biosystems

Bioanalyzer RNA 6000 Pico Assay, Agilent

DNA isolation Kit, Qiagen

First-Strand cDNA Synthesis SuperScript II RT Kit, Life Technologies

Gateway Cloning Kits, Life Technologies

Gene Pulser II Electroporation System, Bio-Rad

High Pure PCR Product Purification Kit, Roche

Human sAPPα/sAPPβ Multiplex Kit, Meso Scale Discovery

Mouse/Rat Aβ (1-40) Assay Kit, Immuno Biological Laboratories (IBL)

Mouse/Rat Aβ (1-42) Assay Kit, IBL

Mouse/Rat sAPPα Assay Kit, IBL

pGEM-T Easy Vector, Promega

Pierce BCA Protein Assay Kit, Thermo Fisher Scientific

Prime-It II Random Primer Labelling Kit, Strategene

qPCR Mastermix, Eurogentec

RNA Easy Mini Kit, Qiagen

Rodent/Human (4G8) Abeta 3-Plex Ultra-Sensitive Kit, Meso Scale Discovery

SuperSignal West Femto/Pico Maximum Sensitivity Kits, Thermo Fisher Scientific

3.7. Technical equipment

ABI 7900HT Fast Real-Time PCR System, Applied Biosystems

Bioanalyzer 2100, Agilent

Cryostat HM 560, Thermo Scientific Microm

DNA sequencer 377, Applied Biosystems

Laser Scanning Microscope SPE, Leica

Laser Scanning Microscope LSM 710, Zeiss

Luminescent Image Analyzer LAS-1000 plus, Fuji

Microscope System DM 6000B, Leica Microsystems

NanoDrop ND-1000 Spectrophotometer, Thermo Fisher Scientific

Radioluminographic Scanner FLA 3000-2R, Fuji

Rotary Microtome HM 355S, Thermo Scientific Microm

Sector Imager 2400, Meso Scale Discovery

Sliding Microtome SM2000R, Leica Biosystems

Synergy HT Multi-Mode Microplate Reader, Bio-Tek

Ultrospec 2100 pro UV/Visible Spectrophotometer, GE Healthcare

3.8. Brain autopsy material

Brain autopsy samples from prefrontal cortex were obtained from the Netherlands Brain Bank (Netherlands Institute for Neuroscience, Amsterdam) and the MRC London Brain Bank for Neurodegenerative Diseases (Institute of Psychiatry, King's College London). Samples were of Caucasian origin. Written informed consent for a brain autopsy and the use of the material and clinical information for research purposes had been collected by the respective brain banks. Detailed personal information including age, gender, neuropathological stage, apolipoprotein E (*APOE*) genotype, of the individuals were provided by the brain banks along with the tissue specimens.

3.9. Mouse lines and husbandry

Mice were kept at standard conditions according to the German animal protection act.

To generate mice homozygous for the SORLA transgene (*Rosa26*$^{Tg/Tg}$), heterozygous SORLA overexpressors (*Rosa26*$^{Tg/+}$) were intercrossed.

The PDAPP mouse line, which expresses the platelet-derived growth factor (PDGF)-β promoter driven human APP gene with V717F familial AD mutation (Games, Adams et al. 1995) was used as a rodent model of Alzheimer disease. SORLA deficient mice were generated in our lab as described previously (Andersen, Reiche et al. 2005). The Cre Deleter mouse strain was purchased from Taconic (Otto, Fuchs et al. 2009).

3.10. Generation of transgenic mice overexpressing SORLA

3.10.1. Generation of the targeting construct

To generate the targeting vector, I used the Gateway cloning technology (Life Technologies), which is based on a recombination reaction between the *att*L sequence of the entry clone (pCAG-ENTRY) and the *att*R sequence of the

destination vector (pCAG-DEST). To produce the entry clone, the human SORLA cDNA was cloned into the *att*L-containing donor vector (pENTR/D-TOPO vector) according to the manufacturer's instructions. The destination vector included 1.1 kb 5'- and 4.3 kb 3'- *Rosa26* homology regions for recombination with murine *Rosa26* locus. It also contained the cytomegalovirus early enhancer/chicken β-actin promoter (CAG) element and the neomycin phosphotransferase gene driven by the mouse phosphoglycerate kinase 1 (PGK1) promoter flanked by loxP sites for positive selection. The destination vector was kindly provided by Dr. Richard Mort (University of Edinburgh). Finally, I performed the LR recombination reaction to transfer the human SORLA cDNA from the attL-containing entry clone (pCAG-ENTRY) into the attR-containing destination vector (pCAG-DEST) (Figure 5). The LR recombination reaction is a site-specific recombination between *att*L sequence of an entry clone and *att*R sequence of a destination vector induced by LR Clonase II enzyme (Life Technologies).

The LR reaction mixture consisting of 40 ng of pCAG-ENTRY clone, 80 ng of pCAG-DEST vector, 1 µl of LR Clonase II (Life Technologies) and 1.25 - 5 µl of TE buffer, pH 8.0 was incubated overnight at room temperature. The next day, 0.5 µl of Proteinase K was added to the mixture and incubated for 10 minutes at 37°C. Plasmids obtained from the LR reaction were used to transform XL1 Blue cells. Ampicillin-resistant bacteria clones were picked and the DNA was isolated as described below. To test the proper insertion of the clone into the vector, 0.5 µg of purified DNA was digested with *BamHI* and *NotI*, and run in the agarose gel. Mini-prep cultures of plasmids containing the correct clone were expanded to isolate larger amounts of DNA.

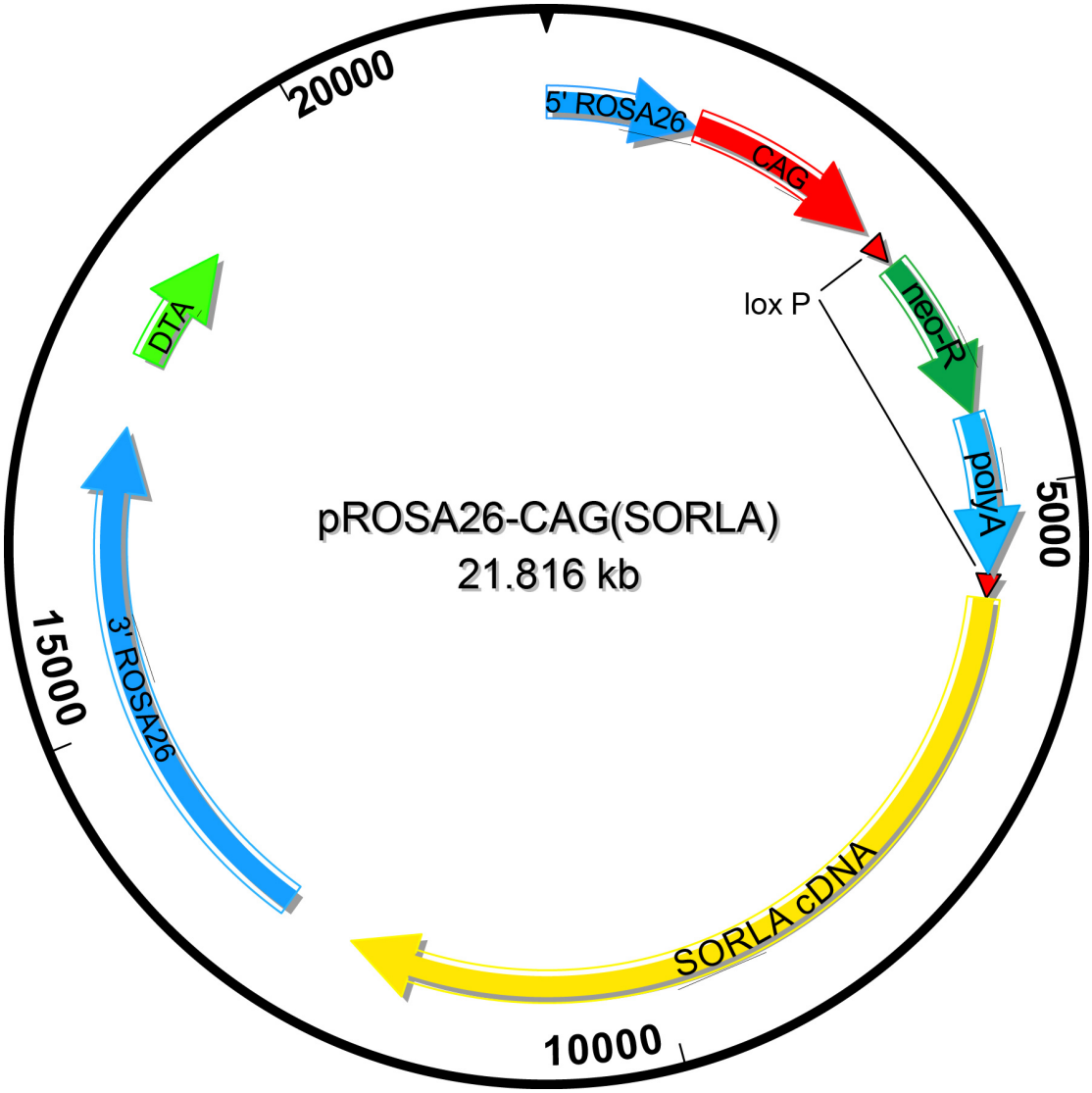

Figure 5. Map of the targeting vector used to generate *Rosa26*$^{CAG(SORLA)}$ mice. The targeting construct was generated by insertion of the human SORLA cDNA from an entry vector into the destination vector using Gateway cloning technology (Life Technologies). Destination vector also included 5' and 3' homology regions of the murine *Rosa26* gene locus for homologous recombination, the cytomegalovirus early enhancer/chicken β-actin promoter (CAG) element to induce transgene transcription, the neomycin phosphotransferase gene driven by the mouse phosphoglycerate kinase 1 promoter (neo-R) for positive selection as well as the diphtheria toxin-A sequence (DTA) for negative selection of embryonic stem cells. Neo-R and the adjacent polyA sequence are flanked by loxP sites and can be removed by Cre-recombinase to induce conditional expression of SORLA driven by CAG. Destination vector was kindly provided by Dr. Richard Mort (University of Edinburgh). The map was drawn using SeqBuilder program (Lasergene, DNASTAR).

The SORLA cDNA and the loxP sites in the final targeting vector were sequenced to confirm lack of mutations that may have been introduced by the polymerase enzymes during the various cloning steps. Next, 35 µg of targeting vector was linearized with *AlwI* restriction enzyme and purified using phenol-chloroform extraction procedures. Complete linearization of the vector was tested by agarose gel electrophoresis.

3.10.2. Introduction of the targeting vector into murine embryonic stem cells

Embryonic stem (ES) cells were previously harvested by our group from the inner cell mass of 129SvEmcTer-derived blastocysts. Before targeting, ES cells were cultured in petri dishes or plates pre-coated with 0.1% gelatin. To support growth of ES cell cultures, dishes and plates were covered with neomycin resistant mouse fibroblasts (feeder cells). Prior to coating, feeder cells were mitotically inactivated by incubation with mitomycin in the cell culture incubator at 37°C with 5% CO_2.

129SvEmcTer derived murine ES cells were targeted with the linearized construct by electroporation. After 1 week of culturing, G418-resistant ES cell clones were picked and screened with Southern blot to identify the homologous recombinants. ES cells heterozygous for the targeted allele were expanded and genotyped with Southern blotting to ensure correct clones were chosen for injection into blastocysts as described in the following.

Approximately $1x10^7$ ES cells were harvested from one 10 cm plate. Cells were washed three times with PBS and collected in 1400 µl of PBS. 700 µl of ES cell suspension was mixed with 100 µl DNA suspension containing 35 µg of targeting plasmid DNA pre-linearized with *Alw*I. The ES cells were electroporated with DNA using a pulse of 250 V and 5 µF in Gene Pulser II Electroporation System (Bio-Rad). Afterwards, the cells were seeded on five 10 cm plates pre-coated with gelatin and feeder cells.

ES cell clones were cultured in ES cell medium containing 0.18 mg/ml geniticin (G418 or neomycin from Gibco) for positive selection. After 7 days

of culturing by replacing the medium of the cells everyday, G418-resistant ES cell clones were picked and transfered into 96-well plates coated with gelatin and feeder cells. After 5 days, each 96-well plate was expanded into four replicate 96-well plates. Two of the replicates plates were coated with gelatin and feeder cells to archive the clones.

Two days later, ES cells in one of the plates without feeder cells were lysed to isolate DNA. After overnight incubation of cells in 75 µl/well lysis buffer (0.1% SDS/0.1 mg/ml RNase A/0.25 mg/ml proteinase K/PBS), the DNA was precipitated by overnight incubation with 75 µl/well 100% isopropanol. After washing with 70% ethanol, the pellet was resuspended in TE buffer by overnight incubation at 55°C.

The remaining ES cell plates were frozen at -80°C until the clones positive for targeting were identified by Southen blotting and/or PCR. Prior to freezing, the ES cells were trypsinized (30 µl 0.05% trypsin/EDTA per well) for 5 min at 37°C. The enzymatic reaction was stopped with 70 µl/well ES cell medium. 100 µl/well ES-cell-freezing medium was added and cells were frozen at -80°C.

After the ES cells were screened for the proper-targeted insertion with Southern blot, positive cells were expanded to confirm the results and to prepare the cells for blastocyst injection. Plates were thawn by incubating at 37°C for 7 min and the ES cells from selected wells were delivered into 24-well plates that were pre-coated with gelatin and feeder cells. After 3 more days, the cells were passaged into 6-well plates. 3 days later, the ES cells in each well were harvested and splitted into 3 equal parts. 2 of them were frozen at -80°C. The third one was cultured for 2 days more in 6-well plate and later used to prepare DNA.

3.10.3. Generation of the germline chimera

After genotyping with Southern blot, the positive ES cell clone was injected into murine blastocyst from C57BL/6 mice to generate germline chimera according to the standard procedures by Dr. Ernst-Martin and Dr. Annette

Fuechtbauer at Aarhus University. These colleagues also crossed the chimeric offspring males with C57BL/6 female mice to generate animals that were heterozygous for the SORLA transgene. These heterozygous mice were obtained by me and used to establish the strain at the MDC.

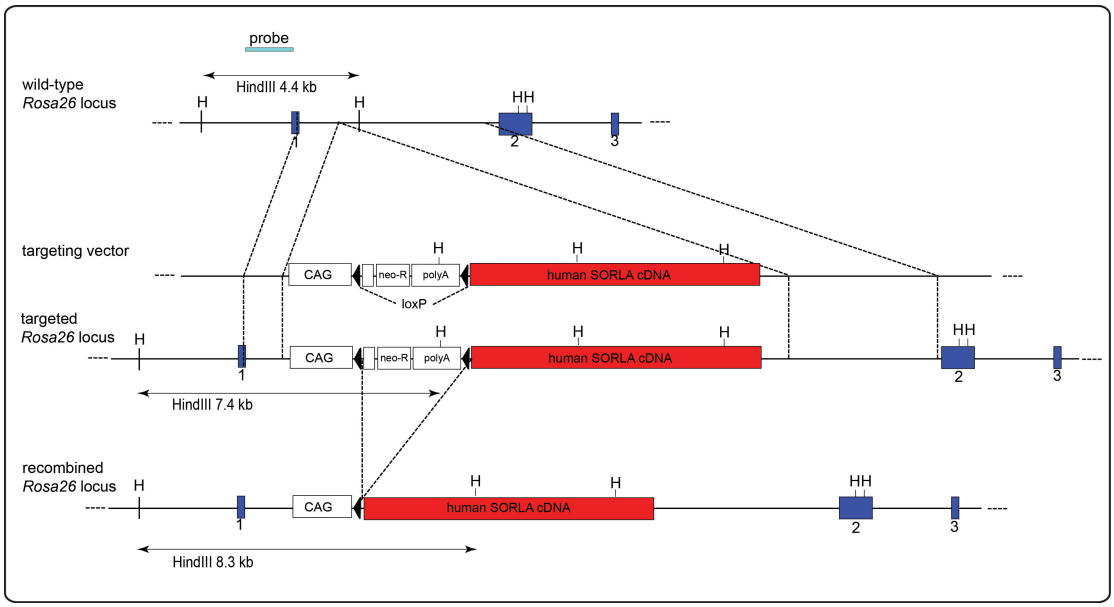

Figure 6. The targeting strategy to generate SORLA overexpressing mice. The targeting vector included the human SORLA cDNA flanked by 3'- and 5'- *Rosa26* homology regions to enable homologous recombination into the murine *Rosa26* locus. To enable conditional overexpressing of SORLA in mice, the neomycin phosphotransferase gene (neo-R) and the poly-A transcription stop element (poly-A) were flanked by two loxP sites. Before Cre-mediated removal of the loxP sites, transcription from the CAG promoter element (cytomegalovirus enhancer and chicken β-actin promoter) will proceed through neo-R but stops at the poly-A signal preceeding the SORLA cDNA. Removal of neo-R and poly-A sequences by Cre-mediated recombination of the loxP sites allows transcription from CAG to proceed through the SORLA cDNA. H denotes *HindIII* restriction site used in Southern blot experiments. Probe stands for 1.5 kb sequence hybridizing to 5' homology region of the Rosa26 locus and targeting vector.

Due to the presence of a transcription stop element in front of the SORLA cDNA in the targeting vector (Figure 6), mice carrying the SORLA cDNA inserted in the *Rosa26* locus did not express the transgene. To induce expression of the gene, the selection marker and transcription stop element were eliminated by breeding the heterozygous mice with the Cre deleter mice (Taconic) (Figure 6). The Cre deleter mouse carries a copy of the Cre recombinase gene inserted in the *Rosa26* locus and is ubiquitously active general Cre deleter line (C57BL/6-*Gt(ROSA)26Sor*$^{tm16(Cre)Arte}$) (Otto, Fuchs et al. 2009).

3.11. Antibodies

Antibodies against the amyloid precursor protein (APP), apolipoprotein E (APOE), carboxy-terminal fragments (CTFs), low-density lipoprotein receptor-related protein 1 (LRP1) -85 subunit and SORLA were produced in-house. Commercial antibodies were used to detect α-tubulin, Na/K ATPase, neuronal nuclei (NeuN) (Millipore), β-actin (Sigma), β -tubulin (Covance), glial fibrillary acidic protein (GFAP, Dako), insulin degrading enzyme (IDE, Abcam), neprilysin (Santa Cruz), Lamp-1 and sortilin (BD Transduction Laboratories). Secondary antibodies were either coupled with peroxidase used for western blotting (Sigma) or coupled with Alexa 488, 555 or 633 fluorophore dyes for immunohistology (Life Technologies).

3.12. DNA isolation from tissues and cells

DNA was isolated from human brain specimens, from ES cells or from mouse-tail biopsies. Tissues were lysed in (10x volume (µl) / weight of the tissue (mg)) tail buffer with proteinase K (0.5 mg/ml) overnight at 55°C. For ES cells in 96-well plates, 75 µl/well tail buffer with proteinase K (0.5 mg/ml) was used for overnight at 55°C. DNA was extracted with phenol/chloroform/isoamylalcohol (25:24:1) (same amount of lysis buffer used) and precipitated with isopropanol. DNA pellets were rinsed with 70% ethanol and resuspended in low-TE buffer.

To genotype mice by PCR, mouse-tail or ear-punch biopsies were lysed in 75 µl alkaline lysis buffer for 30 min at 95°C. After cooling to room temperature, 75 µl neutralization buffer was added.

3.13. Southern blot

Southern blotting was used to screen ES cell clones and to confirm the proper insertion of the targeting vector into the mouse genome via homologous recombination. To do so, 10 µg of ES cell DNA was fragmented by overnight incubation with 40 units of *HindIII* enzyme at 37°C. The digested DNA samples were run in agarose gels. The gels were incubated in NaOH solution (0.4 M) for 30 min to denature the double stranded DNA. Gels were blotted overnight onto the Amersham Hybond-C membranes (GE Healthcare) in 0.4 M NaOH. The following stack was assembled to enable capillary transfer during blotting: 2 sheets of Whatman paper reaching into a reservoir with 0.4 M NaOH solution, the agarose gel containing fragmented DNA, the nylon membrane, 2 sheets of Whatman paper, a pack of paper cloths, and a weight of approximately 0.5 kg.

After overnight transfer, the nylon membrane was baked at 80°C for 10 min and the DNA were fixed to the membrane by exposure to 0.01 Joule of ultraviolet radiation (Crosslinker, Bio-Link). Prior to hybridization with the DNA probe, the membrane was conditioned for 1 hour at 65°C in 10 ml Amersham rapid-hybridization buffer (GE Healthcare). The DNA probe (10 ng/membrane) was labeled with 5 µl radioactive ^{32}P using the Prime-It II Random Primer Labelling Kit (Stratagene) according to the manufacturer's instructions. For hybridization, membranes were incubated with a 1.5 kb probe hybridizing to the 5' region of *Rosa26* locus, overnight at 65°C in a rotator. The probe detects a 4.4 kb band in wild-type *Rosa26* locus, a 7.4 kb band in the targeted locus before recombination and a 8.3 kb band following cre-mediated recombination of *Rosa26* locus (Figure 6). The next day, the membrane was washed in SSC washing buffer at 65°C and exposed to an imaging plate (Fuji) for 16-24 hours at room temperature. The DNA fragments

were visualized using the FLA 3000-2R Radioluminographic Scanner (Fuji) and AIDA Image Analyzer (Rad-Tek Technologies).

3.14. PCR genotyping of mice

DNA templates (1 µl) were amplified in polymerase chain reactions (PCR) with 25 ul of master-mix consisting of 0.025 u/µl Taq polymerase (New England Biolabs), 1x ThermoPol PCR buffer (New England Biolabs), 0.2 mM dNTPs (Life Technologies) and 0.2 µM of each primer pair (sequences are listed in materials section 3.1.). All PCR products were electrophoresed in agarose gels and visualized under UV-light.

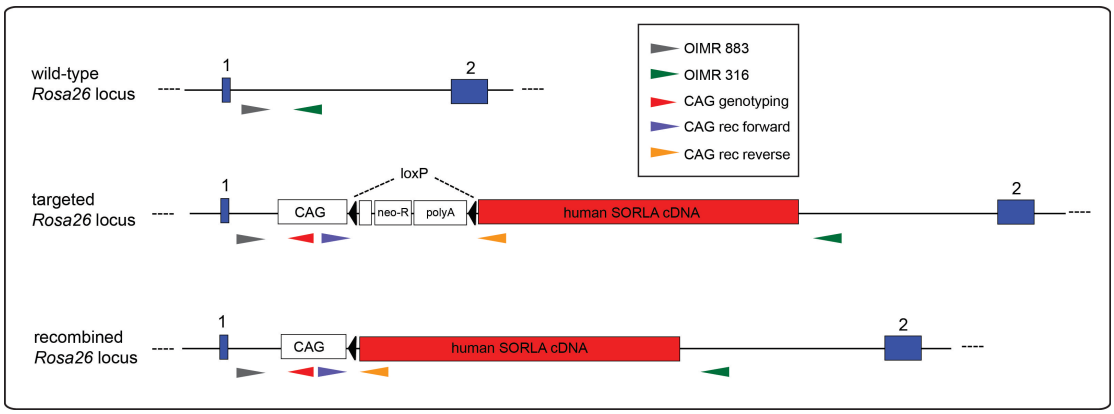

Figure 7. PCR reactions to genotype targeted and recombined *Rosa26* locus. To genotype targeted and wild-type *Rosa26* locus, three primers were designed. OIMR 883 (grey arrowhead) and OIMR 316 (green) are binding to intronic sequences between exon 1 and 2 (blue rectangles) of the *Rosa26* locus. The primers produce a 602 bp long fragment from the wild-type allele in the PCR reaction. As the targeting construct was inserted in between OIMR 883 and OIMR 316, there is no amplification from these primers in the targeted allele. Instead, OIMR 883 and CAG genotyping primer (red), which binds to the CAG promoter produces a fragment of 410 bp length. After the mice were bred with Cre deleter mice, recombination was tested with PCR genotyping. The CAG rec forward (purple) and CAG rec reverse (orange) primers, which bind to CAG promoter and SORLA cDNA respectively, were designed for the analyses. Before the recombination occurs, the DNA isn't amplified from the primers because of the large product size (3-kb) and poly-A tail. When recombination occurs, neo-R and poly-A sequences are removed. As a result, the PCR fragment of 260 bp is seen in the agarose gel.

To determine the presence of the targeted allele in the *Rosa26* locus, the OIMR 883 primer was used as common primer that can bind both to the wild type and to the targeted allele (Figure 7). A CAG genotyping primer was designed to specifically amplify the targeted allele as it binds to the CAG promoter. OIMR 316 binding to the Rosa26 locus was used to distinguish the wild type allele. On the targeted locus amplification from OIMR 883 and OIMR 316 doesn't occur as the targeting vector was inserted between the two primers (Figure 7). The PCR reaction consisted of activation of Taq polymerase and initial denaturation of DNA at 94°C for 3 min, 35 cycles of denaturation (15 sec, 94°C), annealing (15 sec, 53°C) and elongation (15 sec, 72°C), and was terminated with final elongation at 72°C for 10 min. PCR product amplified from the targeted allele was 410 base pair (bp) long and that amplified from wild-type allele was 602 bp long.

To determine elimination of selection marker by Cre recombinase action, the CAG rec forward and reverse primers were used with same conditions used to genotype the targeted allele (Figure 7). When recombination doesn't take place, DNA isn't amplified from the primers due to poly-A tail. In case of successful recombination, which removes neo-R and poly-A, amplification from the former primer binding to the CAG promoter and the latter primer hybridizing to the SORLA cDNA results in a PCR product of 260 bp size.

The presence of the Cre recombinase transgene in the mice was determined by PCR using Deleter-forward and -reverse primers. The PCR amplification reaction, which consisted of initial denaturation at 94°C for 2 min followed by 35 cycles of denaturation at 94°C for 15 sec, annealing at 60 °C for 15 sec and elongation at 72°C for 30 sec, and finished with final elongation at 72°C for 10 min, gave a band at 420 bp size for the transgene.

The PDAPP transgene was detected by PCR using the PDAPP forward and PDAPP reverse primers. The PCR reaction encompassed an initial denaturation step at 94°C for 2 min followed by 35 cycles of denaturation at 94°C for 15 sec, annealing at 62°C for 15 sec and extension at 72°C for 30 sec. The amplification of the transgene resulted in a band of 150 bp size.

3.15. PCR

PCR reactions during cloning steps were performed using Phusion High Fidelity DNA polymerase (Finnzymes). 100-200 ng of template was amplified in a 50 µl master-mix consisting of 1x Phusion HF buffer (Finnzymes), 0.2 mM dNTPs (Life Technologies), 0.5 µM of each primer pair, and 0.02 u/µl Phusion High Fidelity DNA polymerase. Phusion GC buffer and 5% DMSO was used if the desired sequence is GC-rich region. PCR reaction including initial denaturation (3 min, 98°C), amplification (30 steps of denaturation (10 sec, 98°C), annealing (10 sec, 53-70°C) and elongation (1 min per amplification product size (kb)) and final elongation (10 min, 72°C) took place in a thermal cycler.

PCR products were run in agarose gels and DNA was purified using the High Pure PCR purification Kit (Roche) according to the manufacturer's instructions.

3.16. DNA ligation

To insert a DNA fragment into a vector, both plasmids were cut with the appropriate restriction enzymes and run in an agarose gel. The DNA was purified from the gel using a DNA purification kit (Life Technologies). The purified DNA fragments were ligated overnight at 16°C in 10 µl master-mix consisting of 1 µl T4 ligase (Promega) and 1x rapid ligation buffer (Promega).

3.17. Bacteria transformation

Purified plasmids or ligated DNA fragments were transformed into XL1 Blue or DH5α bacteria strains. An aliquot of bacteria was thawed on ice. Two µl of the plasmid (ligation product) was mixed with 40 µl of bacterial cells and electroporated at 1.8 kV.

The cell suspension was incubated with 1 ml SOC medium at 37°C for 30 min. Cells were collected by centrifugation at 800xg for 5 min at room temperature. Cells were re-suspended in 100 µl SOC medium and plated

onto LB medium with Ampicillin (50 µg/ml). The LB-Amp plates were incubated overnight at 37°C.

3.18. DNA isolation from bacteria

Antibiotic-resistant bacterial clones were picked from LB-Amp (50 µg/ml) agar plates and inoculated into 3 ml of LB medium. Cultures were grown overnight at 37°C with vigorous shaking. Cells were harvested next day by centrifuging at 800xg for 10 min at room temperature. The pellet was resuspended in buffer P1 (DNA isolation kit from Qiagen) and cells were lysed in buffer P2. After neutralization with buffer P3, samples were centrifuged at 12000xg for 10 min at 4°C. Supernatant containing the plasmid DNA was collected and the DNA precipitated with LiCl (8 M, 0.1x volume of supernatant) and 100% isopropanol (1 volume of supernatant) followed by centrifugation at 12000xg for 10 min at 4°C. The pellet was washed with 70% ethanol and resuspended in sterile water. The purified plasmid DNA was stored at -20°C.

For isolation of larger amounts of plasmid DNA, the Maxi-Prep DNA Isolation Kit (Qiagen) was used according to the manufacturer's instructions.

3.19. Sequencing

DNA sequencing was performed using the BigDye Terminator v3.1 Cycle Sequencing Kit (Applied Biosystems) according to the manufacturer's instructions. In short, 100 ng of purified DNA was amplified with 0.5 µM of designed sequencing primer, 1x BigDye sequencing buffer and 1x BigDye primer and terminator mix (Applied Biosystems). The BigDye terminator mix includes a fluorescein donor dye linked to one of four dichlororhodamine acceptor dyes. The amplification reaction included initial denaturation (1 min, 96°C) followed by 30 cycles of denaturation (10 sec, 96°C), annealing (10 sec, 48°C) and elongation (4 min, 60°C). The amplified DNA was purified on Sephadex G-50 column (Amersham). The fluorescence signal of the sequences were read in an ABI PRISM 377 DNA Sequencer and analyzed using the Lasergene program (DNASTAR).

3.20. Primary neuronal culture

Primary hippocampal neurons were prepared from newborn (Postnatal day 1) mice. Hippocampi of the mice were dissected and trypsinized (500 µl enzyme medium per animal) for 20 min at 37°C. Enzymatic digestion of the hippocampi was terminated by incubating with 500 µl stopping medium for 5 min at 37°C. The neurons were finely separated in 500 µl dissociating medium and collected by centrifuging with 100xg for 10 min at room temperature. Cells were resuspended in 1 ml Neurobasal-A medium supplemented with B27 and GlutaMAX (Life Technologies) (neuronal medium) and plated on pre-coated chamber slides (Lab-Tek, Thermo Fisher Scientific). Two days later, neuronal medium was replaced and the cells were cultured for 7-10 days *in vitro* in neuronal medium.

To perform Aβ uptake assays in primary neurons, 50 µM stock solution of Aβ-Hilyte-488 recombinant peptide (AnaSpec) was prepared in 1% NH_4OH and diluted with PBS. Neuronal cultures were incubated with Aβ40 (200 nM) diluted in Neurobasal-A medium for 1 hour in the cell incubator. Afterwards, the proteins were collected by extraction with lysis buffer for 1 hour on ice. Aβ levels were measured by ELISA (Mesoscale Discoveries) and normalized to total protein concentrations determined with bicinchoninic acid (BCA) assay.

To show cellular localization of SORLA in the primary cultures, the cells were fixed in 4% paraformaldehyde (PFA)/PBS solution for 10 min and permeabilized by incubating with 0.05% Triton X-100/PBS for another 10 min. Following blocking with 2% donkey serum in PBS, the cells were incubated with primary antibodies directed against SORLA (1:3000 in PBS) or β-tubulin (1:3000 in PBS). To perform immunocytochemistry for Aβ uptake, the primary neurons were incubated with 500 nM of Aβ-Hilyte-488 for 4 hours in the cell incubator. Afterwards, the cells were fixed in PFA, and treated with an anti-Lamp-1 antiserum (1:2000 in PBS) overnight at 4°C. After staining with Alexa Fluor Dye-labeled secondary antibodies (Life Technologies, 1:1000 in PBS) directed against the respective primary

antibodies for 2 hours at room temperature, the cell layers were covered with fluorescent mounting medium (Dako) and coverslips.

3.21. Western blot analyses and ELISA kits

Protein extraction from the frozen human autopsy specimens and mouse tissues was carried out in two steps to separate Tris-buffered saline (TBS)-soluble proteins and detergent-soluble proteins. The tissues were weighed and homogenized in homogenization buffer (10x µl of tissue weight in mg) with 1x proteinase inhibitor (Roche). To remove tissue debris and nuclei, the homogenates were centrifuged at 2500xg and 12000xg for 15 min at 4°C. The supernatants were collected and subjected to a final centrifugation step at 100000xg for 1 hour at 4°C. Membrane-associated proteins, which were resuspended in lysis buffer (with 1x proteinase inhibitor), and supernatant containing cytosolic proteins were aliquoted and stored at -80°C until further use.

Protein concentrations were determined using either Bradford protein assay (Bradford MM, 1976) or the bicinchoninic acid (BCA) assay. In the Bradford assay, 2 µl of protein sample was diluted in Bradford solution (Sigma). The colorimetric reaction was measured in an Ultrospec 2100 pro spectrophotometer (GE Healthcare) at 595 nm wavelengths. The BCA assay was performed using the Pierce BCA Protein Assay Kit (Thermo Fisher Scientific) according to the manufacturer's instructions. The colorometric reaction was measured on Multi-Mode Microplate reader (Bio-Tek) at 562 nm wavelengths.

Protein expression levels were determined either by western blotting or ELISA. For western blotting of medium sized proteins, SDS-polyacrylamide, Tris-Glycine gels were used. To separate small carboxyl terminal fragments, NuPAGE 12% Bis-Tris gels from Life Technologies were used. Equal amounts of proteins were separated on the gels for 2-3 hours in running buffer at room temperature. The gels were transferred onto Amersham Hybond-C extra nitrocellulose membranes (GE Healthcare) by blotting for 2

hours in transfer buffer at room temperature. The membranes were stained with 0.1% Ponceau S solution/1% acetic acid and incubated with blocking buffer for 30 min at room temperature. Subsequently, the membranes were incubated in primary antibody solutions (diluted to 1 µg/ml concentration in blocking buffer) overnight at 4°C, followed by incubation in the respective anti-mouse, -goat, or –rabbit IgG-peroxidase coupled secondary antibody solution (diluted 1:2500 in blocking buffer) for 2 hours at room temperature. Immunoreactive protein bands were detected by chemiluminescence reaction using SuperSignal West Femto or Pico Maximum Sensitivity Kits (Thermo Fisher Scientific) and visualized in a Luminescence Image Analyzer (Fuji). For quantification of expression levels, the intensities of immunoreactive bands were determined by optical densitometry using the AIDA Image Analyzer (Raytest) software.

Commercial ELISA kits for amyloid precursor protein (APP) (Life Technologies), human soluble (s) APPα, sAPPβ and Aβ (Meso Scale Discovery), as well as murine sAPPα and Aβ (IBL) were used according to the manufacturers' instructions to measure the respective protein levels in tissue extracts and cell lysates. Electrochemiluminescence assays of Meso Scale Discovery were read in a Sector Imager 2400 (Meso Scale Discovery). Colorimetric reaction for APP, murine sAPPα and murine Aβ ELISA were measured in a Multi-Mode Microplate reader (Bio-Tek) at 450 nm wavelengths. The concentrations of target proteins were determined against a standard curve of recombinant proteins provided by the manufacturers, and normalized to total protein concentrations measured by BCA assay.

3.22. SORLA ELISA

To determine SORLA levels in cells and tissues, a custom-made sandwich ELISA was developed. In brief, 96-well plates (Nunc Maxisorb F96 from Thermo Fisher Scientific) were coated with 1 µg/ml of rabbit anti-SORLA IgG (IgG 5387) as capture antibody in 0.1 M $NaHCO_3$, pH 9.8, overnight at 4°C. After washing 3 times with PBS-T, the plate was incubated with blocking buffer (2.5% casein/PBS-T) overnight at 4°C. The next day, protein lysates or

recombinant SORLA protein standards (provided by Dr. Claus Munck Petersen, Aarhus University) were diluted in PBS-T and incubated in the plate overnight at 4°C. On the 4th day, after 3 times washing with PBS-T, the plates were incubated with 1 µg/ml of mouse monoclonal anti SORLA antibody (IgG 20c11) as detection antibody in PBS-T, overnight at 4°C. The next day, the signal was amplified by incubation with 0.2 µg/ml goat anti-mouse poly horseradish peroxidase (HRP) IgG (Thermo Scientific Pierce) for 2 hours at room temperature. After washing 3 times with TBS-T, HRP-conjugates were detected with Stable Peroxide Substrate Buffer supplemented with o-phenylenediamine (Thermo Scientific Pierce). Colorimetric reactions were measured on Multi-Mode Microplate reader (Bio-Tek) at 450 nm wavelengths. The SORLA concentrations in the samples were determined by comparing the measurements against a standard curve of recombinant protein, and normalizing to total protein concentrations measured by BCA assay.

3.23. Immunohistochemistry

Mice were anesthetized and transcardially perfused first with PBS, followed by 4% PFA/PBS solutions. The dissected brains were kept in 4% PFA/PBS for 24 hours.

To prepare free-floating sections, the brain samples were placed in 30% sucrose/PBS for 48 hours at 4°C. 40 µm-thick free-floating sections were cut on dry ice using a Sliding Microtome SM2000R (Leica Biosystems). Sections were stored at -20°C in cryoprotective buffer (25% glycerol/ 25% ethylene glycol/ 0.05 M phosphate buffer in PBS) until further use. Prior to staining, the sections were permeabilized with 0.5% Triton X-100/PBS for 45 min at room temperature and incubated with blocking buffer (1% BSA/10% normal donkey serum/0.5% Tween20/PBS) for subsequent 30 min at room temperature. Primary antibody solutions directed against SORLA (polyclonal anti-SORLA serum raised in goat, 1:750), neuronal nuclei (monoclonal anti-NeuN IgG, clone A60 from Millipore, 1:1000) or glial fibrilary acidic protein (polyclonal anti-GFAP rabbit serum from Dako, 1:1000) were prepared in

blocking buffer. Following overnight incubation with primary antibody solutions at 4°C, the sections were washed 3 times (30 min each) with PBS at room temperature. Fluorescence staining of the sections was performed in dark using the respective Alexa Flour (Life Technologies) dye-coupled secondary antibody solutions (1:250 in 0.05% Triton X-100/PBS) for 2 hours at room temperature. After washing 3 times (30 min each) with PBS at room temperature, sections were mounted onto Superfrost Ultra Plus Adhesion Slides (Thermo Scientific) and covered with fluorescent mounting medium (Dako) and coverslips (Roth).

Nissl staining was performed to identify neurons in the brain. To do Nissl staining, paraffin embedded sections were prepared. Brain samples were dehydrated through a series of graded ethanol solutions (25%, 50%, 75%, and 100%; 30 min each). Afterwards, they were incubated in xylene (Roth) (3 times for 2 hours), and infiltrated with paraffin at 67°C (2 times for 2 hours, followed by overnight incubation). The next day, the samples were embedded in paraffin and stored at 4°C until further use. 10 µM paraffin sections were cut on a rotary microtome (Microm HM 355S, Thermo Scientific) and stored at 4°C until staining. Prior to staining, sections were deparaffinized in xylene (3 times for 5 min) and dehydrated in graded ethanol solutions (100%, 90%, 80%, 70%, 50%, 2 times for 3 min each) and H_2O (3 min). Sections were stained in 0.1% Cresly violet solution for 30 min at room temperature and differentiated in 95% ethanol for 10 min. The sections were dehydrated in 100% ethanol and cleared in xylene before mounting with permanent mounting medium (Sigma).

Fluorescent mages were recorded using Zeiss LSM 700 or Leica TCS SPE confocal laser scanning microscopes and analyzed using Fiji software (ImageJ, NIH). Bright-field pictures were taken using the Microscope System DM 6000B (Leica Microsystems).

3.24. Measurements of RNA levels

Tissue samples or cells were homogenized in TrIzol (Life Technologies). Total RNA samples were purified using the RNeasy Mini Kit (Qiagen) according to the manufacturer's instructions. Concentration and integrity of RNA samples were measured by Bioanalyzer RNA 6000 Nano Assay (Agilent) and evaluated in BioAnalyzer 2100 program (Agilent) according to the manufacturer's instructions.

The cDNA was synthesized from prepared mRNA by a reverse-transcriptase reaction using the High Capacity RNA-to-cDNA Kit from Applied Biosystems. 2 µg of RNA template was transcribed into cDNA with 1x enzyme mix (MuLV reverse transcriptase and RNase inhibitor protein) and 1x buffer mix (dNTPs, random octamers and oligo dT-16) at 37°C for 60 min. The reaction was stopped by incubating at 95°C for 5 min.

Prior to quantitative (q) PCR reaction, the cDNA samples were diluted 1/50 in RNase-free H_2O. The transcript levels were measured using FAM dye-labeled TaqMan Gene Expression primer/probe sets (Applied Biosystems). One µl (40 ng) of cDNA dilution was mixed with 1x qPCR Mastermix (Eurogentec) and 1x primer/probe mix (Applied Biosystems). The PCR reaction was run in an ABI 7900HT Fast Real-Time PCR instrument (Applied Biosystems). The reaction included AmpliTaq Gold activation at 95°C for 10 min, followed by PCR amplification with 40 cycles of denaturation at 95°C for 15 sec and annealing and extension at 60°C for 1 min each. Fluorescence signal intensities in each PCR cycle were measured using the Sequence Detection System (SDS) program (Applied Biosystems) and used to calculate mRNA levels.

For each reaction, a standard curve was prepared from serial dilutions of the cDNA mixture. Transcript levels of 18S ribosomal RNA (18S rRNA) or β-2-microglobulin were measured as internal controls to calculate relative expression levels of the target cDNAs. Differences in expression levels were calculated using the Pfaffl method (Pfaffl 2001).

To determine transcript levels of the Zeocin resistance cassette and 18S ribosomal (r) RNA in Chinese hamster ovary (CHO) cells, primer sequences (18S rRNA forward, 18S rRNA reverse, Zeocin forward and Zeocin reverse) were designed using Internet website of IDT (Integrated DNA Technologies, http://eu.idtdna.com/site). For each reaction, 1 µl (40 ng) of cDNA solution was mixed with 5 µl of Power SYBR Green PCR Master Mix (SYBR Green Dye, Taq Gold DNA polymerase, dNTPs) and 0.5 µM of primer pairs. Thermal cycler conditions were the same as that one used for TaqMan Gene Expression Assays.

3.25. SNP genotyping

TaqMan SNP genotyping assays (Applied Biosystems) were used to determine the SNP alleles (Figure 8). Thus, 10 ng of genomic DNA samples isolated from human brain specimens were delivered to the bottom surface of 384-well plates (Applied Biosystems). DNA samples were dried down by overnight evaporation at room temperature. The next day, 10 µl reaction mix including 0.25 µl Primer and TaqMan probe (FAM) dye mix, and 5 µl TaqMan universal PCR master mix (Applied Biosystems) was prepared and added onto the dried DNA samples. The DNA templates were amplified in a thermal cycler with initial denaturation for 1 min at 95°C, followed by 40 cycles of denaturation for 15 sec at 92°C and annealing and extension steps for 1 min 60°C each. Fluorescence intensities were measured with the 7900HT Fast Real-Time PCR system (Applied Bisosystems) and analyzed using the Sequence Detection System (SDS) program (Applied Biosystems). Plotted fluorescence signals were used to determine alleles in each sample.

3.26. *APOE* genotyping

For individuals, whose apolipoprotein E (*APOE*) allele genotypes weren't provided by the brain banks, genotyping using restriction fragment length polymorphism analysis was performed as described (Ingelsson, Shin et al. 2003). In short, this method included the PCR amplification of genomic DNA using APOE forward and APOE reverse primers, followed by restriction of the

PCR product using *HhaI* enzyme. Fragmented PCR products were run in 4% agarose gels, and the *APOE* allele genotypes were determined based on the size of the fragmented products as described (Ingelsson, Shin et al. 2003).

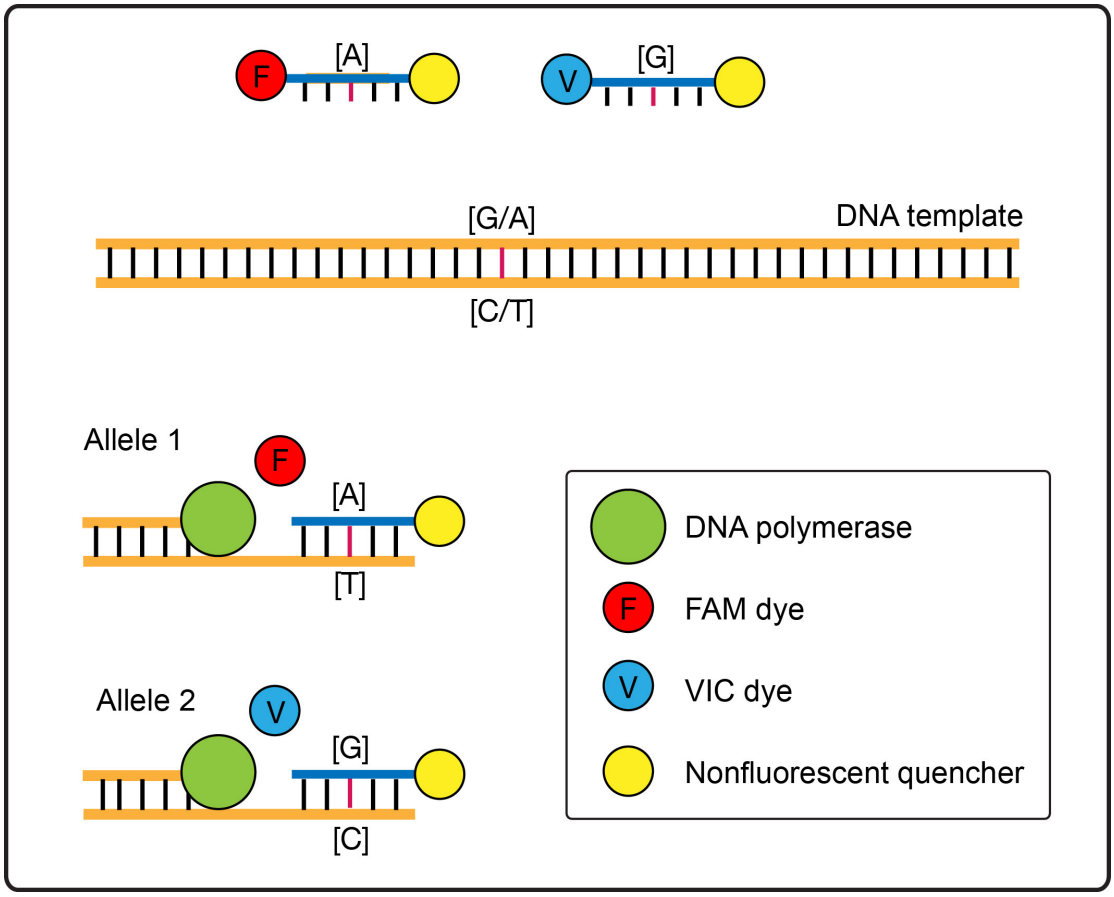

Figure 8. *SORL1* gene variants were determined using TaqMan SNP genotyping assays. TaqMan SNP genotyping assays (Applied Biosystems) employ two specific primer probes, which are fluorescently labeled with FAM or VIC dyes, to distinguish the alleles. Each probe can only bind to a single allele due to sequence specifity. When the probe hybridizes with its complimentary allele, amplification of the DNA by the DNA polymerase liberates the fluorescence tag bound to that probe. Alleles were determined according to the graph plotted based on amplification of each fluorescence signal. Increase of the FAM signal only indicated homozygosity of the allele 1 whereas increase of the VIC signal only indicated homozygosity of the allele 2. Increase of the both signal indicated heterozygosity of the allele 1 and 2. Figure is modified from TaqMan SNP genotyping assay protocol (Applied Biosystems).

3.27. Statistical analysis

Statistical analyses were performed using Prism 5.0 software (GraphPad Prism Software). Parametric tests were used to evaluate the data obtained from mouse samples or cell cultures. Student's *t*-test was used to compare differences between two groups. Linear regression analysis was performed to test correlation between two variables-measurements. Significance levels were set as $p<0.05$.

To evaluate the data obtained from human samples, nonparametric tests were employed. Mann-Whitney test was applied to compare 2 groups. Kruskal-Wallis one-way analysis of variance (ANOVA) test with a Dunn post hoc test was used to compare more than 2 groups. Since several SNPs were included in the association analyses, results were adjusted for multiple comparisons. The association tests with the SNPs were highly correlated as the SNPs displayed high linkage disequilibrium. Because of this, a permutation-based method to control the experiment-wise error rate was applied (Churchill and Doerge 1994) as multiple comparisons test.

MaCH program (Li, Willer et al. 2010) was used to estimate the haplotype distribution in *SORL1*. Haploview program (MIT/Harvard Broad Institute; www.broad.mit.edu/mpg/haploview/) was used to estimate the linkage disequilibrium (LD) between the SNPs and to plot the haplotype structures as heat map. Strength of the pairwise LD was shown as D' values ranging between 0 and 100. Logarithm of odds (LOD) score showed the significance of the linkage analyses. Standard color scheme was used to display the LD with D' and LOD scores. Accordingly, if the LOD score was equal or greater than 2, boxes were shown colored as shades of pink/red based on D' value (bright red when D'=100). If the linkage analysis was not significant (LOD<2), boxes were white (D'<100) or blue (D'=100). Pearson's $\chi 2$ test (Haploview) was applied to analyze deviation of genotype distribution from Hardy-Weinberg equilibrium.

4. Results

4.1. Identification of Alzheimer disease risk genotype that predicts efficiency of SORLA/SORL1 expression in the brain

SORLA/SORL1 is an established genetic risk factor in sporadic Alzheimer disease (AD). Initially, it was shown that patients with late-onset AD have less receptor expression in the cortex and hippocampus (Scherzer, Offe et al. 2004). A second line of evidence for a role of SORLA in AD came from genetic analyses in humans. Case-control studies showed association of several single nucleotide polymorphisms (SNPs) in *SORL1* (the gene encoding SORLA) with late-onset AD in several populations with different ethnicities (Rogaeva, Meng et al. 2007). Since SORLA expression is decreased in the patients with AD, the genetic variants may confer the disease risk by altering the receptor levels. However, direct association of genetic variants in *SORL1* with receptor expression levels was not shown previously. Thus, I wanted to correlate the individual *SORL1* genotypes with the protein concentration in the brain.

4.1.1. Sample set

Towards this aim, the sample set of brain autopsy material from 88 confirmed cases of AD was recruited from the Netherlands Brain Bank (NBB) and Medical Research Council London Brain Bank for Neurodegenerative Diseases (LBB). The samples were obtained from frontal cortex of donors who were of white ancestry. Because the samples from the brain banks displayed similar characteristics such as gender, age, and neuropathological score (Table 2), I pooled the two sample sets into a single group.

Table 2. Characteristics of sample set.

	NBB	LBB
No. of subjects	44	44
Male, %	40.9	25.0
Age at death, y, mean (SD)	79 (10)	81 (9)
Braak stage, No. of individuals		
V-VI	36	36[a]
III-IV	8	5[a]
Unknown	0	3
APOE4 allele frequency in population, %	39.8	36.0

Abbreviations: LBB, Medical Research Council London Brain Bank for Neurodegenerative Diseases; NBB, Netherlands Brain Bank

[a] The estimation of Braak stage was based on Consortium to Establish a Registry for Alzheimer's Disease criteria diagnoses.

4.1.2. Genotyping of *SORL1* SNPs in the sample set

Before starting protein expression analyses, I selected SNPs to genotype my samples sets. Thus, I screened previously published association studies to derive the genetic variants in *SORL1* associated with the late onset AD. Since the donors of the specimens were of European origin, I selected the SNPs that show association in Caucasian populations. Based on this screening, I selected 12 SNPs (Table 3). Two of these variants were exonic and others were intronic alterations distributed across the *SORL1* locus.

Table 3. *SORL1* SNPs genotyped in the study.

Marker number	SNP rs number	Alleles	Physical map location (bp)	SNP type	Risk allele	Reference study
1	rs668387	C/T	120873131	intron	C	(Rogaeva, Meng et al. 2007; Bettens, Brouwers et al. 2008)
2	rs689021	A/G	120876330	intron	G	(Rogaeva, Meng et al. 2007; Bettens, Brouwers et al. 2008)
3	rs641120	A/G	120886175	intron	G	(Rogaeva, Meng et al. 2007; Bettens, Brouwers et al. 2008)
4	rs11218313	A/G	120888081	intron	G	(Webster, Myers et al. 2008)
5	rs2276346	G/T	120919686	intron	T	(Rogaeva, Meng et al. 2007)
6	rs7131432	A/T	120932080	intron	A	(Webster, Myers et al. 2008)
7	rs2070045	G/T	120953300	S1187S	G	(Rogaeva, Meng et al. 2007; Li, Rowland et al. 2008)
8	rs1699102	C/T	1209621172	N1246N	C	(Rogaeva, Meng et al. 2007)
9	rs2282649	C/T	120984168	intron	T	(Rogaeva, Meng et al. 2007; Li, Rowland et al. 2008)
10	rs726601	C/T	120986617	intron	T	(Meng, Lee et al. 2007)
11	rs1784931	A/C	120988148	intron	C	(Meng, Lee et al. 2007)
12	rs1010159	C/T	120988611	intron	C	(Rogaeva, Meng et al. 2007)

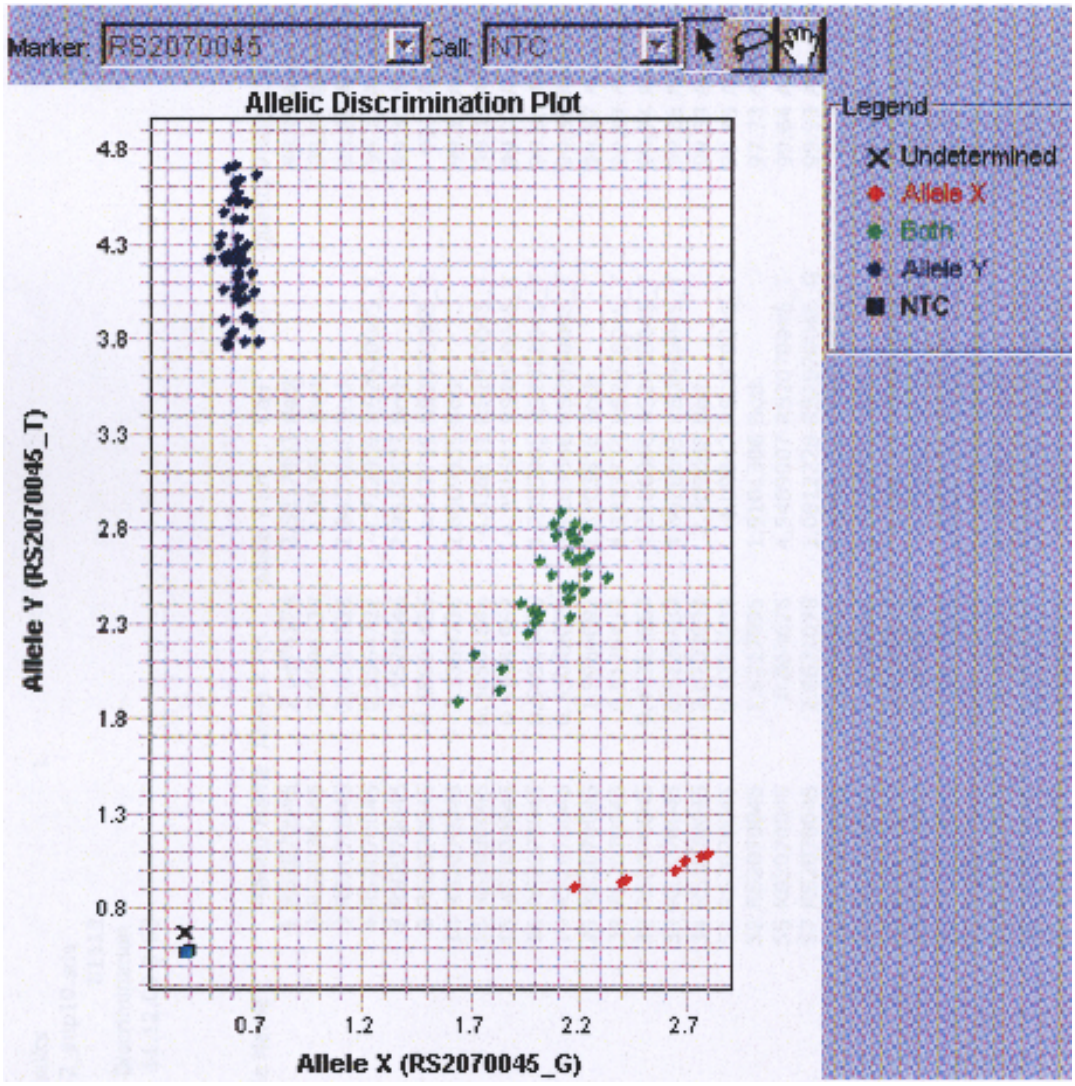

Figure 9. The graph illustrating the allele distribution of rs2070045 in the sample set. *SORL1* single nucleotide polymorphisms (SNPs) were genotyped using TaqMan SNP genotyping assays as described in Materials and Methods section (Figure 8). Alleles were determined according to the graph plotted based on amplification of the FAM or VIC fluorescent signals as exemplified here for rs2070045. Bias of the signal to the X- (red dots) or Y- (blue dots) axis showed either alleles of the SNP. Heterozygous samples (green) didn't favor any of the axes. Black dots close to zero indicate negative control reactions without any templates (NTC).

I decided to use Taq Man SNP Genotyping Assay (Applied Biosystems) to genotype the risk variants in *SORL1*. This assay was superior to the alternative method of the Big Dye Sequencing Kit (Applied Biosystems) as it provided simple and ready-to-use genotyping workflow. Taq Man SNP Genotyping Assay included optimized sequence-specific forward and reverse primers to amplify the region of interest containing the target SNP. In each assay there were also two different Taq Man probes to distinguish two alleles of the SNP. One probe labeled with VIC® (Applied Biosystems) dye was detecting one of the alleles and the other one labeled with FAM® was detecting the other allele. Allelic discrimination was based on the generated signal from each probe at the end of the polymerase chain reaction (Figures 8 & 9, please see Materials and Methods section for further details).

I isolated DNA samples from the frozen human brain specimens and genotyped the SNPs using the Taq Man SNP genotyping assays as described above (SNP genotypes of the sample set were listed in Table 6 in the Appendix section.). Before getting started with association analysis, I wanted to analyze the genotype distribution of the SNPs in the sample set to confirm the validity of the sample set and the genotyping results. I compared frequency of major and minor alleles in my sample set to the previously reported genotype data from the Human HapMap website (http://www.hapmap.org). Genotype distribution fitted the Hardy-Weinberg equilibrium, meaning that there was no significant deviation of allele frequencies in the sample set from the reported distribution data (Table 4).

Next, I analyzed the linkage disequilibrium (LD) in the genetic data using the Haploview software (Barrett, Fry et al. 2005). I found that the first 3 SNPs at the 5' end of *SORL1* were forming one haplotype block. A second block with high LD was formed by the last 6 SNPs at the 3' end of *SORL1* (Figure 10). With these results, I confirmed the high LD at the 5' and 3' end of the *SORL1* locus that was previously published (Rogaeva, Meng et al. 2007). Overall, the results showed that my genetic data were appropriate and could be used further for association with protein expression data in the sample set.

Table 4. Distribution of *SORL1* genotypes in the sample set.

SNP ID	Genotypes			HW p value
rs668387	C/C	C/T	T/T	
	0.35	0.50	0.15	0.90
rs689021	G/G	A/G	A/A	
	0.35	0.48	0.17	1.00
rs641120	G/G	A/G	A/A	
	0.35	0.50	0.15	0.90
rs11218313	A/A	A/G	G/G	
	0.83	0.16	0.01	1.00
rs2276346	G/G	G/T	T/T	
	0.41	0.45	0.14	1.00
rs7131432	T/T	A/T	A/A	
	0.99	0.01	0.00	1.00
rs2070045	T/T	G/T	G/G	
	0.50	0.43	0.07	0.80
rs1699102	T/T	C/T	C/C	
	0.38	0.49	0.14	0.96
rs2282649	C/C	C/T	T/T	
	0.45	0.43	0.11	0.97
rs726601	C/C	C/T	T/T	
	0.41	0.47	0.13	1.00
rs1784931	A/A	A/C	C/C	
	0.36	0.47	0.17	0.89
rs1010159	T/T	C/T	C/C	
	0.39	0.47	0.15	1.00

Abbreviation: HW, Hardy-Weinberg

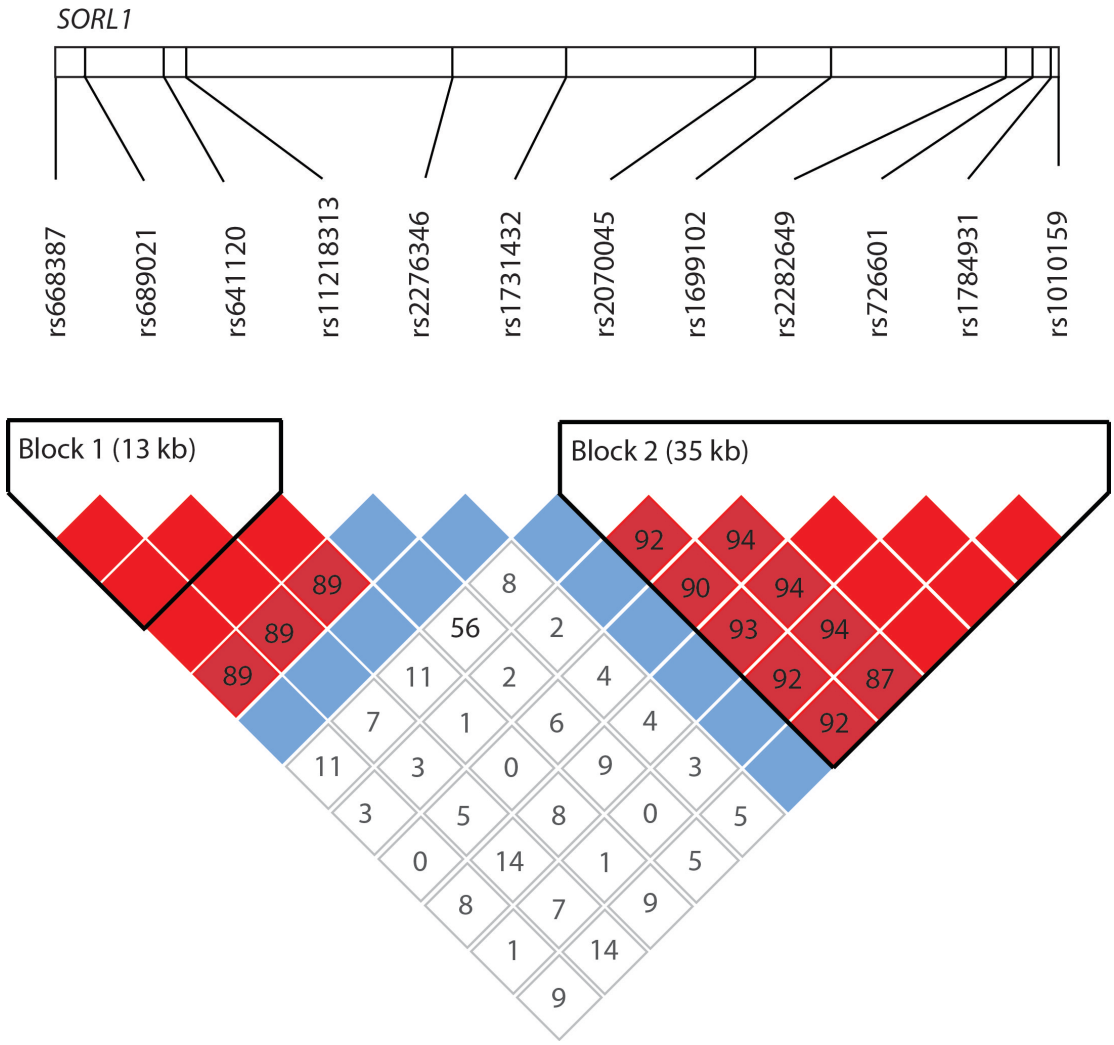

Figure 10. Genetic map of the 12 single nucleotide polymorphisms (SNPs) in the sample set. SNPs were genotyped in the sample set and the genetic data were evaluated using the Haploview program (http://www.broad.mit.edu/mpg/haploview/, Broad/MIT Institute). The SNPs at the 5' and 3' end of the *SORL1* locus showed high linkage disequilibrium (LD) and formed two haplotype blocks of 13 and 35 kb size, respectively. Haplotype structures were drawn according to the standard Haploview color scheme: LOD > 2 and D' = 1 (red), LOD < 2 and D' = 1 (blue), and LOD <2 and D' < 1 (white). LOD score is the logarithm of the odds for LD between two blocks, D' represents the degree of LD between two markers, and kb indicates kilobase.

4.1.3. Quantification of SORLA levels in human brain specimens

To measure SORLA expression in human brain specimens, I needed a highly sensitive and reproducible assay. Towards this aim, I wanted to optimize the SORLA enzyme-linked immunosorbent assay (ELISA), a sandwich ELISA developed in our lab by Dr. Vanessa Schmidt (please see Materials and Methods section for the assay protocol). Initially, I tested the reproducibility of the immuno-assay with human samples. Thus, I extracted proteins from the frozen human brain specimens and measured SORLA levels in selected samples loaded in several different plates. The measurements of the same samples gave similar results in different plates showing high inter-assay precision of ELISA (Figure 11).

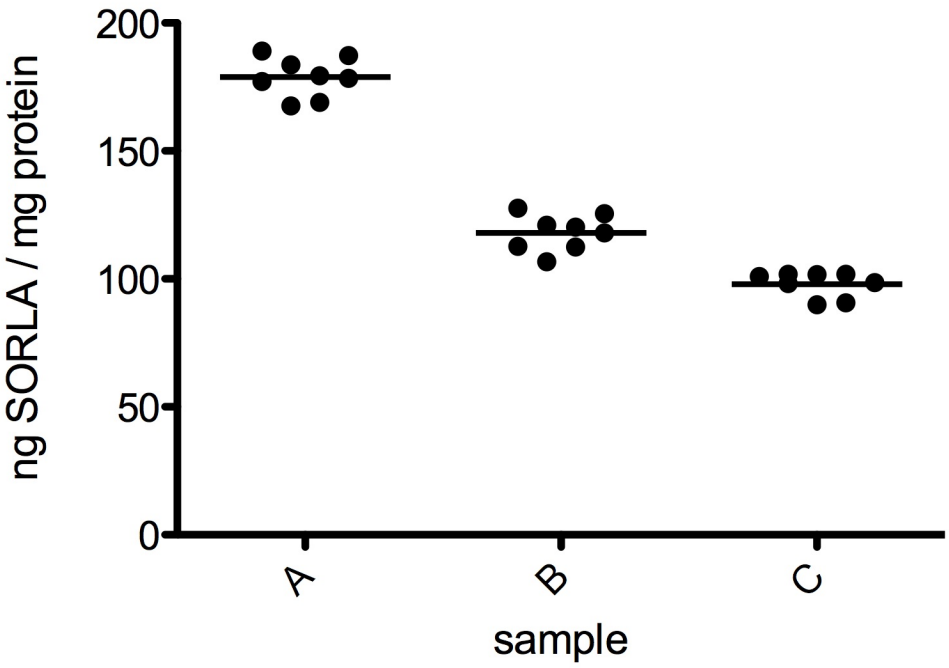

Figure 11. Inter-assay precision of the SORLA ELISA. To compare the reproducibility of measurements amongst different ELISA plates, three selected samples (A, B, C) were loaded into 8 different ELISA plates and quantified. The plotted quantifications show a highly reproducible interassay precision of the homemade immuno-assay.

Next, I wanted to check the accuracy of the ELISA measurements with semi-quantitative western blotting. To do so, I selected some samples and measured SORLA levels using these two methods. I have found that SORLA levels measured by the immuno-assay were correlating well with the band intensities shown in the western blot (Figure 12). These results showed that ELISA could be used to determine SORLA expression levels efficiently and accurately in the human samples.

A

No.	SORLA (ng/mg)
163	17.3
115	22.8
118	22.3
73	59.9
70	71.3
173	142.3
170	160.3

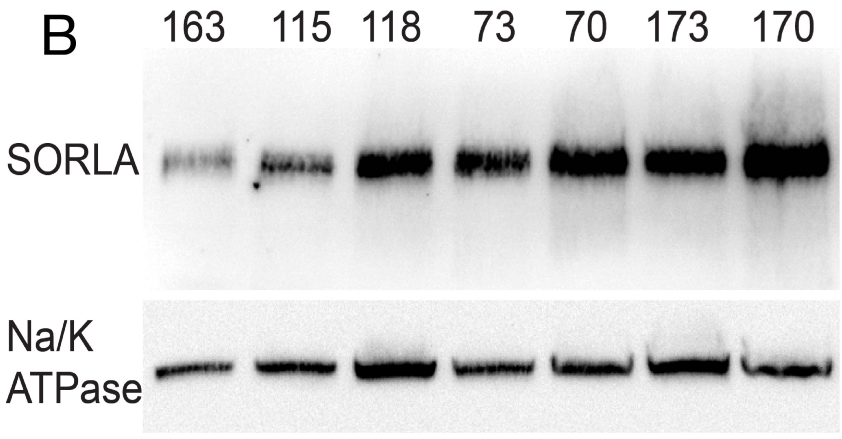

Figure 12. SORLA levels measured by ELISA correlate with results from western blots. SORLA expression levels in 7 selected samples were tested using both ELISA and western blot. The relative intensities of the SORLA immunoreactive bands in the western blot (B) paralleled the distribution of levels measured by ELISA (A). Detection of Na/K-ATPase was used as loading control in the western blot.

After validating my ELISA, I completed the quantification of SORLA levels in all 88 brain specimens (SORLA concentration of each individual in the sample set is listed in Table 7 in the Appendix section). Initially, I wanted to find out whether personal parameters, including age, gender or neuropathological score, of the donors were affecting SORLA levels in the brain. However, I failed to see any significant correlation of SORLA levels with age or gender (Figure 13A & B). Additionally, neuropathological severity (Braak stage) of the samples didn't show any effects on SORLA levels, indicating that reduction of the receptor expression is a primary (genetic cause) not a secondary consequence of neurodegeneration seen in AD (Figure 13C).

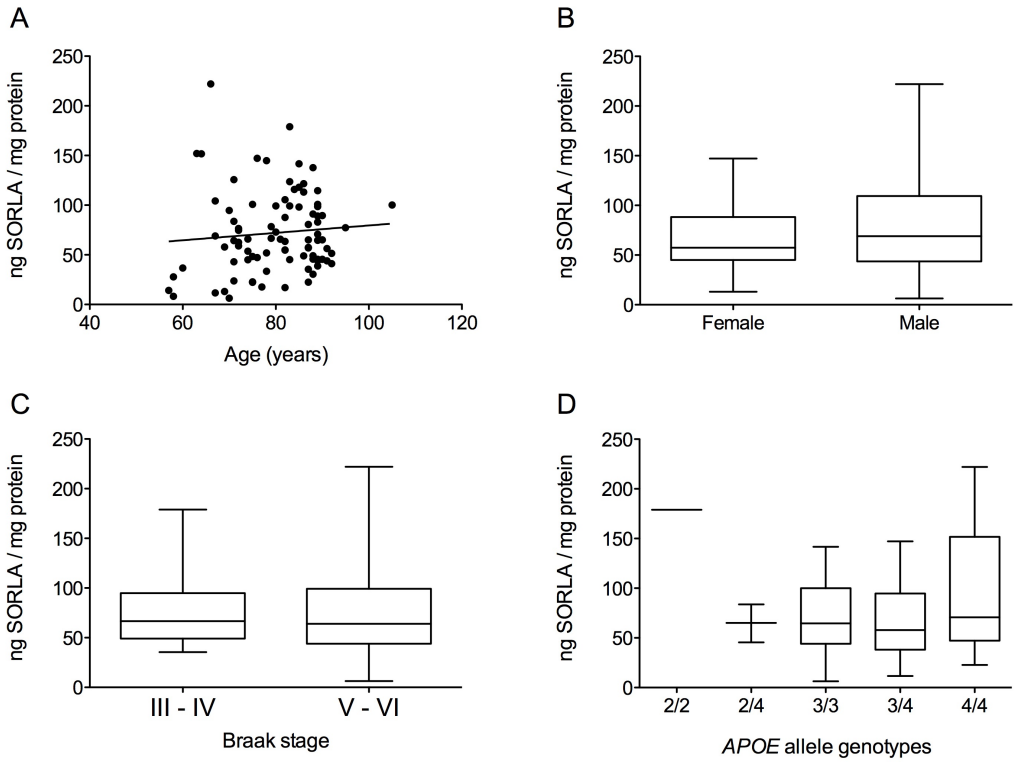

Figure 13. Age, gender, neuropathology, and APOE allele do not affect SORLA expression levels in the brain. To find out possible modifiers of protein expression in the brain, I correlated different parameters with SORLA concentrations. Age (years) (A) and gender (B) didn't have significant affects on SORLA levels. Also, the severity of the neuropathological condition measured by Braak stage (C) or being carrier of the risk variant of *APOE* (D) does not change SORLA levels.

The apolipoprotein (*APO*) *E*4 allele is the major risk factor in late-onset AD (Payami H et al. 1993 Lancet) while the *APOE2* allele is assumed to be protective (Corder EH et al. 1994 Nature Genetics). As SORLA is a receptor for APOE peptide (Jacobsen, Madsen et al. 2001), I further wanted to analyze whether *APOE* alleles were modifiers of SORLA levels. The brain banks provided the *APOE* genotype for some of the donors. For the remaining, I genotyped the *APOE* alleles using their DNA samples. Comparison of SORLA expression among different *APOE* genotype groups didn't reveal any significant changes (Figure 13D). These results showed that age, gender, Braak score and *APOE* genotype are not significant modifiers of SORLA expression in the brain and that protein expression data can be used for genetic association analysis.

4.1.4. rs2070045 and rs1699102 were associated with decreased SORLA levels in the human brain

To find effects of AD risk variants on SORLA levels, I next performed association analyses between protein concentrations and SNP genotypes in *SORL1* in all individuals of my sample set. I applied Kruskal-Wallis one-way analysis of variance test to compare SORLA levels among the homozygous carriers of minor allele or major allele, and the heterozygous individuals. With these analyses, I identified two SNPs (rs2070045 and rs1699102) that were significantly associated with SORLA levels in the patients with AD ($p=0.03$ and $p=0.01$ respectively; Figure 14A & C). SORLA concentrations in homozygous carriers of the minor (risk) alleles were significantly less compared to those in homozygous major allele carriers. These results were consistent with the previous studies showing decreased receptor expression as disease promoting (Scherzer, Offe et al. 2004; Dodson, Gearing et al. 2006; Rogaeva, Meng et al. 2007). Heterozygous individuals had intermediate SORLA levels; further supporting that these two SNPs were affecting protein expression in the human brain (Figure 14A & C).

Although age, gender and *APOE4* status didn't affect overall SORLA levels, they might have cumulative effect together with the SNPs. Indeed, when

protein concentrations were adjusted for age, gender and *APOE4* status, I found an improved correlation between the rs2070045 and rs1699102 genotypes and SORLA levels (p=0.027 and p=0.006 respectively; Figure 14B & D).

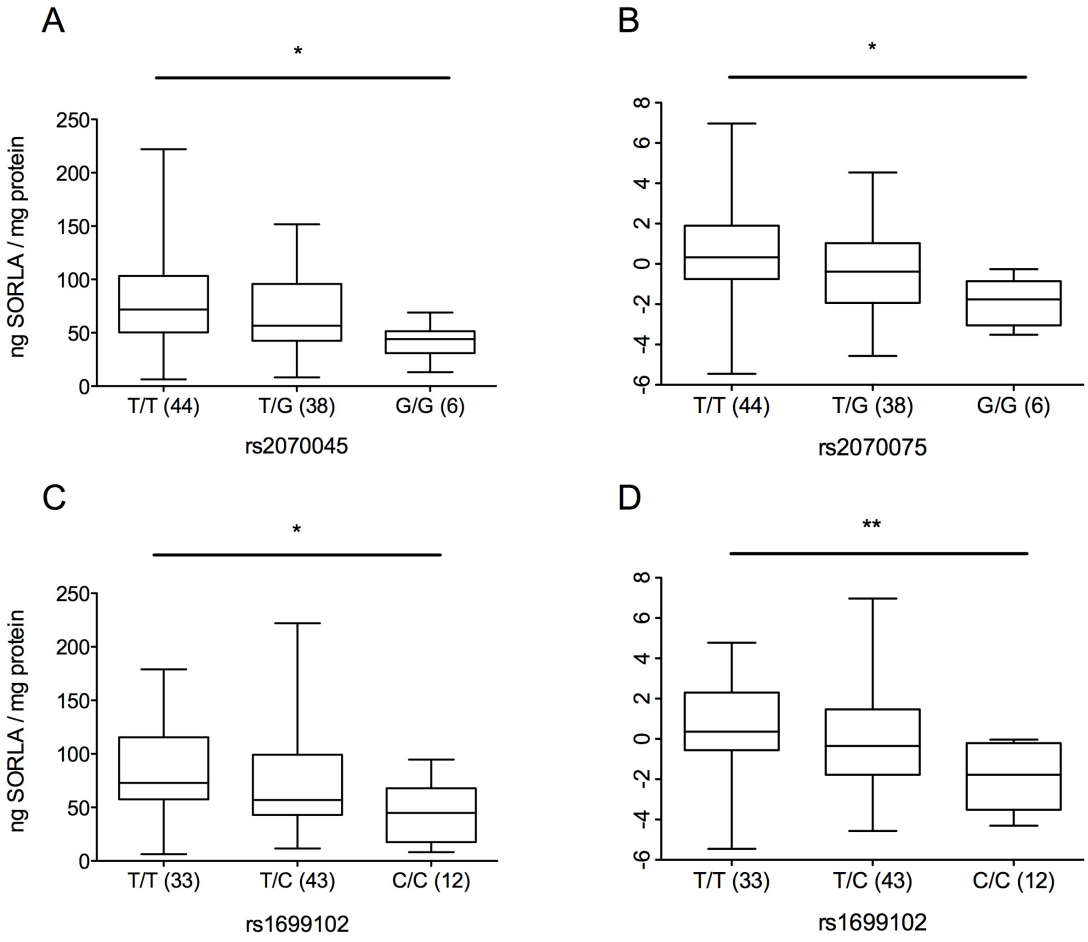

Figure 14. rs2070045 and rs1699102 are associated with SORLA expression in the brain. Statistical analyses reveal a correlation of 2 SNPs among the 12 tested with SORLA protein levels in the human brain (A & C). In line with a role of decreased receptor levels in late-onset AD development, carriers of the *SORL1* risk variants show reduced protein expression. Heterozygous carriers of the variants have intermediate levels of SORLA expression. Effects of the SNPs on the SORLA levels are even better seen when protein concentrations are adjusted for age, gender and number of *APOE*4 alleles (B & D). Expression measurements are normalized (square root transformation) in the panels B and D. The number of samples in each genotype is given in parentheses. Kruskal-Wallis test was applied to evaluate the differences among the groups (* $p<0.05$, ** $p<0.01$).

Interestingly, rs2070045 and rs1699102 cluster in a haplotype block in the 3' region of *SORL1* (Block 2 in Figure 10). The SNPs in that block are in high linkage disequilibrium (D' value is 90-94%; Figure 10) although they aren't completely linked (in this case D' value would be 100%). Consistent with this notion, the SNPs in the 3' haplotype block other than rs2070045 and rs1699102 seemed to affect protein levels as well but only with a tendency not reaching the significance level (Figure 15G, H, I & J). The remaining SNPs in the 5' region of *SORL1* didn't show association with SORLA levels probably because of high genetic heterogeneity associated with *SORL1* variants in different populations (Figure 15A, B & C). Since testing various SNPs increased the probability of detecting effects on phenotype, all analyses were next adjusted for multiple comparisons. Significant association of rs1699102 with SORLA levels (p= 0.02) was confirmed and a trend for association of rs2070045 (p= 0.10) was found in multiple comparison test (please see Materials and Methods section for details of the statistical analyses).

Haplotype blocks can also affect protein expression as they display cumulative effects of selected SNPs as well as unidentified SNPs in that region. Because of this, I wanted to evaluate the association of SNP haplotypes with SORLA levels. Similar to single SNP analysis, 3' haploytpe block (block 2) consisting of minor variants of SNPs (GCTTCC; frequency 26.5%) was associated with lower SORLA expression (p=0.04) whereas the major 3' haplotype (TTCCAT; frequency 58.7%) was correlated with higher protein expression (p=0.049) (Table 5). In contrast, the 5' haplotype block (block 1) didn't have any effects on protein levels similar to the previous results obtained with the single SNPs in that region. Taken together, these results showed that SORLA protein levels in the human brain were influenced by two single SNPs, rs2070045 and rs1699102, as well as by the 3' haplotype encompassing these 2 variants.

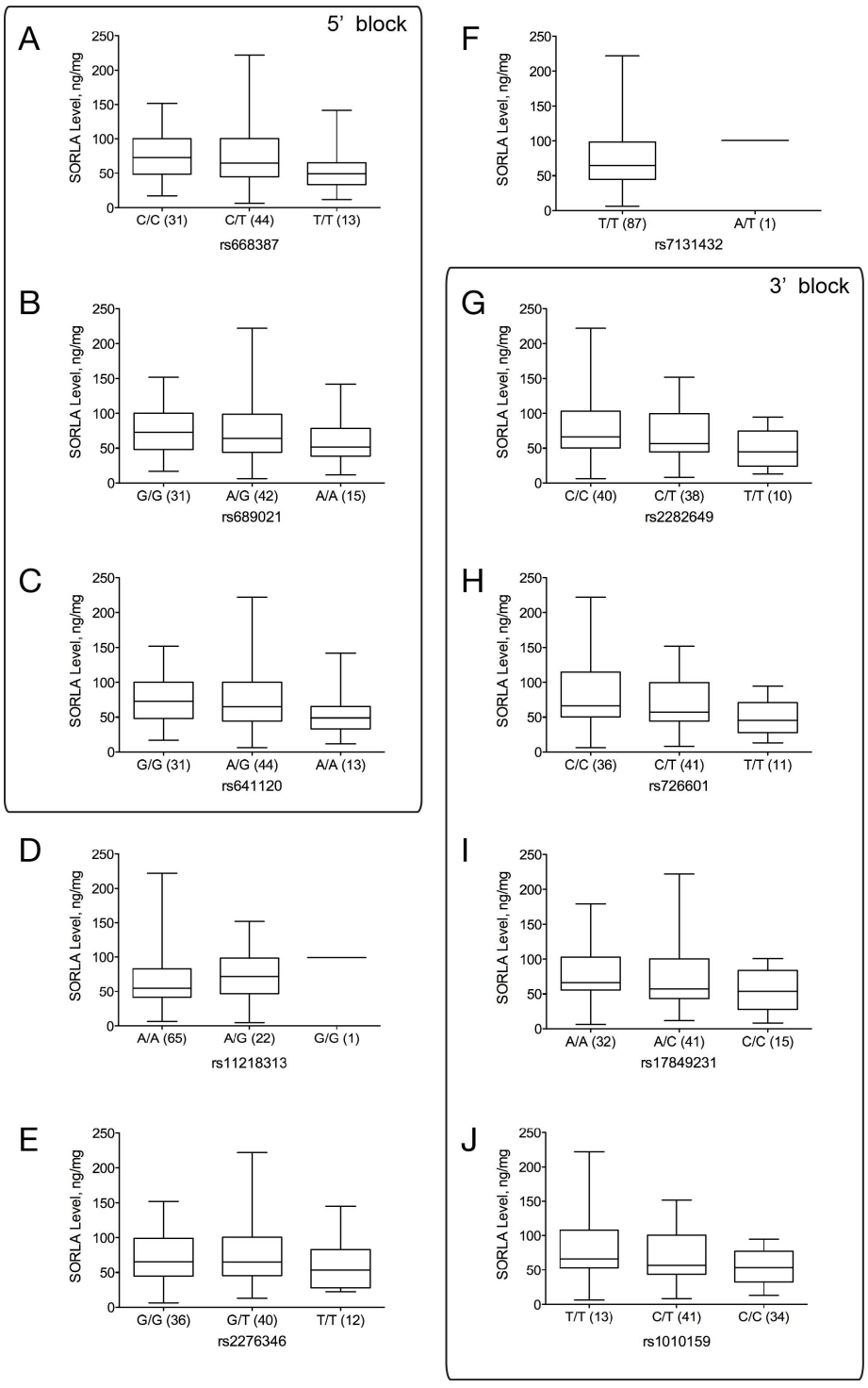

Figure 15. Additional tested SNPs do not show a significant association with SORLA levels. Statistical analyses reveal a trend for association of SNPs in 3' haplotype block with SORLA expression (G, H, I & J), however this does not reach significance level at p=0.05. The remanining SNPs do not show any effects on receptor expression. The number of samples in each genotype is given in parantheses. Kruskal-Wallis test was applied to evaluate the differences among the groups.

Table 5. Correlation of *SORL1* haplotypes with receptor expression.

	No. (%)	p value
Haplotype block 1 (5' block)		
CGG	114 (58.2)	0.42
TAA	80 (40.8)	0.13
CAG	2 (1.0)	0.06
Haplotype block 2 (3' block)		
TTCCAT	115 (58.7)	0.049
GCTTCC	52 (26.5)	0.04
All others	(<5)	>0.05

4.1.5. rs2070045 and rs1699102 have no effects on *SORL1* mRNA expression in the human brain

Interestingly, rs2070045 and rs1699102 were the only exonic variants among the 12 SNPs tested. As these sequence variations represent silent mutations, they are changing the mRNA sequence without affecting the polypeptide sequence. Rs2070045 is a TCT to TCG variant coding for amino acid serine and rs12699102 converts AAT to AAC coding for asparagine. Since changes in the codon sequences may have the potential to affect rate of gene transcription or mRNA stability, I wanted to know whether rs2070045 and rs1699102 were changing transcription levels and thereby control protein expression. Therefore, I extracted total RNA from selected samples that were homozygous for the major rs2070045 and rs1699102 (T/T, T/T) or that carry minor risk (G/G, C/C) genotypes. Since the RNA samples were prepared from post-mortem specimens, I needed to check for integrity of the samples. As measured by the Bioanalyzer platform (Agilent Technologies), the RNA integrity values were comparable in major (mean (SD), 5.54 ± 0.26) and minor genotype carriers (5.45 ± 0.52). To measure the RNA expression levels of *SORL1*, I used the TaqMan gene expression assays (Applied Biosystems), as they constituted validated assays for quantitative reverse-transcriptase-polymerase chain amplification of cDNA in a dye (FAM)-based assay. I quantified mRNA transcript levels of *SORL1* using TaqMan assays and

normalized the values to the expression of the selected normalization gene, β2-microglobulin (β2M) (Carlo, Gustafsen et al. 2013). There was no significant difference in *SORL1* transcript levels in minor variant carriers compared to samples homozygous for major variants (Figure 16). These results demonstrated that the risk variants rs2070045 and rs1699102 are associated with protein expression levels without affecting mRNA levels of *SORL1*.

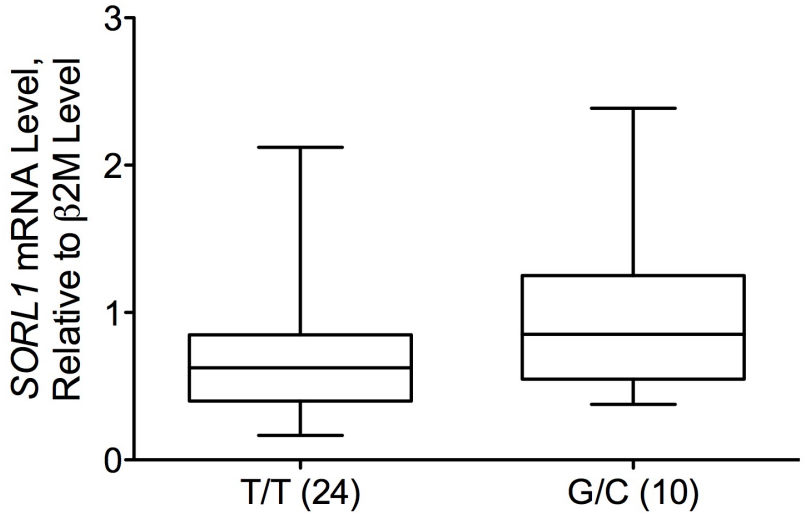

Figure 16. mRNA levels of *SORL1* are not affected by the risk variants of rs2070045 and rs1699102. Total RNA samples were extracted from 24 specimens carrying the major (T/T) and 10 specimens carrying the minor (G/C) variants of indicated SNPs. Transcript levels of *SORL1* were determined using quantitative reverse transcriptase-polymerase chain reaction and normalized to the levels of the internal control gene, β2-microglobulin (β2M). Analyses of RNA expression levels do not show any differences between carriers of minor and major variants. RNA integrity values of the samples were also similar (mean (SD) 5.54 ± 0.26) in major and in minor genotype carriers (5.45 ± 0.52) as determined using the Bioanalyzer platform. Mann-Whitney test was used to evaluate the differences among the groups.

4.1.6. Risk haplotype composed of rs2070045 and rs1699102 decreased translation efficiency of SORLA in CHO cells

Since rs2070045 and rs1699102 weren't affecting transcription efficiency of *SORL1*, I wanted to investigate alternative effects of the SNPs on protein expression levels. For this aim, I intended to use a cell culture system. Accordingly, I generated expression constructs encoding the SORLA cDNA carrying either the major haplotype of rs2070045 and rs1699102 (T/T, T/T) or the minor risk variants (G/G, C/C). I used the pcDNA-SORLA construct (Schmidt, Sporbert et al. 2007) as the control vector that expresses major genotypes ($SORLA^{major}$). I converted major variants into minor genotypes by a PCR-based mutagenesis approach using mutant primers. Then, I replaced the wild-type sequence in $SORLA^{major}$ with the mutant PCR products using a standard cloning approach to generate $SORLA^{minor}$ (Figure 17). For the cell culture experiments, I used Chinese hamster ovary (CHO) cells, as they were easy to transfect with 20-30% transfection efficiency. To control for transfection efficiency in each experiment, I also measured mRNA levels of the zeocin resistance cassette included in both vectors (Figure 17).

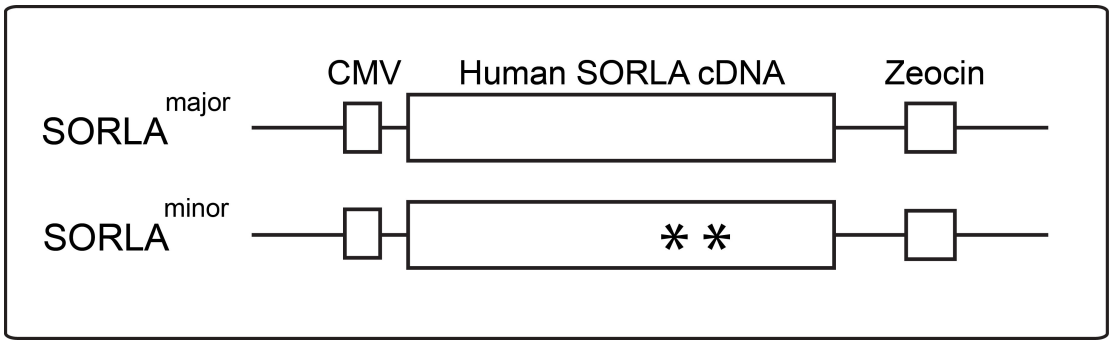

Figure 17. Map of the SORLA cDNAs carrying rs2070045 and rs1699102 variants. The SNPs were inserted into wild-type human SORLA cDNA sequence in the pcDNA vector ($SORLA^{major}$) using PCR-based mutagenesis to generate the $SORLA^{minor}$ cDNA. Both cDNAs were expressed under control of cytomegalovirus (CMV) promoter. The zeocin resistance gene encoded in the vector backbone was used to determine the transfection efficiency. Asterisks denote the locations of the minor variants of rs2070045 and rs1699102 in the cDNA sequence.

I transfected cells with the constructs using Lipofectamine (Life Technologies). After 2 days, I harvested the cells and isolated protein and RNA samples. To test SORLA expression in the transfected cells, initially I performed western blot experiments. I found that cells expressing SORLA^{minor} had less SORLA compared to the cells transfected with SORLA^{major} (Figure 18). This result was consistent with the results obtained in human brain specimens.

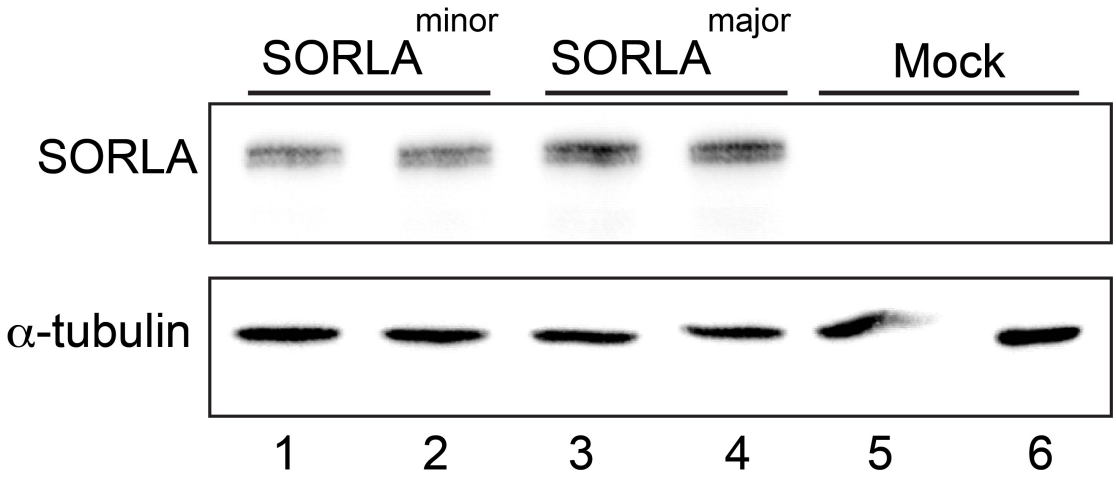

Figure 18. SORLA levels are decreased in SORLA^{minor} expressing Chinese hamster ovary (CHO) cells. Confluent CHO cells were transfected with SORLA cDNAs carrying the major or minor variants of rs2070045 and rs1699102. Two days later, the cells were harvested and used for protein extraction. Western blot experiments show decreased SORLA expression in cells transfected with the SORLA cDNA carrying the minor alleles. Mock transfected cells lack SORLA expression. α-tubulin was used as loading control.

Next, I checked the transfection efficiency by comparing the expression of the zeocin resistance cassette in the vector backbone. I did quantitative reverse transcriptase-polymerase chain reaction (RT-PCR) to determine RNA levels and normalized them to the RNA levels of the internal control 18S ribosomal (r) RNA. The transfection efficiencies were comparable among the replicate cell layers expressing SORLA^{minor} or SORLA^{major} (Figure 19A). I also

measured the *SORL1* transcript levels and didn't find any differences between the two genotypes (Figure 19B). Finally, I performed an ELISA to measure SORLA concentrations. Similar to my western blot results, I found that the SORLA protein levels were decreased approximately 30% in cells expressing SORLA^{minor} compared to cells with SORLA^{major} cDNA (Figure 19C). These results indicated that rs2070045 and rs1699102 were affecting SORLA protein concentration without modulating RNA expression.

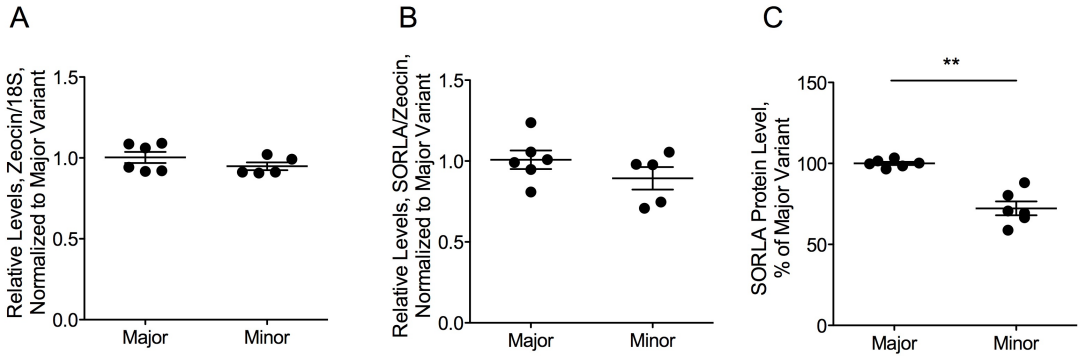

Figure 19. rs2070045 and rs1699102 modulate protein expression without affecting transcription levels. CHO cells were transfected with SORLA^{major} and SORLA^{minor} constructs. Two days later, the cells were lysed and used to isolate protein and RNA. To determine transfection efficiency expression of zeocin resistance cassette was determined using quantitative reverse-transcriptase polymerase chain reaction (qRT-PCR). Transcript levels of SORLA were also determined using qRT-PCR. 18S ribosomal (r) RNA expression was measured to normalize gene expression levels. (A) Transfection efficiency and (B) SORLA transcription levels in cells expressing SORLA^{minor} minigene are similar compared to the cells with SORLA^{major}. (C) SORLA protein concentration as quantified by ELISA is decreased in cells transfected with SORLA carrying minor genotype. Mann-Whitney test was used to evaluate the differences among the groups (** $p<0.01$).

4.2. Novel role for SORLA as clearance receptor for amyloid-β peptide

In the above project, I identified genetic mechanisms regulating SORLA expression in the brain. Additionally, above data supported decreased SORLA levels as a causative factor in AD development. Next, I wanted to test whether alterations in SORLA expression are in fact linked to disease development. Our group along with other labs already showed that SORLA-deficient mice (*Sorl1*$^{-/-}$) display elevated processing of APP along with accumulation of more amyloid (A)-β and plaques in the brain (Andersen, Reiche et al. 2005; Offe, Dodson et al. 2006). But effects of SORLA overexpression *in vivo* weren't tested before. Thus, I wanted to investigate whether increasing the receptor levels may reduce amyloidogenic processing in the brain and be protective.

4.2.1. Generation of SORLA overexpressing mice

To understand the effects of SORLA overexpression *in vivo*, I wanted to generate a transgenic mouse model overexpressing the receptor. Since the murine *Rosa26* locus was already shown to have high targeting efficiency and there is no documented defect in mice due to targeting of that locus (Soriano 1999), I decided to insert the human SORLA cDNA into the murine *Rosa26* locus (Figure 6). To achieve robust overexpression of SORLA, I decided to express the receptor under control of CAG enhancer (cytomegalovirus enhancer with chicken β-actin promoter). To construct the targeting vector, I took advantage of the Gateway technology (Life Technologies, please see Materials & Methods for details). I inserted the human SORLA cDNA into the targeting vector encompassing 5'- and 3'-*Rosa26* sequence for homologous recombination with murine *Rosa26* locus. Additionally, the vector included the neomycin phosphotransferase gene driven by the mouse phosphoglycerate kinase 1 (PGK1) promoter between the SORLA cDNA and CAG enhancer to select targeted embryonic stem (ES) cells with antibiotics G418 (Life Technologies). In addition, the neo resistance expression cassette (neo-R) and poly-A tail inserted in front of the SORLA cDNA served as a transcription stop site. To generate a transgenic mouse

strain that can be inducible with Cre recombinase, the neo-R and poly-A sequences were flanked with loxP sites (Figure 6).

As mutations may be introduced during the various cloning steps, I sequenced the final targeting construct to show the absence of any mutations in the SORLA encoding sequence and the presence of the loxP sites.

Prior to targeting of ES cells (please see Materials and Methods for details), I linearized 35 ug of the vector with *Alo*I. I used ES cells collected from 1x10 cm plate (approximately $1x10^7$ cells) to electroporate with the linearized targeting vector and distributed the cells on 5x10 cm plates pre-coated with gelatin and mouse fibroblasts (feeder cells). After culturing the cells for 7 days in ES cell medium with G418 to select for targeted cells, I picked 96 antibiotic-resistant ES cell clones and delivered each clone to a well in 96-well plates pre-coated with gelatin and feeder cells. 5 days later, the cells were split into 4 replicate 96-well plates. Three of the plates, which were reserved for further expansion and injection, were frozen. The cells in the remaining plate were used to isolate genomic DNA for genotyping.

To identify the ES cell clones for blastocyst injections, I needed to identify those cells that contained the targeting vector in the proper localization in the *Rosa26* locus. I decided to genotype the cells with Southern blot and isolated DNA of ES cells in one 96-well plate. Fifty ES cell clones out of 96 yielded enough amount of DNA for Southern blotting and screened further. Ten ug of DNA was digested with restriction enzyme *Hind*III. The fragmented DNA samples were electrophoresed in agarose gels and blotted onto membranes. To screen the clones, I used a ^{32}P labeled 1.5 kb length DNA fragment as a probe, which hybridizes with the 5' region of the *Rosa26* locus outside the genomic region included in the targeting vector (Figure 6). I identified 2 ES cell clones, which were positive for targeted insertion, among the 50 tested. This result showed an average of 4% recombination efficiency for targeting of the *Rosa26* locus. Before proceeding with the blastocyst injection step, I needed to expand the clones and confirm the Southern blot results to ensure

that the correct clones are being processed. For this aim, I thawed one of the three remaining 96-well plates and seeded the selected ES cell clones to 24-well plate. To expand the cells, I cultured them for 6-7 days and split them into three aliquots of 2 ml each. Two of them were frozen at -80°C. The ES cells in the third vial was expanded and used to isolate DNA for Southern blotting. With the DNA from these replicate cells, I confirmed the proper insertion of the targeting vector into the murine *Rosa26* locus (Figure 20).

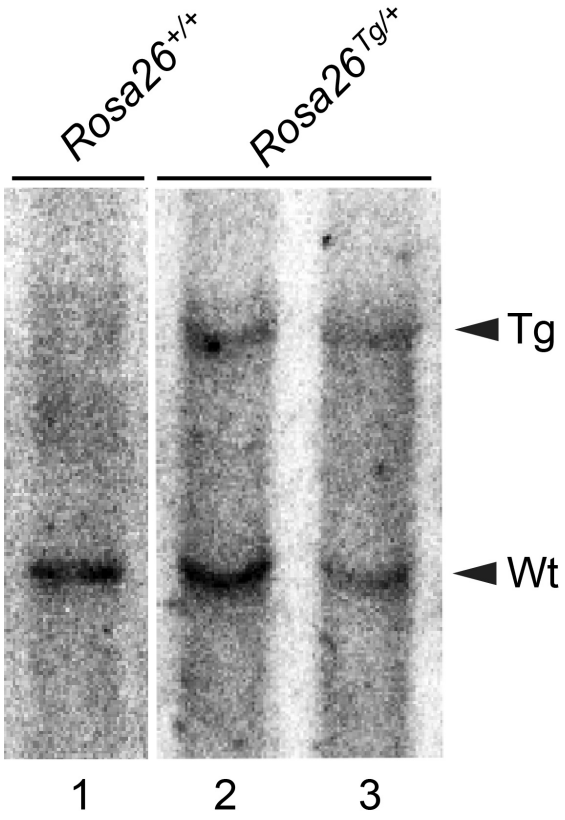

Figure 20. Insertion of the targeting vector into the *Rosa26* locus in ES cells as shown by Southern blot analysis. To genotype embryonic stem (ES) cells derived from the gene targeting experiment, genomic DNA was extracted from G418-resistant ES cell clones and fragmented with *HindIII* enzyme. The digested samples were run in agarose gels and blotted onto Hybond membranes. A radiolabeled (^{32}P) external probe of 1.5 kb length was used to screen the clones. Transgenic cells (*Rosa26*$^{Tg/+}$) display two bands in Southern blot. The wild-type *Rosa26* allele (Wt) is represented by a 4.4 kb band whereas the 7.4 kb band identifies the insertion of the targeting vector (Tg) (please see Figure 6 for the locus map). DNA from wild-type ES cells (*Rosa26*$^{+/+}$) that were used as negative control displayed only the band corresponding to the Wt allele (lane 1).

I picked one of the ES cell clones to be injected into C57BL/6 blastocysts. The blastocysts were implanted into the uterus of pseudo-pregnant foster mothers to obtain chimeras. Dr. Ernst-Martin Fuechtbauer and Dr. Annette Fuechtbauer performed these experiments targeted according to the standard protocols at the University of Arhus in Denmark. Injected ES cell lines were initially derived from 129SvEmcTer blastocysts, and they were injected back into C57BL/6 blastocyst. The pups are called chimeric as they consist of tissues deriving from both the injected ES cell and the host blastocyst. Contribution of injected ES cells to organs and tissues can be predicted based on the color of the fur of the pups. 129 mouse substrains are agouti colored and C57BL/6 mice are black. So, chimeric mice were further bred with C57BL/6 mice for germline transmission of the targeted ES cell genome. Agouti-colored pups were indicative of germline transmission of the injected ES cell clones. These mice were imported to establish the new mouse strain at the MDC.

To make genotyping procedure of mice simpler and more efficient, I also optimized a PCR-based method (Figure 7). To do so, I selected one common primer which binds to the 5' of *Rosa26* homology region, so can amplify both wild type and targeted allele. I provided specificity for the targeted allele by designing a second primer binding to the CAG promoter. An additional primer binding to *Rosa26* locus was designed to amplify wild type *Rosa26* locus (Figure 7).

At this point, in the mice having the targeted *Rosa26* locus, expression from the CAG promoter was terminated by the transcription stop element localized before SORLA cDNA (Figure 6). To remove the neomycin resistance cassette and to induce SORLA expression under control of CAG promoter, I needed to cross my mouse line with a rodent strain expressing Cre recombinase. Expression of the Cre enzyme can be induced in different tissues depending on the promoter used to derive transcription of the recombinase gene. However, many available Cre lines to derive brain-specific expression of the target protein had several limitations. For example, some of them showed an

incomplete pattern of Cre activity in the brain. Also, to study APP processing in mice, I was planning to cross my mouse strain with a rodent model of AD. This AD mouse model, called PDAPP (Games, Adams et al. 1995) expresses platelet-derived growth factor (PDGF)-β promoter driven human APP gene with V717F familial AD mutation. So, I needed to overexpress SORLA in the neurons where the endogenous murine receptor and transgenic human APP are also expressed. Based on all these reasons, I decided to use a ubiquitously active general Cre deleter line (C57BL/6-*Gt(ROSA)26Sor*$^{tm16(Cre)Arte}$ from Taconic). I bred the mice heterozygous for the targeted allele with mice carrying a single copy of the Cre recombinase transgene derived from the *Rosa26* locus (Otto, Fuchs et al. 2009).

To test whether the recombination was successful, first I wanted to eliminate the Cre recombinase transgene. For this aim, I next bred the mice heterozygous for the recombined allele (*Rosa26*$^{Tg/+}$; Cre$^{+/-}$) with C57BL/6 mice. As a result I obtained mice heterozygous (*Rosa26*$^{Tg/+}$) or null (*Rosa26*$^{+/+}$) for the SORLA transgene and lacking Cre recombinase gene. Homozygous SORLA overexpressing animals (*Rosa26*$^{Tg/Tg}$) were obtained by intercrossing *Rosa26*$^{Tg/+}$ mice. To see the efficiency of recombination, I took tail biopsies from the *Rosa26*$^{+/+}$, *Rosa26*$^{Tg/+}$, and *Rosa26*$^{Tg/Tg}$ mice, and did Southern blot to show Cre-induced recombination of the targeted allele in *Rosa26* locus (Figure 21).

Next, I showed presence of the targeted allele in *Rosa26*$^{Tg/+}$ and *Rosa26*$^{Tg/Tg}$ mice with the PCR-based genotyping (Figure 21B). Additionally, I optimized another PCR to determine the targeted allele, which is recombined. To do so, I designed two primers binding either side of the sequence flanked by the loxP sites (Figure 7). When recombination occurs, and the neomycin resistance cassette (neo-R) and poly-A tail were removed, the PCR product amplified from the locus was used to distinguish the recombined allele (Figure 21C).

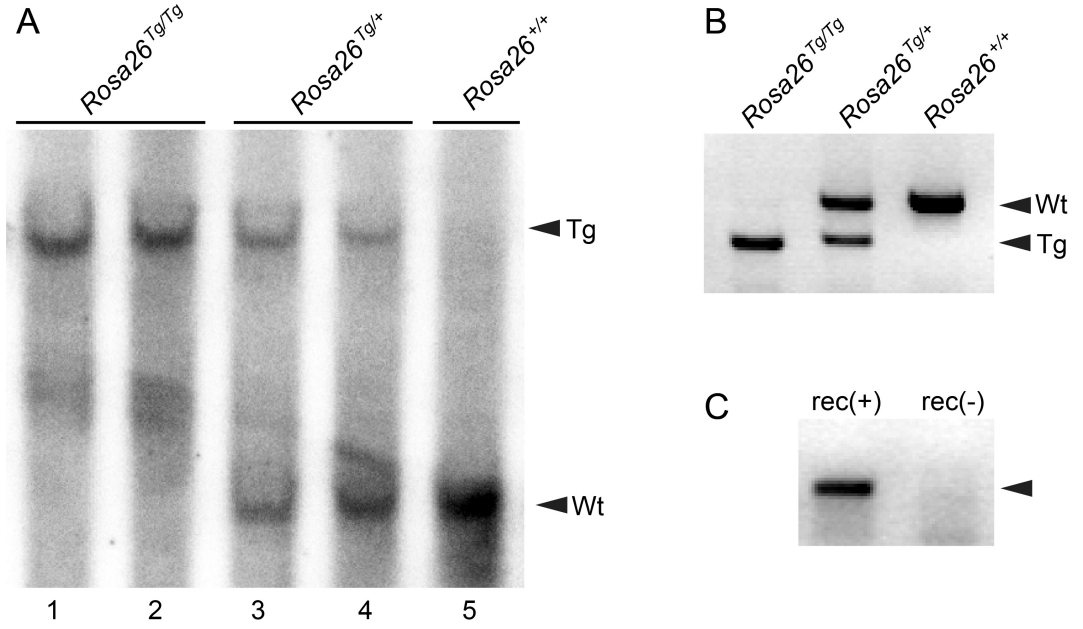

Figure 21. Genotyping of mice by Southern blot and PCR. To remove the neo-R and poly-A encoding sequences and induce SORLA expression in the murine genome, mice were bred with the Cre deleter strain of mice (Taconic). (A) Offspring were genotyped by Southern blot to confirm Cre-mediated recombination in the *Rosa26* locus. *Rosa26*$^{+/+}$ mice (lane 5) display only one band of 4.4 kb for wild-type allele whereas heterozygous *Rosa26*$^{Tg/+}$ mice (lanes 3 & 4) show two bands at 4.4 kb and 8.3 kb for the wild-type (Wt) and the recombined (Tg) alleles, respectively. Mice that are homozygous for the recombined allele (*Rosa26*$^{Tg/Tg}$) are identified by single band at 8.3 kb (lanes 1 & 2). (B & C) For faster genotyping of mice, polymerase chain reaction (PCR) was designed with allele-specific primers (please see Figure 7 for primer binding sites). DNA was isolated from the tail or ear clips. (B) One common forward primer and two different reverse primers were used to distinguish between the Wt and Tg alleles. Accordingly, the primer binding to the CAG enhancer in the transgene generates a PCR product of 410 bp size and the Wt allele specific primer amplifies a product of 602 bp size. (C) Cre-mediated recombination of the *Rosa26* locus can be detected with a primer pair binding to CAG enhancer and SORLA cDNA (Figure 7). Removal of the sequence between the loxP sites generates a PCR product of 260 bp length. Lack of recombination yields no PCR amplification in the region because of the poly-A tail and product size that is too long to be amplified.

4.2.2. SORLA expression in the brain of *Rosa26*$^{+/+}$, *Rosa26*$^{Tg/+}$ and *Rosa26*$^{Tg/Tg}$ mice

I started analysis of the new mouse model by determining expression of SORLA in the brain. I dissected cortex, hippocampus and cerebellum of the mice and extracted membrane proteins from these tissues. For western blotting, I used an antibody that recognizes both the endogenous murine receptor as well as the human protein derived from the *Rosa26* insertion. As seen in figure 22, SORLA immunoreactivity was lowest in *Rosa26*$^{+/+}$ mice and increased gradually in *Rosa26*$^{Tg/+}$ and *Rosa26*$^{Tg/Tg}$ mice. This effect was seen in all three brain regions analyzed (Figure 22). Additionally, to quantify concentrations of SORLA levels, I analyzed protein extracts by SORLA ELISA. *Rosa26*$^{Tg/+}$ mice showed a 4-5-fold increase in the receptor expression in the cortex and hippocampus compared to wild-type *Rosa26*$^{+/+}$ mice (Figure 23). I also analyzed SORLA deficient mice (*Sorl1*$^{-/-}$) to show specifity of the immunoassay. As expected, there was no SORLA detected in *Sorl1*$^{-/-}$ mice (Figure 23). These results showed that *Rosa26*$^{Tg/+}$ and *Rosa26*$^{Tg/Tg}$ mice overexpress SORLA successfully in the brain.

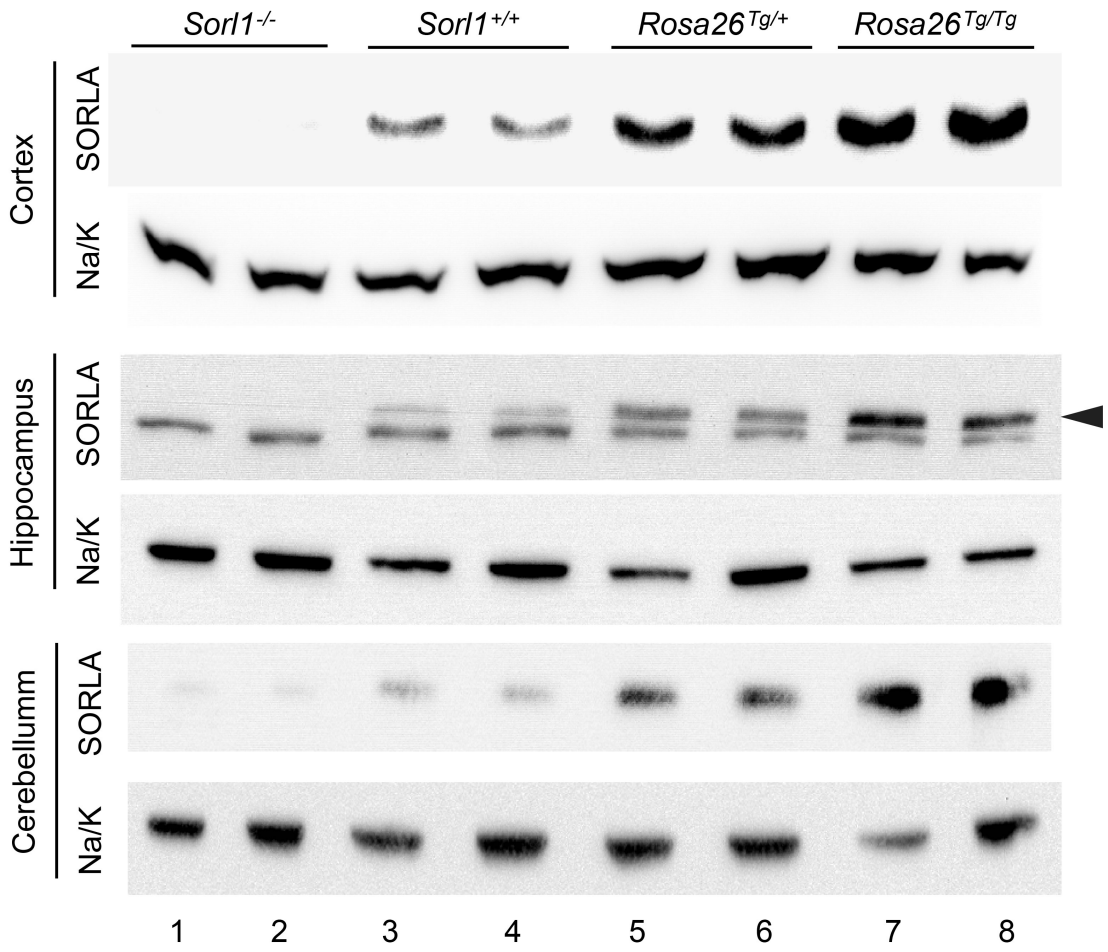

Figure 22. Expression of SORLA is elevated in the brain of *Rosa26*$^{Tg/+}$ and *Rosa26*$^{Tg/Tg}$ mice. Proteins were extracted from cortex, hippocampus and cerebellum of the 8 weeks-old mice of the indicated genotypes and analyzed by western blotting. Gene dosage-dependent overexpression of SORLA is seen comparing *Rosa26*$^{Tg/+}$ (lanes 5 & 6) and *Rosa26*$^{Tg/Tg}$ (lanes 7 & 8) animals with *Rosa26*$^{+/+}$ mice (lane 3 & 4) that expressing the endogenous receptor only. SORLA-deficent mice (*Sorl1*$^{-/-}$) mice (lanes 1 & 2) were used as negative control for specificity of the antibody. Two bands were seen in western blot analyses of the hippocampal extracts. The arrowhead indicates the immunoreactive band representing SORLA band. The lower band represents an unspecific signal also seen in *Sorl1*$^{-/-}$ animals (lanes 1 & 2). Na/K ATPase (Na/K) levels were detected as loading control.

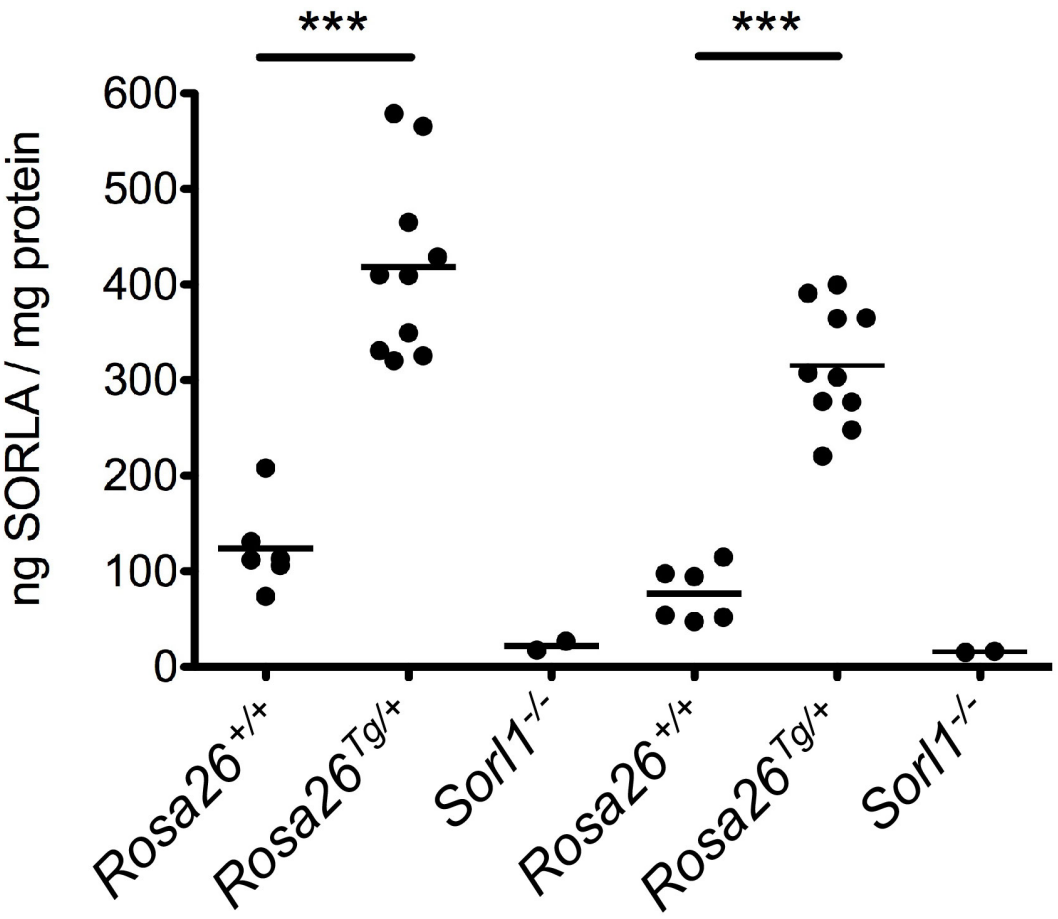

Figure 23. Overexpression of SORLA in cortex and hippocampus of *Rosa26*$^{Tg/+}$ mice as quantified by ELISA. SORLA concentrations were measured in protein extracts from the cortex and hippocampus of 8 weeks-old mice using ELISA. *Rosa26*$^{Tg/+}$ mice (n=10) had 4-5-fold more expression of the receptor in cortex and hippocampus compared to *Rosa26*$^{+/+}$ mice (n=6). *Sorl1*$^{-/-}$ mice (n=2) were used as negative control to document specifity of the ELISA. Each group included both genders and mean of duplicate measurements were shown. Student's *t*-test was applied to evaluate the differences between two genotypes (*** $p<0.001$).

4.2.3. Neuronal expression of SORLA in the brain of transgenic mice

To analyze the impact of SORLA overexpression on APP processing, it is important to have elevated receptor expression in neurons where APP is also expressed. Therefore, I wanted to determine the cell types expressing human SORLA in the brain of *Rosa26*$^{Tg/+}$ mice. To distinguish human SORLA from the murine receptor that is also expressed in *Rosa26*$^{Tg/+}$ animals, I needed to eliminate the murine receptor gene. To do so, I crossed the *Rosa26*$^{Tg/+}$ animals with mice with targeted disruption of the murine *Sorl1* gene (*Sorl1*$^{-/-}$). I prepared free-floating brain sections of adult (*Rosa26*$^{Tg/+}$; *Sorl1*$^{-/-}$), *Rosa26*$^{+/+}$ (equal *Sorl1*$^{+/+}$), and *Sorl1*$^{-/-}$ mice and stained for SORLA, neuronal marker (neuronal nuclei, NeuN), and astrocyte marker (glial fibrillary acidic protein, GFAP). Immunofluorescence stainings demonstrated localization of human SORLA in the same cell type as the murine receptor (Figure 24). In the cortex and hippocampus, SORLA was expressed in neurons as shown by colocalization with NeuN, but not expressed in GFAP positive astrocytes (Figure 24). In the cerebellum, both endogenous murine and human SORLA were expressed in Purkinje cells (Figure 24). These data showed that SORLA is overexpressed in the neurons of cortex and hippocampus along with endogenous murine receptor. Therefore, I could use this model to investigate the impact of SORLA overexpression on processing of APP in the brain of PDAPP mice.

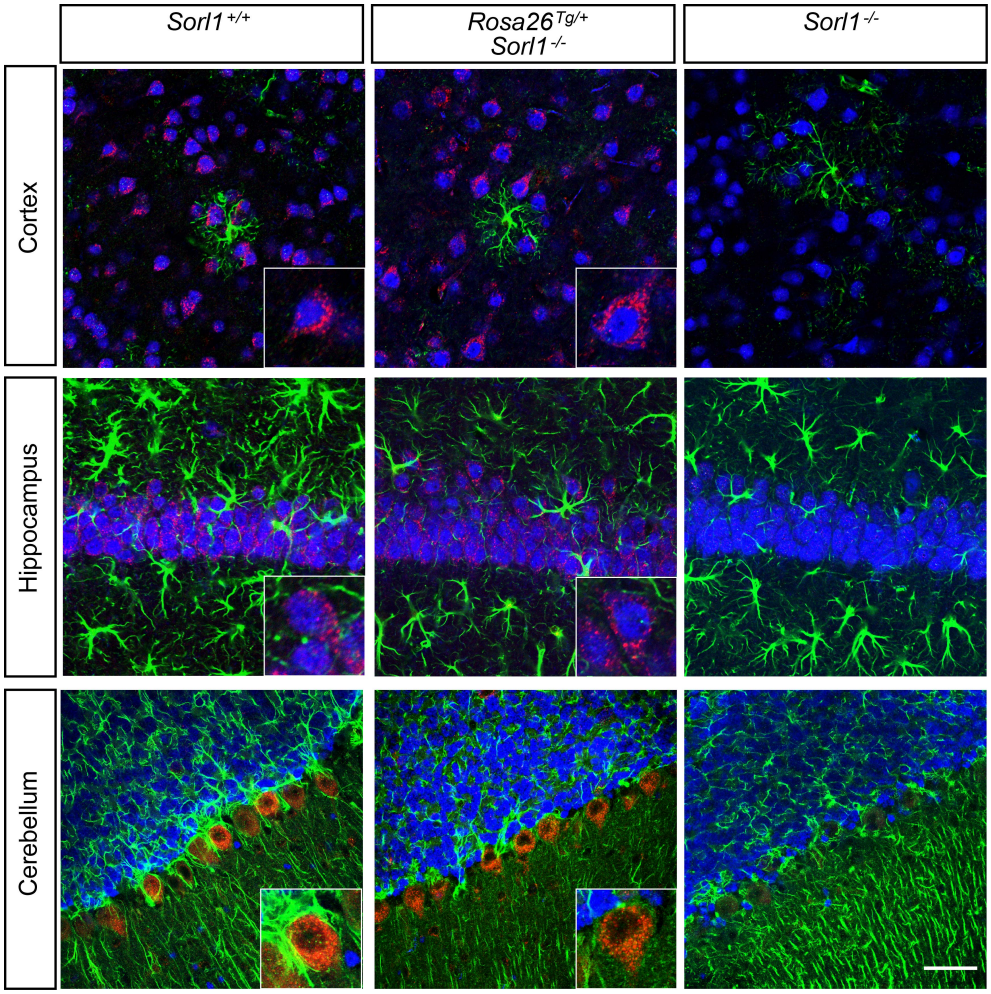

Figure 24. Human SORLA is expressed in neurons of *Rosa26*$^{Tg/+}$ mice. To determine the localization of human SORLA expressed from the transgene, endogenous receptor expression was eliminated by breeding *Rosa26*$^{Tg/+}$ mice with *Sorl1*$^{-/-}$ animals. The localization of SORLA was shown in sagittal free floating sections of 8-12 weeks-old *Rosa26*$^{+/+}$ and *Rosa26*$^{Tg/+}$ mouse deficient for murine *Sorl1* (*Rosa26*$^{Tg/+}$; *Sorl1*$^{-/-}$). *Sorl1*$^{-/-}$ mice were used as negative control for specificity of the antibody directed against SORLA. Neurons of the brain were counterstained for neuronal nuclei (NeuN, depicted in blue). Glial fibrillary acidic protein (GFAP, green) was detected as marker of astrocytes. Representative immunofluorescence pictures shown from cortical layer V and hippocampal CA1 region demonstrate SORLA signals (red) that colocalize with NeuN but not with GFAP in transgenic mice. This pattern parallels the localization of murine SORLA in wild-type mouse (*Sorl1*$^{+/+}$) shown as well. In the cerebellum, human SORLA is expressed in the Purkinje cells of (*Rosa26*$^{Tg/+}$; *Sorl1*$^{-/-}$) mice similar to murine SORLA in *Sorl1*$^{+/+}$ mice. The perinuclear localization of SORLA can be seen in the insets that represent higher magnifications of the micrographs. Scale bar: 50 µM

4.2.4. Impaired viability of homozygous *Rosa26*$^{Tg/Tg}$ mice

I intercrossed *Rosa26*$^{Tg/+}$ mice to obtain even higher expression levels with *Rosa26*$^{Tg/Tg}$ animals. I was successful in obtaining some *Rosa26*$^{Tg/Tg}$ animals. Yet, only 10% of the weaned animals at postnatal day (P) 21 were homozygous contrary to expected Mendelian ratio of 25% (Figure 25A). Thus, I hypothesized that the *Rosa26*$^{Tg/Tg}$ mice may suffer from impaired viability and die before being weaned. To test for early lethality, I decided to start analyzing animals at embryonic day (E) 13.5. Thus, I set up timed-matings with *Rosa26*$^{Tg/+}$ mice. Female *Rosa26*$^{Tg/+}$ mice were checked every morning for vaginal plugs. The presence of a vaginal plug was counted as E0.5 of pregnacy and the pregnant mice were sacrificed 13 days later. I collected fetuses and analyzed them by PCR. The observed genotype distribution was similar to expected Mendelian ratio implying that mice do not have early embryonic complications (Figure 25A). Next, I tested newborn (P1) animals from intercrossings of *Rosa26*$^{Tg/+}$ mice to find out whether mice are born with normal genotype distribution. Interestingly, some of the P1 animals died on the day they were born. To analyze these offspring further, I used their tail for PCR analysis and kept their brains for protein extraction and immunohistochemistry. Genotyping of the animals showed that *Rosa26*$^{Tg/Tg}$ mice were born at normal Mendelian ratios, yet approximately half of them died at P1 (Figure 25A). The only obvious difference between the pups was that *Rosa26*$^{Tg/Tg}$ newborns were slightly smaller compared to *Rosa26*$^{+/+}$ or *Rosa26*$^{Tg/+}$ pups as shown in the photographs in figure 25B, and by determination of body weights (Figure 25C). These results showed that *Rosa26*$^{Tg/Tg}$ mice display perinatal lethality with an incomplete penetrance.

A

	Genotype		
	Rosa26$^{+/+}$	*Rosa26*$^{Tg/+}$	*Rosa26*$^{Tg/Tg}$
Adult (n)	16 (24%)	44 (66%)	6 (10%)
E13.5 (n)	14 (28%)	21 (44%)	14 (28%)
P1 all (n)	17 (27%)	32 (51%)	14 (22%)
P1 survived (n)	17 (30%)	32 (56%)	8 (14%)

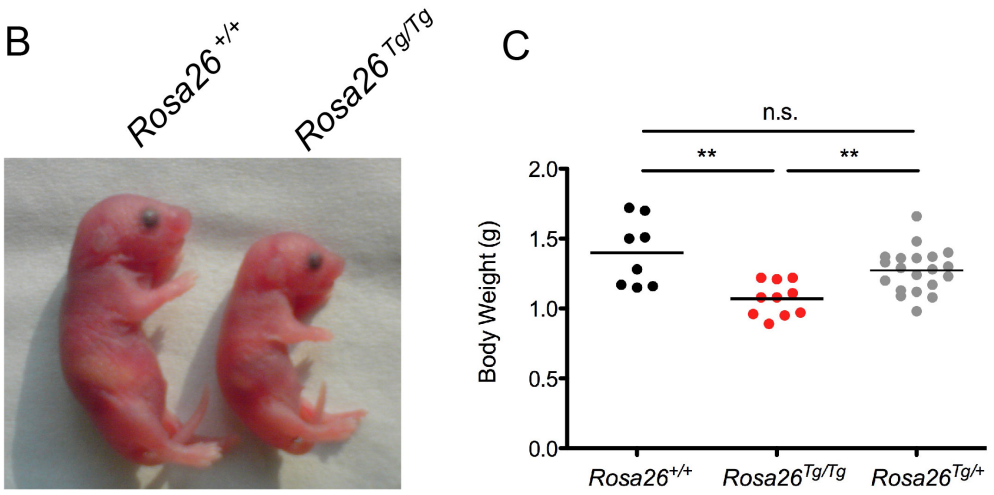

Figure 25. Impaired viability in *Rosa26*$^{Tg/Tg}$ mice. (A) *Rosa26*$^{Tg/+}$ animals were bred to obtain *Rosa26*$^{Tg/Tg}$ mice. Genotyping of offspring at postnatal day (P) 21 (adult) showed that only 10% of the mice were *Rosa26*$^{Tg/Tg}$ although the expected Mendelian ratio was 25%. To identify the time-point of death of *Rosa26*$^{Tg/Tg}$ mice, embryos and newborn animals from heterozygous breeding were analyzed as well. Genotyping of animals at embryonic day 13.5 and newborn mice (P1 all) failed to display any deviations in genotype distribution from the expected ratios showing that embryonic development wasn't affected. However, only half of the *Rosa26*$^{Tg/Tg}$ newborn mice survived the first day (P1 survived) and this ratio was comparable to that of weaned animals at P21.This finding indicated perinatal lethality of *Rosa26*$^{Tg/Tg}$ animals. (B) Anatomical inspections did not reveal any gross abnormalities comparing newborn *Rosa26*$^{+/+}$, *Rosa26*$^{Tg/+}$, and *Rosa26*$^{Tg/Tg}$ mice. The only obvious difference between *Rosa26*$^{+/+}$ and *Rosa26*$^{Tg/Tg}$ pups was the reduced body size of the later genotype. (C) Measurements of body weight showed that *Rosa26*$^{Tg/+}$ pups (n =20) are indistinguishable from their wild-type littermates (n=8) at P1. However, P1 *Rosa26*$^{Tg/Tg}$ mice (n=10) exhibit a reduced body weight. Differences between two groups were analyzed using student's *t*-test (** $p<0.01$, n.s., not significant).

I wanted to find whether the impaired lethality of the *Rosa26*$^{Tg/Tg}$ mice was due to compromised vital body functions. I examined several organs of the mice including the kidneys, liver, lung, and heart. However, I didn't observe any gross abnormalities in *Rosa26*$^{Tg/Tg}$ pups by visual anatomical inspection. To dissect potential side effects of SORLA overexpression in detail, I analyzed tissue sections and protein extractions from brains of *Rosa26*$^{+/+}$, *Rosa26*$^{Tg/+}$ and *Rosa26*$^{Tg/Tg}$ newborn animals. First, I compared their brain morphologies and neuro-anatomical structures. I prepared paraffin embedded tissue sections and performed Nissl staining. Histological analysis of the brains showed that the brain structure of the *Rosa26*$^{Tg/Tg}$ animals that died was comparable to that of their viable wild-type littermates (Figure 26A).

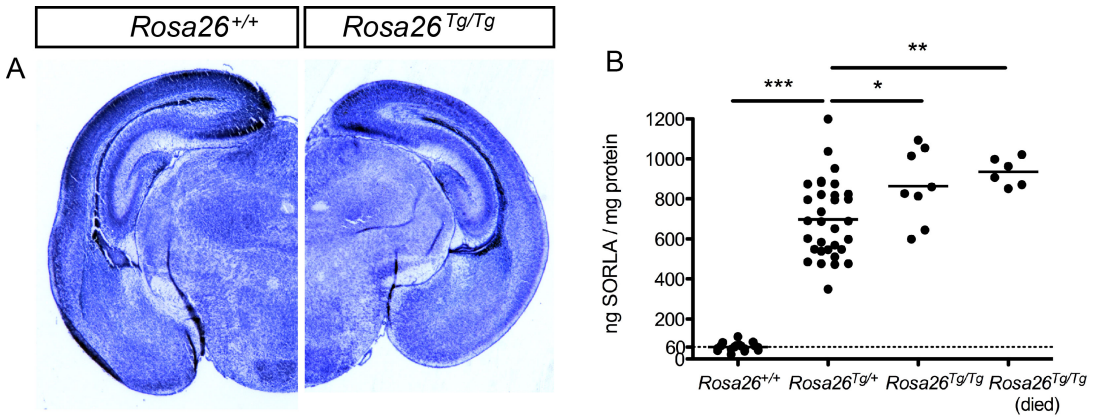

Figure 26. Neuroanatomical analysis and SORLA expression in newborn mice. (A) Coronal brain sections of newborn mice were stained with cresyl violet acetate solution that labels *Nissl* bodies of neurons. Bright-field microscopy pictures of the sections show no discernable differences in brain structures of *Sorl1*$^{+/+}$ mice compared to *Rosa26*$^{Tg/Tg}$ mice that had died perinataly. (B) Protein extracts from the brains of P1 mice were analyzed using the SORLA ELISA. The concentration of the receptor in *Rosa26*$^{Tg/+}$ animals (n=32) was 10-fold higher compared to the situation in *Rosa26*$^{+/+}$ littermates (n=17). There was also significant difference in SORLA levels between *Rosa26*$^{Tg/Tg}$ and *Rosa26*$^{Tg/+}$ newborn mice. However, the increase was only 1.5 fold. Brain expression levels of SORLA were not significantly different between *Rosa26*$^{Tg/Tg}$ animals that died (n=8) or that survived (n=6). Differences between two groups were analyzed using student's *t*-test (* $p<0.05$, ** $p<0.01$, *** $p<0.001$).

Additionally, to understand whether there was a direct relation between overexpression of SORLA and impaired viability of *Rosa26*$^{Tg/Tg}$ animals, I quantified receptor levels in brain protein extracts using the SORLA ELISA. Again, I didn't find any significant differences in the protein expression between *Rosa26*$^{Tg/Tg}$ animals that died and that survived (Figure 26B). Overall, I observed a significant overexpression (8-10 fold) of SORLA in the brain of *Rosa26*$^{Tg/+}$ animals compared to their *Rosa26*$^{+/+}$ littermates. Remarkably, the levels of SORLA increased only modestly further when a second transgene was introduced in the *Rosa26*$^{Tg/Tg}$ mice (1.5 fold) (Figure 26B). These results implied that overexpression of SORLA in the brain might not be the underlying reason of the perinatal lethality seen in *Rosa26*$^{Tg/Tg}$ animals. The results also document that *Rosa26*$^{Tg/+}$ mouse is already an adequate model to explore the effects of SORLA overexpression on amyloidogenic processing in the brain.

4.2.5. Murine Aβ accumulation is decreased in the brain of *Rosa26*$^{Tg/+}$ mice

After measuring SORLA concentrations in the newborn *Rosa26*$^{+/+}$, *Rosa26*$^{Tg/+}$, and *Rosa26*$^{Tg/Tg}$ animals, I continued my analysis by quantifying processing products of the murine APP. Accordingly, I extracted protein samples from the brains and measured levels of soluble APP processing products using ELISA (International Biological Laboratories, IBL). Intriguingly, in line with protective role of SORLA in APP processing, I found a 2-fold decrease in murine Aβ40 and Aβ42 levels in *Rosa26*$^{Tg/+}$ and *Rosa26*$^{Tg/Tg}$ animals compared to *Rosa26*$^{+/+}$ mice (Figure 27A & B). In line with the modest increase in SORLA levels, murine Aβ levels weren't decreased significantly in *Rosa26*$^{Tg/Tg}$ animals compared to *Rosa26*$^{Tg/+}$ (Figure 27A & B). Additionally, I compared Aβ levels with SORLA expression using linear regression analysis and found that the decrease of Aβ levels was correlated with elevated receptor expression (Figure 27C). In contrast to the decrease in Aβ concentrations, measurement of murine sAPPα levels didn't reveal any significant differences among *Rosa26*$^{+/+}$, *Rosa26*$^{Tg/+}$ and *Rosa26*$^{Tg/Tg}$ animals

(Figure 27D). I could not analyze murine sAPPβ levels, as no commercial ELISA kits are available to measure this peptide. Overall, my results implied that expression of SORLA didn't affect non-amyloidogenic processing of APP, but decreased Aβ levels in the brain of mice.

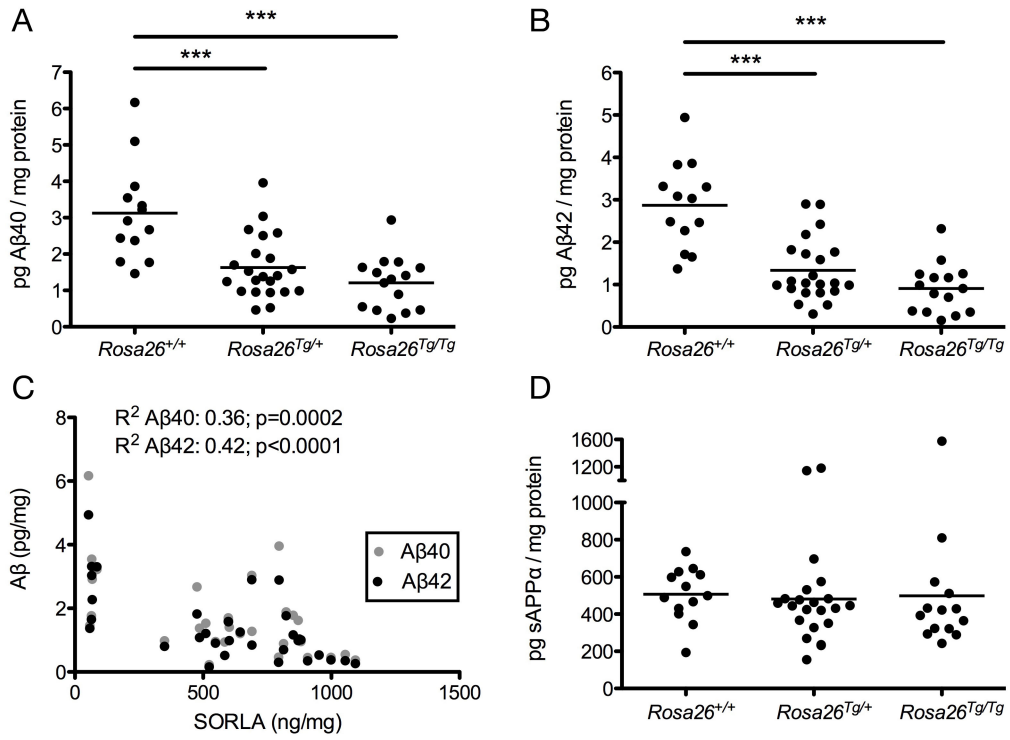

Figure 27. Overexpression of SORLA reduces murine Aβ levels in the brain. Tris-buffered saline (TBS) soluble proteins were extracted from total brains of newborn *Rosa26*$^{+/+}$, *Rosa26*$^{Tg/+}$ and *Rosa26*$^{Tg/Tg}$ mice. Processing products of murine APP were analyzed in TBS soluble fractions using commercial ELISA kits. Statistical analyses revealed a significant decrease in murine Aβ40 (A) as wells as Aβ42 (B) levels in newborn *Rosa26*$^{Tg/+}$ mice (n=21) compared to *Rosa26*$^{+/+}$ animals (n=13). *Rosa26*$^{Tg/Tg}$ mice (n=15) didn't show significantly different soluble Aβ levels compared to *Rosa26*$^{Tg/+}$ animals. In line with a role for SORLA as negative regulator of amyloidogenic processing, linear regression analysis (C) revealed an inverse correlation of soluble Aβ levels with receptor concentration in the brain. In contrast to the decrease in Aβ levels, murine soluble (s) APPα levels remain unchanged in *Rosa26*$^{Tg/+}$ and *Rosa26*$^{Tg/Tg}$ animals. Aβ levels were quantified as single measurements of each animal. Mean of duplicate measurements are shown for sAPPα. Differences between two groups were evaluated using student's *t*-test (***, $p<0.001$).

4.2.6. Human Aβ accumulation is decreased in the brain of (PDAPP; *Rosa26*$^{Tg/+}$) mice

Next, I wanted to analyze the processing of human APP, as this was more relevant for the disease condition in patients. To do so, I used PDAPP mice expressing platelet-derived growth factor (PDGF)-β promoter driven human APP. It is also possible to measure more processing products of human APP compared to murine APP since there are more assays and antibodies available such as ELISA kits for human sAPPβ (Meso Scale Discovery) and full-length human APP (Life Technologies). Thus, I crossed *Rosa26*$^{Tg/+}$ mice with (PDAPP; *Rosa26*$^{Tg/+}$) animals to obtain *Rosa26*$^{+/+}$, *Rosa26*$^{Tg/+}$, and *Rosa26*$^{Tg/Tg}$ newborn animals expressing human APP. I extracted proteins from the total brain samples and performed ELISA to test APP processing products in tris-buffered saline (TBS) soluble fractions. Similar to the decrease of murine amyloid peptide levels, I observed a significant reduction in soluble human Aβ40 and Aβ42 levels in (PDAPP; *Rosa26*$^{Tg/+)}$) and (PDAPP; *Rosa26*$^{Tg/Tg}$) mice compared to control animals, (PDAPP; *Rosa26*$^{+/+}$) (Figure 28A & B). Similar to the murine sAPP levels, there was no significant difference in sAPPα and sAPPβ concentrations among (PDAPP; *Rosa26*$^{+/+}$) (PDAPP; *Rosa26*$^{Tg/+}$), and (PDAPP; *Rosa26*$^{Tg/Tg}$) animals (Figure 28C & D). To ensure that APP levels were not affected by SORLA overexpression, I also measured full-length APP in membrane fractions. Comparable to soluble processing products, full-length APP levels weren't altered among genotypes (Figure 22F). These results showed that human Aβ as well as murine Aβ accumulation is decreased by overexpression of SORLA without changing processing of APP in the brain of mice.

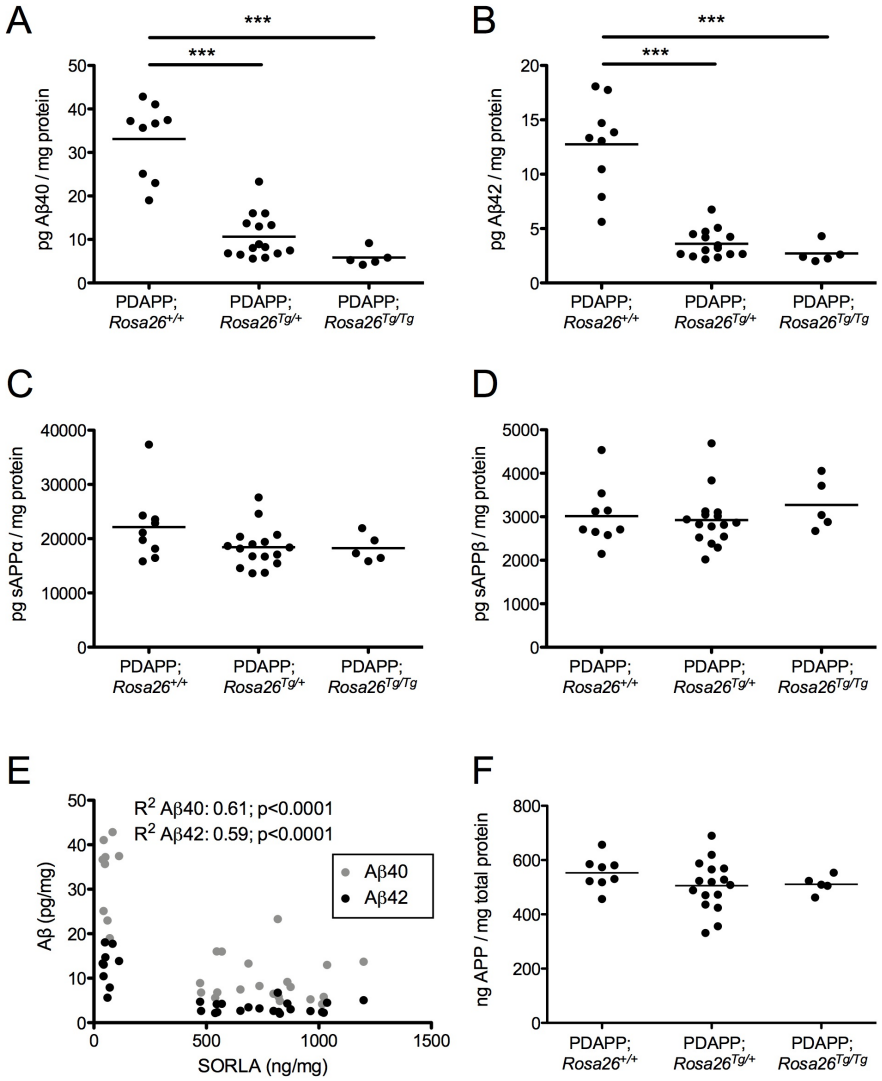

Figure 28. Overexpression of SORLA decreases human soluble Aβ accumulation in the brain of newborn PDAPP mice. PDAPP mice were used as model for human APP processing. Total brains of newborn (PDAPP; *Rosa26*$^{+/+}$), (PDAPP; *Rosa26*$^{Tg/+}$), and (PDAPP; *Rosa26*$^{Tg/Tg}$) animals were used to prepare TBS soluble protein extracts. The protein fractions were analyzed using ELISA kits. Similar to the situation with murine Aβ, levels of human Aβ40 (A) and Aβ42 (B) levels are also reduced in (PDAPP; *Rosa26*$^{Tg/+}$) (n=15) compared to (PDAPP; *Rosa26*$^{+/+}$) (n=9) animals. However, there is no difference in Aβ levels comparing (PDAPP; *Rosa26*$^{Tg/+}$) and (PDAPP; *Rosa26*$^{Tg/Tg}$) mice (n=5). The levels of sAPPα (C) and sAPPβ (D) as well as of full-length APP protein (F) were comparable among the three genotypes. (E) Linear regression confirmed the inverse correlation of Aβ and SORLA levels. Each sample was measured as duplicates and student's *t*-test was applied to analyze the differences between two groups (*** $p<0.001$).

Since AD is a disease associated with aging, next, I wanted to analyze APP processing in the adult animals. To understand regional differences in the brain, I dissected cortices and hippocampi of the 20 weeks-old (PDAPP; *Rosa26*$^{+/+}$), (PDAPP, *Rosa26*$^{Tg/+}$) and (PDAPP, *Rosa26*$^{Tg/Tg}$) mice, and prepared protein extractions as described before. I pooled (PDAPP, *Rosa26*$^{Tg/+}$) and (PDAPP, *Rosa26*$^{Tg/Tg}$) mice into a single group (PDAPP, *Rosa26*$^{Tg/}$) as number of the (PDAPP, *Rosa26*$^{Tg/Tg}$) mice (n=2-4) weren't enough to perform a strong statistical analysis. Similar to the results obtained from newborn animals, (PDAPP, *Rosa26*$^{Tg/}$) mice had significantly lower soluble Aβ40 and Aβ42 levels in the cortex compared to (PDAPP, *Rosa26*$^{+/+}$) animals (Figure 29A & B). In the hippocampus, Aβ40 levels were decreased in the (PDAPP, *Rosa26*$^{Tg/}$) animals compared to the (PDAPP, *Rosa26*$^{+/+}$) mice. However Aβ42 measurements didn't show any significant changes in the hippocampus among the genotypes. In line with the findings in the newborn animals, the concentrations of sAPPα and sAPPβ were similar in (PDAPP, *Rosa26*$^{Tg/}$) and (PDAPP, *Rosa26*$^{+/+}$) mice (Figure 29C & D). These results showed that overexpression of SORLA in AD vulnerable regions such as the cortex and hippocampus decreased Aβ accumulation also during disease progression in the brain of adult mice.

In the SORLA deficient mice (*Sorl1*$^{-/-}$), amyloidogenic processing is enhanced, and Aβ levels were increased along with sAPPα and sAPPβ levels compared to *Sorl1*$^{+/+}$ mice (Andersen, Reiche et al. 2005). So, it was interesting to find that sAPPα and sAPPβ levels weren't affected by overexpression of SORLA. sAPPα and sAPPβ are produced by cleavage of APP by α- or β-secretases respectively. Other products of these proteolytic reactions are carboxyl terminal fragments (CTFs). One of them, C83, is a by-product of α-cleavage, and the other one, C99, is a derivative of β-cleavage (Figure 2). I decided to check for the levels of these peptides to ensure that the activity of α- or β-secretases weren't altered by SORLA overexpression.

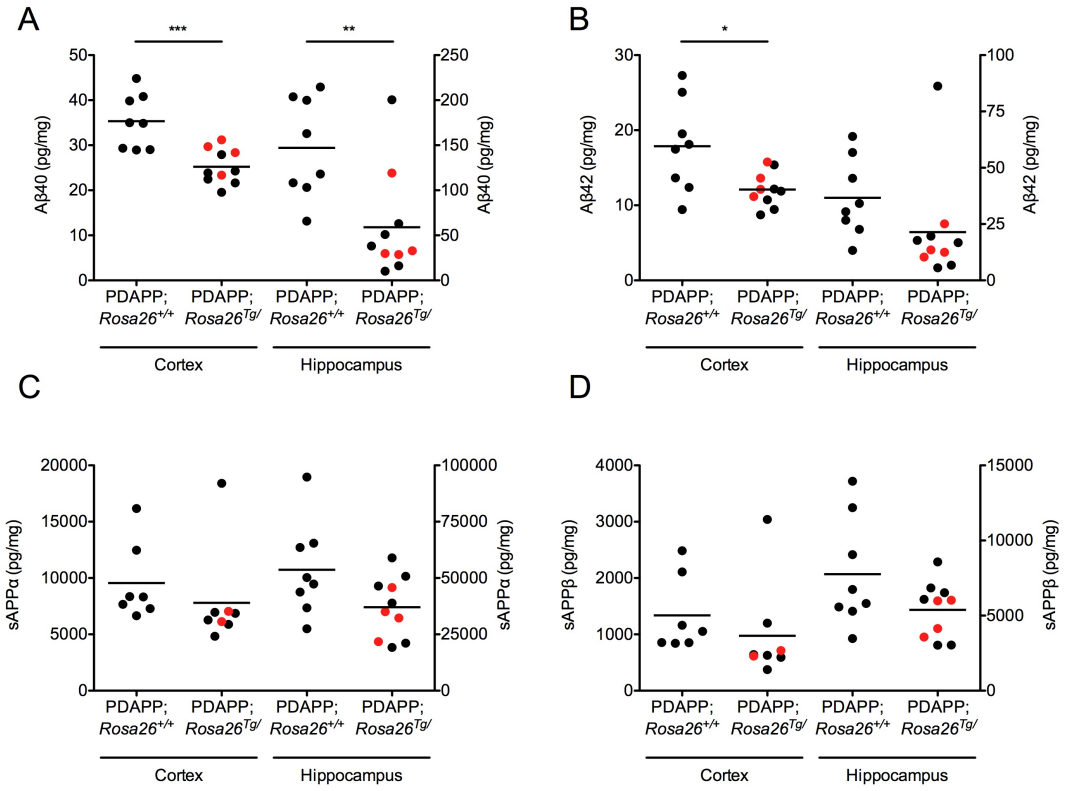

Figure 29. SORLA overexpression decreases human soluble Aβ levels in the brain of 20 weeks-old PDAPP mice. 20 weeks-old male PDAPP mice were used to analyze processing of human APP. Cortices and hippocampi of (PDAPP; *Rosa26*$^{+/+}$) (n=8), (PDAPP; *Rosa26*$^{Tg/+}$) (n=6), and (PDAPP; *Rosa26*$^{Tg/Tg}$) (n=2-4) animals were dissected and TBS soluble proteins were extracted. Aβ40, Aβ42, sAPPα and sAPPβ concentrations were measured by ELISA and normalized to total protein content. (PDAPP; *Rosa26*$^{Tg/+}$) (black), and (PDAPP; *Rosa26*$^{Tg/Tg}$) (red) animals were pooled into one SORLA overexpressor group (PDAPP; *Rosa26*$^{Tg/}$) for statistical analysis. Aβ40 (A) and Aβ42 (B) concentrations were significantly decreased in the cortex of 20 weeks-old (PDAPP; *Rosa26*$^{Tg/}$) mice compared to (PDAPP; *Rosa26*$^{+/+}$) animals. In the hippocampus, there was a significant decrease in Aβ40 levels in (PDAPP; *Rosa26*$^{Tg/}$) mice compared to (PDAPP; *Rosa26*$^{+/+}$) animals, but there was no significant difference in Aβ42 levels (p=0.14). Concentrations of sAPPα (C), and sAPPβ (D) fragments were similar between genotypes in the cortex as well as in the hippocampus. Each sample was measured as duplicates and student's *t*-test was applied to analyze differences between the groups (* p<0.05, ** p<0.01, *** p<0.001).

Thus, I extracted proteins from cortices of PDAPP animals and I measured levels of C83 and C99 in the membrane protein fractions by western blotting. Quantifications of the blots didn't reveal any differences in CTF levels comparing (PDAPP, *Rosa26*$^{+/+}$) and (PDAPP, *Rosa26*$^{Tg/+}$) mice (Figure 30). These results showed that overexpression of SORLA didn't alter APP processing or Aβ production, but it rather increased catabolism of Aβ.

4.2.7. Pathways of Aβ catabolism aren't altered in the brain of *Rosa26*$^{Tg/+}$ mice

Secreted Aβ peptides can be catabolized by degrading enzymes neprilysin and insulin degrading enzyme (IDE). Another pathway involved in Aβ catabolism is cellular uptake of free or APOE-bound Aβ by lipoprotein receptors, such as sortilin and low-density lipoprotein receptor-related protein 1 (LRP1). Internalized Aβ is then degraded in the lysosomes. Therefore, I wanted to check whether overexpression of SORLA decreases Aβ levels by promoting these pathways directly or indirectly. I extracted RNA and protein samples from the brains of *Rosa26*$^{+/+}$, *Rosa26*$^{Tg/+}$, and *Rosa26*$^{Tg/Tg}$ mice and performed quantitative real-time PCR and western blotting. I did not observe any significant differences in mRNA and protein levels of neprilysin and IDE comparing *Rosa26*$^{+/+}$ and *Rosa26*$^{Tg/+}$ animals. Similarly, mRNA and protein expression of APOE, sortilin as well as LRP1 weren't changed between the genotypes (Figure 31). *Rosa26*$^{Tg/Tg}$ mice had less neprilysin expression compared to *Rosa26*$^{+/+}$, situation expected to result in elevation rather than in decrease in Aβ levels.

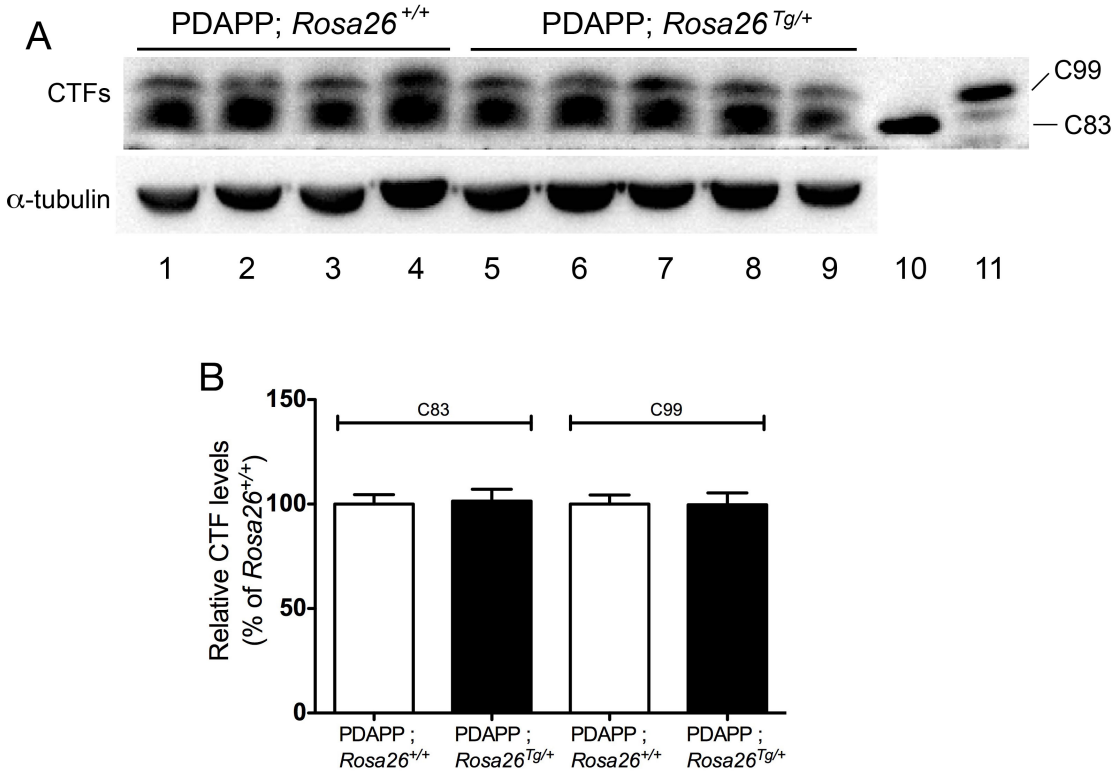

Figure 30. SORLA overexpression does not affect production of carboxyl-terminal APP fragments in the brain of 20 weeks-old PDAPP mice. (A) Membrane bound carboxyl-terminal fragments (CTFs) of APP were checked to determine the activity of α- and β-secretases. To do so, membrane protein fractions were prepared from cortices of 20 weeks-old (PDAPP; *Rosa26*$^{+/+}$), and (PDAPP; *Rosa26*$^{Tg/+}$) mice and analyzed by western blotting. (B) Densitometric scanning of replicate blots (n=8-10 samples per genotype) failed to reveal a difference in CTF C83 and C99 between (PDAPP; *Rosa26*$^{+/+}$) and (PDAPP; *Rosa26*$^{Tg/+}$) mice. Recombinant C83 and C99 peptides (lanes 10 & 11, respectively, in panel A) were used as reference for the position of migration of CTFs in the gel. These peptides were obtained from protein extractions of Chinese hamster ovary cells transiently transfected with expression constructs for C83 and C99. α-tubulin was used as loading control in western blots.

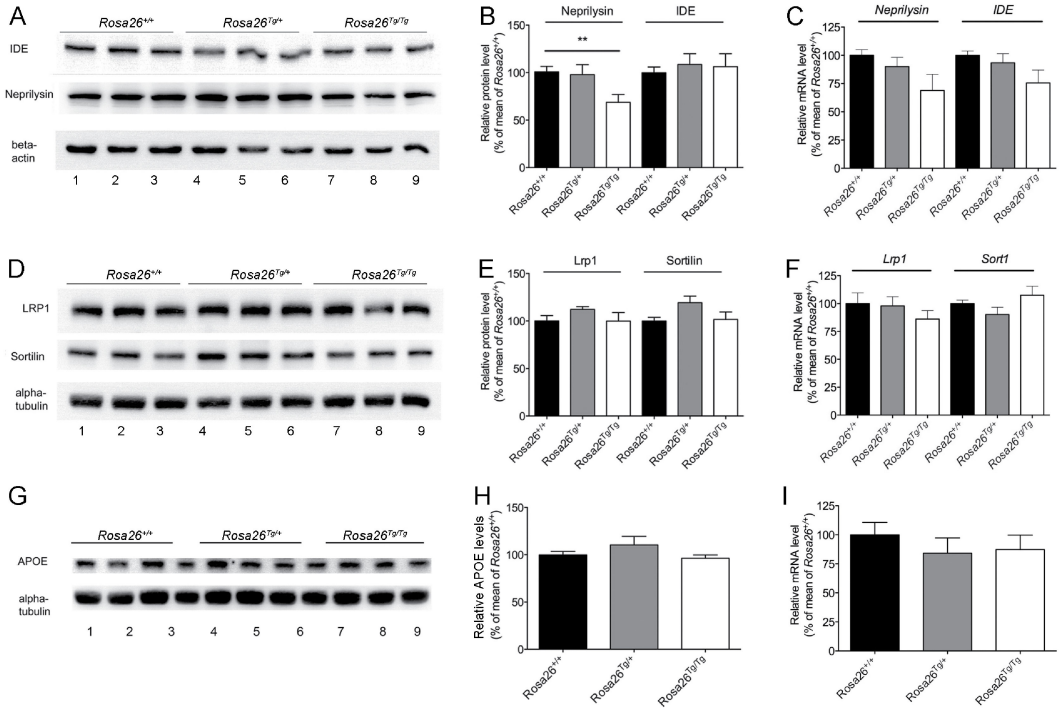

Figure 31. Pathways in Aβ catabolism in the brain are not altered by SORLA overexpression. To evaluate components of the Aβ catabolism pathways, brain tissues of newborn *Rosa26*$^{+/+}$, *Rosa26*$^{Tg/+}$, and *Rosa26*$^{Tg/Tg}$ mice were analyzed by western blotting and quantitative real-time polymerase chain reaction. Insulin degrading enzyme (IDE) and neprilysin are Aβ degrading enzymes. LRP1, sortilin, APOE factors are involved in cellular uptake and degradation of Aβ. (A, D & G) Protein samples were analyzed by western blotting. (B, E & H) Immunoreactive bands representing the indicated proteins in replicate blots (n=5-7 per genotype) were quantified by densitometric scanning. There is no difference in levels of IDE and neprilysin (A & B), or of LRP1, sortilin (D & E), and of APOE levels (G & H) comparing *Rosa26*$^{+/+}$ and *Rosa26*$^{Tg/+}$ mice. (B) There is only a slight decrease in neprilysin levels in *Rosa26*$^{Tg/Tg}$ animals compared to *Rosa26*$^{+/+}$ mice. α-tubulin and β-actin were used as loading controls in western blotting experiments. Transcriptional analyses of the Aβ catabolism pathway components were performed using TaqMan gene expression assays. Transcript levels of *neprilysin* and *Ide* (C), of *Lrp1* and *Sort1* (the gene encoding sortilin) (F) and of *Apoe* (I) were measured as triplicates in n=4 samples per genotype. The transcript levels of each gene were normalized to the expression level of 18S ribosomal RNA as internal control. Analyses of RNA expression levels do not show any significant alterations amongst the various genotypes (C, F, and I). Differences between two groups were analyzed using student's *t*-test (** $p<0.01$).

4.2.8. SORLA acts as an Aβ clearance receptor in the neurons

Based on these results, I hypothesized a novel function for SORLA in clearance of Aβ. To test this ability of SORLA, I performed Aβ uptake experiments using cell culture systems. Initially, I used Chinese hamster ovary (CHO) cells. I cultured parental CHO cells and cells stably overexpressing SORLA until they reach 70-80% confluency. Before I started with the uptake experiments, I confirmed overexpression of SORLA in the stably transfected cells by western blotting (Figure 32). To show uptake of Aβ, I incubated the cells with 200 nM of recombinant human Aβ40 (Ana Spec.). After 30 min of incubation at 37°C, I lysed the cells and measured the Aβ concentrations in the cells using ELISA. In line with decreased Aβ levels in the brain, the CHO cells overexpressing SORLA had 3-fold higher uptake of Aβ compared to parental cells (Figure 32).

To study the role of SORLA in Aβ uptake in a more relevant experimental system, I next used primary neuronal cultures. I lysed the hippocampus of newborn *Sorl1*$^{-/-}$, *Sorl1*$^{+/+}$ (same as *Rosa26*$^{+/+}$), and *Rosa26*$^{Tg/+}$ mice and cultured the cells for 7-10 days. First, I analyzed expression of SORLA in these neurons. Immunofluorescence experiments using antibody against SORLA along with the neuronal marker β-tubulin showed that the receptor has a vesicular expression pattern in the neurons (Figure 33A). Next, I performed western blotting to document overexpression of the receptor in the *Rosa26*$^{Tg/+}$ neurons. I also confirmed that LRP1 expression didn't change in the primary neurons of *Sorl1*$^{-/-}$, *Sorl1*$^{+/+}$, and *Rosa26*$^{Tg/+}$ mice (Figure 33B).

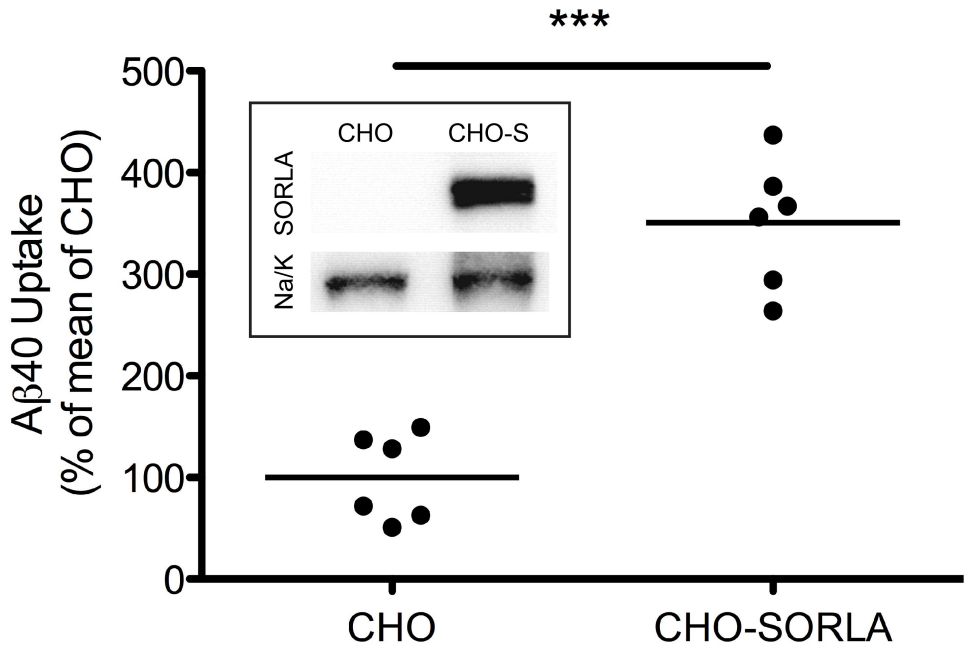

Figure 32. Uptake of human Aβ40 by CHO cells overexpressing SORLA. To test SORLA dependent Aβ uptake, parental Chinese hamster ovary (CHO) cells and CHO cells stably overexpressing SORLA were used. Overexpression of SORLA in stably transfected CHO cells (CHO-S) is documented by western blot in the inset. Detection of Na/K ATPase served as loading control. CHO and CHO-S cells were incubated with 200 nM of recombinant human Aβ40 for 30 min at 37°C. Subsequently, the cells were lysed and proteins were extracted to determine the levels of internalized Aβ by ELISA. The quantification of Aβ40 levels normalized to total protein concentrations revealed a 3-fold increase in endocytosed Aβ by CHO-S cells compared to parental CHO cells. Values are the mean of duplicate measurements from n=3 experiments and are shown as percentage of the mean of the parental CHO cells. Differences were evaluated using student's *t*-test (*** $p<0.001$).

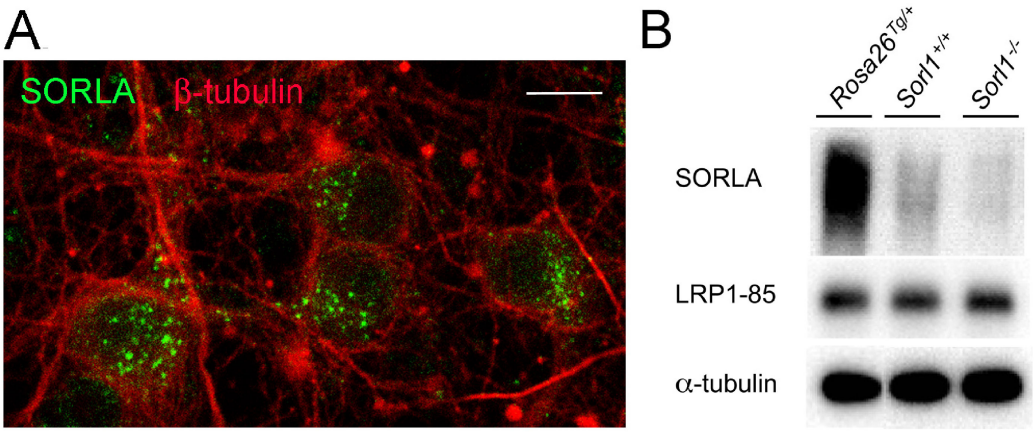

Figure 33. Human SORLA is overexpressed in primary hippocampal neurons of mice. (A) Hippocampi of newborn *Rosa26*$^{Tg/+}$ mice were trypsinized and neurons were plated on pre-coated chamber slides (Thermo Fisher Scientific). After 7-10 days in culture, the cells were stained using antibodies directed against SORLA (green) and the neuronal marker β-tubulin (red). Immunofluorescence pictures show a vesicular pattern for SORLA (green) in these neurons. Scale bar: 10 µm. (B) SORLA overexpression is documented in primary neuronal cultures from *Rosa26*$^{Tg/+}$ mice compared to *Sorl1*$^{+/+}$ animals by western blotting. In contrast, the levels of the 85 kDa subunit of LRP1 were similar in neuronal cultures derived from *Rosa26*$^{Tg/+}$, *Sorl1*$^{+/+}$ or *Sorl1*$^{-/-}$ mice. α-tubulin detection was used as loading control.

Finally, I performed an Aβ uptake assays using primary hippocampal cultures. I incubated the neurons of *Sorl1*$^{-/-}$, *Sorl1*$^{+/+}$, and *Rosa26*$^{Tg/+}$ mice with 200 nM of recombinant human Aβ40 for 1 hour at 37°C. Thereafter, I measured the concentration of Aβ peptides in the lysed cells by ELISA and normalized the data to the total protein content. Replicate experiments showed 2-fold higher Aβ uptake by *Rosa26*$^{Tg/+}$ neurons compared to *Sorl1*$^{+/+}$ neurons (Figure 34A). There was also a significant 25% decrease in Aβ levels taken up by *Sorl1*$^{-/-}$ cells showing that endogenous murine SORLA is also involved in Aβ clearance. One fate of the endocytosed proteins is delivery to lysosome. To test for lysosomal targeting of Aβ taken up by SORLA, I blocked the lysosomal pathway in primary neurons by treating the cells with 100 µM chloroquine (Sigma). Aβ levels in *Rosa26*$^{Tg/+}$ cells under these

conditions increased compared to neurons not treated (Figure 34B). This increase in cellular Aβ content was also evident in *Sorl1*$^{-/-}$ neurons implicating other receptors in neuronal Aβ uptake and lysosomal targeting as well. To explore the subcellular localization of internalized Aβ, I also performed immunocytochemistry in primary neurons. The recombinant human Aβ40 used in these assays was labeled with Hilyte-488 dye enabling easy detection of the peptide. Co-stainings of neurons with Lamp-1, a lysosomal marker, showed the presence of endocytosed Aβ in lysosomal compartments of the neurons (Figure 34C).

Taken together, my data obtained in this part of the thesis work elucidated a novel function for SORLA in uptake and lysosomal degradation of Aβ in neurons of the brain.

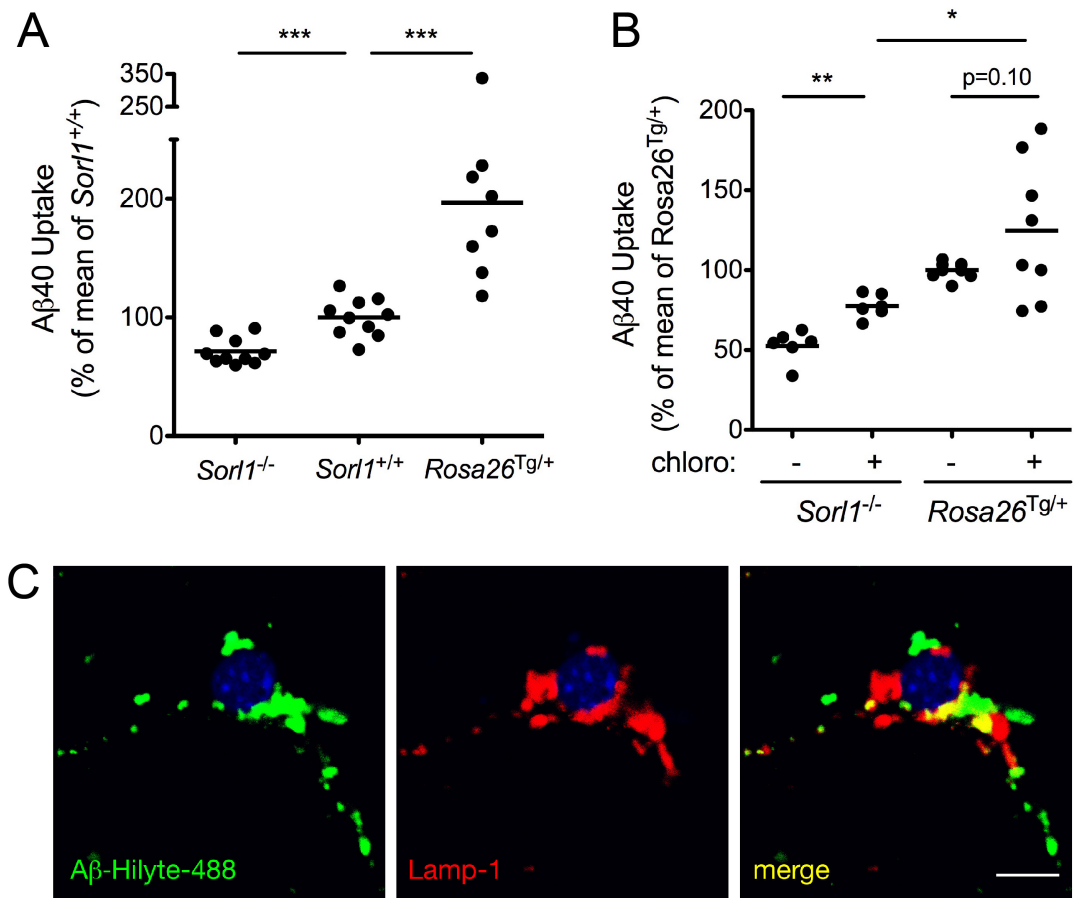

Figure 34. Endocytosis and lysosomal targeting of Aβ by SORLA in primary hippocampal neurons. (A) Primary hippocampal neurons from *Rosa26*$^{Tg/+}$, *Sorl1*$^{+/+}$ and *Sorl1*$^{-/-}$ mice were cultured for 7-10 days in pre-coated chamber slides.

Thereafter, the cells were incubated with 200 nM of recombinant human Aβ40-Hilyte-488 (AnaSpec) for 1 hour at 37°C. The amount of internalized Aβ was measured by ELISA and normalized to the total protein content. Neurons lacking SORLA show less Aβ uptake compared to *Sorl1*$^{+/+}$ cells whereas primary neurons of *Rosa26*$^{Tg/+}$ animals exhibit significantly more Aβ uptake compared to *Sorl1*$^{+/+}$ cultures. (B) To determine whether Aβ is targeted to lysosomes, neurons were treated with 100 µM of the lysosomal inhibitor chloroquine 2 hours prior to performing the uptake assay. Subsequently, neurons were treated with 200 nm of Aβ40-Hilyte-488 and 100 µM of chloroquine for another 1 hour. Inhibition of the lysosomal degradation resulted in a significantly more Aβ accumulation in *Sorl1*$^{-/-}$ neurons but only a modest increase (p=0.10) in *Rosa26*$^{Tg/+}$ neurons compared to non-treated cells as measured by ELISA. In A and B, results of n=3 experiments are shown. Student's *t*-test was used to compare 2 groups (* $p<0.05$, ** $p<0.01$, *** $p<0.001$). (C) To determine the localization of internalized Aβ, neurons were incubated with 500 nM of Aβ40-Hilyte-488 for 4 hours. Afterwards, co-staining was performed using antibody directed against the lysosomal marker Lamp-1. Immunofluorescence pictures show colocalization of Aβ40-Hilyte-488 (green) with Lamp-1 (red) suggesting lysosomal targeting of the internalized peptide in neurons. Arrowheads indicate vesicles positive for Lamp-1 and Aβ. Nuclei were stained with DAPI (blue). Scale bar: 10 µm.

5. Discussion

In my PhD study, I wished to explore the connection between genetic control of SORLA expression and development of AD. My project was based on prior evidences suggesting SORLA as a risk factor for AD. Loss of expression of the receptor was seen in a subset of patients with sporadic AD (Scherzer, Offe et al. 2004) but not in patients with familial AD (Dodson, Gearing et al. 2006). In patients with sporadic AD, SORLA expression was reduced in brain regions vulnerable to neurodegeneration like the hippocampus, but it was unaltered in protected brain regions such as the cerebellum (Offe, Dodson et al. 2006). Association analysis in humans also identified risk variants in *SORL1* gene predisposing to sporadic AD. Additionally, SORLA-deficient mice were shown to accumulate more Aβ and plaque deposits in their brain (Andersen, Schmidt et al. 2006; Rohe, Carlo et al. 2008). Taken together, these results suggested that SORLA negatively regulates amyloidogenic processing and loss of its expression might be a causal factor in development of sporadic AD. However, how genetic risk factors in *SORL1* may control receptor expression and confer risk for AD was not clear. Additionally, whether amyloidogenic processing and thus risk of AD might be decreased by experimentally elevating levels of the receptor was not evaluated thoroughly. To address these open questions, I investigated genetic factors that might regulate expression levels of SORLA in the human brain. In parallel, I generated a novel transgenic mouse model to test whether increasing expression of the receptor impairs amyloidogenic processing in the brain of mice and may represent a therapeutic option for treatment of AD.

5.1. Heterogeneity of risk variants in *SORL1*

To study the effects of genetic variants in *SORL1* on SORLA expression in the human brain, I collected a sample set composed of 88 autopsy specimens from the frontal cortex. Half of the specimens were recruited from the NBB and the second half was provided by the LBB. Initially, I compared the characteristics of the sample sets since there can be variations among the samples obtained from different brain banks due to subject selection,

handling and storage of the samples (Mattsson, Blennow et al. 2010). However, in my sample set there were no major differences in characteristics of the subjects such as age at death, and neuropathological severity level (Braak stage) comparing the subsample sets of the two brain banks (Table 2). The frequency of *APOE4* allele in the sample sets from the NBB and LBB was 39.8% and 36.0% respectively, which was also in consistent with previously published *APOE4* allele ratios in patients with AD (St Clair, Norrman et al. 1994). These features confirmed the validity of my samples to proceed with genotyping.

Next, I selected 12 SNPs located in the *SORL1* locus, which is spanning 180 kb and harbors several variations both in intronic and exonic sequences. In the initial study showing association of *SORL1* with AD, 29 SNPs were tested (Rogaeva, Meng et al. 2007). In the following studies, multiple genetic tags covering the entire gene including the 5' and 3' untranslated regions were genotyped for association analyses. These studies showed that different risk SNPs of *SORL1* are associated with the disease in diverse populations suggesting high allelic heterogeneity, which suggests that different mutations in the same locus can cause a similar phenotype. Since my sample set was of Caucasian origin, I chose the SNPs associated with the disease in the European populations in prior studies.

Analyses of SNP genotypes showed that the frequencies of SNP alleles in my sample set didn't show any deviations from the Hardy-Weinberg equilibrium (Table 3). This observation means that the genotype frequencies are in line with general population average. Additionally, the haplotype analysis of the 12 SNPs that were genotyped in my sample set revealed that there were two major haplotype blocks formed by these variants (Figure 8). The distribution of the SNPs in the 5' and 3' of the gene showed high linkage disequilibrium (LD) within each block. The presence of these LD blocks was shown previously in other reports. In particular, SNPs in the 3' haplotype block were associated with AD in European case-control sets as well as families (Rogaeva, Meng et al. 2007). These results highlighted that the genotyping

assays worked accurately in my hands and that my sample set was valid for a solid genetic association study.

In parallel, I quantified SORLA levels in the brain specimens using a specific ELISA developed in our lab. Expression of SORLA at the mRNA level was quantified in lymphoblasts samples before (Rogaeva, Meng et al. 2007). Supporting less SORLA expression as risk factor, it was found that carriers of AD-associated haplotype have less SORLA expression compared to non-carriers. However, expression of the receptor in lymphoblasts might not be truly indicative of brain expression. Additionally, mRNA expression doesn't always accurately reflect the corresponding protein levels. An immunoassay, which was able to detect SORLA protein levels was developed previously (Matsuo, Ebinuma et al. 2009). Since concentration of circulating SORLA fragments is associated with progression of atherosclerosis, the authors designed a specific ELISA to measure shedded SORLA fragments in serum samples. In another study employing this ELISA, the authors showed that patients with AD have more SORLA in their CSF compared to the control individuals (Ikeuchi, Hirayama et al. 2010). However, the authors did not correlated CSF levels with SORLA levels in brain parenchyma to substantiate that CSF levels are indicative of brain receptor mass. In another study, SORLA expression in brain specimens was measured semi-quantitatively using western blotting. However, I needed a much more sensitive and reliable assay to measure numerous samples simultaniously. Thus, I developed an ELISA to measure SORLA levels in brain specimens and I showed that this immunoassay is highly specific and correlates well with data obtained by western blotting (Figures 11 & 12). Accordingly, I applied this ELISA to determine SORLA concentration in all brain specimens.

Next, I correlated protein levels with SNP markers for each individual. In this study, I identified two risk variants in *SORL1*, rs2070045 and rs1699012 that correlated with the protein concentrations in the brain (Figure 14). Association of rs2070045 with AD was shown in North European families and case-control population as well as in another Caucasian sample set in the

USA (Rogaeva, Meng et al. 2007). Association of rs2070045 with AD was replicated in another study in a UK population (Li, Rowland et al. 2008). In the Rogaeva *et al*.'s report, the effect of rs1699102 on AD did not reach significance when it is tested as single SNP in Caucasian population. However, when it was tested together with its neighboring SNPs as a haplotype, a significant association with AD was found in North European and American Caucasian data sets (Rogaeva, Meng et al. 2007). Moreover, associations of rs2070045 as well as the 3' haplotype block with AD risk were replicated in several meta-analyses (Reynolds, Hong et al. 2010; Reitz, Cheng et al. 2011). Finally, a genome-wide association study identified rs3781835, which is in the 3' haplotype block between rs2070045 and rs1699102, as a risk variant for AD (Naj, Jun et al. 2011). These results showed that rs2020745 and 1699102 are important genetic risk factors. In line with this notion, my data suggest a significant effect of these SNPs on SORLA concentrations in the brain.

At this point, I need to acknowledge certain limitations of my study. Although the sample size was large enough to identify the two most significant SNPs, there were additional variants in the 3' haplotype block of *SORL1*, which were in linkage disequilibrium with rs2070045 and rs1699102 (Figure 10). However, they didn't show significant association with protein levels (Figure 15). This result implies that even though other SNPs in the 3' haplotype block might be relevant for the disease risk, my sample size might have been too small to detect the association between these SNPs and SORLA levels. As the 3' risk haplotype block is significantly associated with lower receptor concentrations (Table 5), there might be additional causative variants, which weren't tested in this study. Another limitation of the study is that sample set consisted of only patients with AD who display neurodegeneration. However, confounder effect of the disease status on SORLA levels due to neuronal loss is unlikely, as comparable levels of RNA expression among major or minor variant carriers of rs2070045 and rs1699102 was detected (Figure 16). Additionally, severity of neuropathology didn't show any effects on SORLA levels (Figure 13). Nevertheless, it is still important to test the variants in

another replication cohort composed of healthy controls to analyze how early the risk variants may start to alter expression level of SORLA.

5.2. Association of genetic risk factors with disease markers

In my study, the minor alleles of rs2070045 and rs1699102 were associated with lower SORLA protein expression in the brain. In contrast, I didn't see any correlations between these two SNPs and mRNA levels of *SORL1* suggesting a specific impact at the post-transcriptional level. There are several studies suggesting association of the 5' and 3' haplotypes in *SORL1* with various AD markers to explain the mechanism how the risk variants/haplotypes may confer risk for AD. For example, it was shown that the 5' risk haplotype is associated with areas of high intensity in white matter of the brain as measured by magnetic resonance imaging (K, Lunetta et al. 2008). Also, a 3' haplotype including rs1699102 was associated with cerebral and hippocampal atrophy in Caucasian patients (K, Lunetta et al. 2008). Another study performed in AD patients from Germany showed a 3' haplotype in *SORL1* consisting of rs2070045 that was associated with CSF Aβ levels (Kolsch, Jessen et al. 2008) and with age of AD onset (Kolsch, Jessen et al. 2009). Finally, consistent with my results, another study from Sweden found that the minor allele of rs2070045 was associated with accelerated cognitive decline in men and a decreased overall cognitive performance in women (Reynolds, Zavala et al. 2013). Taken together, all of these studies showed that the risk variants in *SORL1* are associated with AD as well as with various biomarkers of the disease.

Since decreased levels of SORLA are seen in patients with AD, it is plausible that the risk variants might modulate the disease biomarkers and development by altering expression level of the receptor. Thus, effects of *SORL1* variants on expression level of the receptor were analyzed previously. However these studies were quantifying either the mRNA levels in the brain or the protein fragments in the CSF. For example, it was shown that rs661057 in *SORL1*, which I haven't tested in my sample set, is correlating with mRNA expression of *SORL1* in the human brain specimens (Grear, Ling

et al. 2009). Interestingly, only heterozygous carriers of the risk variant displayed decreased levels of receptor expression. In a recent study in a German cohort, it was reported that two different 3' *SORL1* haplotypes, consisting of rs2070045 and rs1699102 respectively, were associated with decreased Aβ levels (Guo, Westerteicher et al. 2012). The authors also showed correlation of SORLA fragment concentrations in CSF samples with the risk haplotype in the 5' region of *SORL1*. In my study, I failed to replicate the association of the 5' SNPs with SORLA levels in the brain samples of my sample set (Figure 15), emphasizing allelic heterogeneity. Another likely reason for this discrepancy is that SORLA concentrations in the CSF might not be predictive of protein expression levels in the brain. Reliable measurements of protein markers in the CSF are more challenging than in brain autopsy specimens as CSF samples are more sensitive to post-mortem interval and handling conditions. In line with this caveat, one recent study suggested decreased SORLA levels in the CSF of AD patients compared to control subjects (Ma, Galasko et al. 2009), whereas another study showed that patients had higher concentration of SORLA fragments in the CSF compared to controls (Ikeuchi, Hirayama et al. 2010). These different results suggest difficulties in reproducible measurements of SORLA levels in the CSF. Thus, the risk variants identified in my project may be more informative as they directly predict SORLA protein concentration in brain tissue.

5.3. Synonymous variations in *SORL1* affect efficiency of protein expression

Interestingly, rs2070025 and rs1699102 are the only 2 exonic SNPs in the list of risk variants that I tested. They alter the codon sequence of the mRNA without altering the protein sequence. Still, synonymous or silent mutations are implicated in disease and might alter expression and function of the proteins (Sauna and Kimchi-Sarfaty 2011). There are several possibilities how silent variations may change protein expression including their effects on RNA stability or splicing, resulting in differences in gene expression levels (Capon, Allen et al. 2004). In terms of *SORL1*, transcription levels of *SORL1*

were shown to correlate with an AD risk variant, rs665017, in 5' of *SORL1* (Grear, Ling et al. 2009). In another study, association of two other SNPs in 5' of *SORL1* with transcript levels were shown in temporal cortex (McCarthy, Saith et al. 2012).

Rather than affecting RNA stability, I found an alterative explanation how the minor alleles of rs2070045 and rs1699102 impact protein levels. Thus, a SORLA expression construct carrying the minor allele variants was expressed at lower levels in CHO cells than one carrying the major variants (Figure 18). However, mRNA levels were comparable in two cell lines suggesting differences at the level of translation efficiency (Figure 19). Silent mutations can modify the efficiency of protein translation by changing the secondary structure of transcript (Nackley, Shabalina et al. 2006) or by altering the codon usage (Ikemura 1985). Codon usage, in turn, might alter the stability of the protein, as the speed of translation is an important determinant in folding of the peptide. For example it is suggested that rs6332 (change from CCG to CCA) in the *Neurotrophin-3* gene, which is implicated in attention deficit/hyperactivity disorder, might increase speed of translation and affect protein levels, whereas rs2069763 (change from CTG to CTT) might decrease the speed of translation of the *Interleukin-2* gene and be associated with cervical and vulvar cancer (Sauna and Kimchi-Sarfaty 2011). Consistent with this notion, I showed by computational analyses that the efficiency of codon usage for serine is decreased from 18.5% (TCT) to 5.6% (TCG) comparing major to minor allele alteration at rs2070045 (Zeeberg 2002).

While my data strongly argue for inefficient codon usage as the cause of poor receptor expression in the minor allele variant, my results do not exclude possible effects of other genetic and environmental factors on SORLA expression. In a study showing association of 3' *SORL1* haplotype with mRNA expression of SORLA, it was calculated that the risk genotype accounts for only 14% of the difference in mRNA levels seen amongst genotypes (Rogaeva, Meng et al. 2007). Consistent with this notion, other

SNPs in the 3' haplotype block in my study showed a trend for association with SORLA protein levels as well. Moreover, haplotype analysis showed that the 3' minor haplotype is associated with decreased SORLA levels. These results suggest that additional SNPs in 3' haplotype block may also have effects on protein expression levels as well as on biomarkers of AD (K, Lunetta et al. 2008; Kolsch, Jessen et al. 2008). To detect possible significant association of the 3' variants in *SORL1* with these phenotypes, larger sample sets may be required as risk sizes of individual SNPs in *SORL1* are typically modest.

Taken together, I identified two risk genotypes associated with SORLA expression in the human brain. To the best of my knowledge, my study represents the first report of association of risk variants in *SORL1* with SORLA concentrations in the brain. These results suggest a possible mechanism how decreased translational efficiency may predispose to AD in carriers of the respective SNPs variants.

5.4. Neuronal localization of SORLA and mosaic protein expression from the *Rosa26* locus

My above data supported the hypothesis that decreased level of SORLA expression is a risk factor causative of sporadic AD in patients. As a next logical step I wanted to query this model by testing whether increasing the expression levels of SORLA, in turn, may reduce amyloidogenic processing in the brain and be protective.

Direct correlation between SORLA levels and amyloidogenic processing products were previously shown in cells and knockout mouse models. Thus, SORLA deficiency increased accumulation of murine and human Aβ as well as plaque density (Andersen, Reiche et al. 2005; Rohe, Carlo et al. 2008). This effect was gene-dose dependent as *Sorl1*$^{+/-}$ animals had intermediate levels of processing products and plaques burden compared to *Sorl1*$^{+/+}$ and *Sorl1*$^{-/-}$ animals (Dodson, Andersen et al. 2008). In the same study it was also shown that there was an inverse correlation between plaque pathology and

SORLA levels. Although these data showed a specific influence of SORLA on APP processing when being lost completely, total deficiency of SORLA (as in knockout mouse models) only poorly recapitulates the conditions seen in patients with AD. In consistent with the results obtained from knockout animal models, overexpression of SORLA in neuronal cells decreased processing of APP (Andersen, Reiche et al. 2005). A dose-dependent inverse correlation of SORLA activity with levels of APP processing products was shown using a tetracycline-controlled inducible overexpression system in cells (Schmidt, Baum et al. 2012). These data provided first evidence that overexpression of SORLA may have a therapeutic potential. However, *in vivo* effects of SORLA overexpression in mice weren't tested so far. Accordingly, I wanted to analyze the effects of increased receptor levels on APP processing and AD development in mice.

Towards the above goal, I generated a new transgenic mouse line overexpressing SORLA. I obtained high expression level of the receptor by inserting the human SORLA cDNA into the murine *Rosa26* locus (Figure 6). Targeting the *Rosa26* locus is a widely used approach to generate transgenic mouse models because the *Rosa26* transcript is not translated into a protein and no abnormal phenotype was reported in mice with targeted disruption of this locus (Soriano 1999). Another feature of *Rosa26* locus is the high homologous recombination efficiency enabling site-specific transgene insertion. This provides a further advantage compared to random insertion method in which the inserted gene might be subject to local silencing or cause insertional mutagenesis (Irion, Luche et al. 2007). The endogenous *Rosa26* promoter drives expression of the inserted target genes at modest levels. To asure higher amount of SORLA overexpression, I inserted the CAG promoter upstream of the SORLA cDNA. To activate the transgene, I bred the mice with the Cre deleter strain of mice to remove the transcription stop element in front of the SORLA cDNA. In his approach, I obtained high, dosage-dependent expression of the SORLA transgene in the cortex, hippocampus and cerebellum of mice (Figure 22). Quantification of SORLA

levels documented a 4-fold increase in SORLA levels in the cortex and hippocampus of *Rosa26*$^{Tg/+}$ mice compared to *Rosa26*$^{+/+}$ animals (Figure 23).

As the Cre deleter strain initiates recombination in germ cells and as CAG is a ubiquitous promoter element, I expecting SORLA expression in all cell types of the transgenic mice at all stages of ontogeny. However, I failed to see significant SORLA immunoreactivity in the glia cells that express glial fibrillary acidic protein (GFAP) in the brain of mice (Figure 24). Rather in the brain, SORLA transgene expression was restricted to neurons of the cortex and hippocampus as well as the Purkinje cells of the cerebellum, which also express the murine receptor. There can be several reasons for the restricted expression of the transgene in cells that normally also express the endogenous receptor.

For example, efficiency of expression from *Rosa26* locus might be a mechanism to explain my findings. One of the reasons why the *Rosa26* locus is preferred for generation of transgenic mouse lines is the expression efficiency from the locus. In contrast to the random insertion approach, in which the transgenes can be silenced after the onset of ES cell differentiation, *Rosa26* locus drives the robust expression of the transgene in most tissues (Irion, Luche et al. 2007). Consistent with this activity, I also saw overexpression of SORLA in several tissues including the brain, kidney and adipose tissue (data not shown). However, expression within tissues might not be always ubiquitous as shown previously. In a previous study in which the *Myc-Mdm4* gene was inserted into the *Rosa26* locus, the authors found that their target gene displayd mosaic expression in lung and liver. Although in their study Myc expression was shown successfully in all cells in the brain, the immunoreactivity level of the protein wasn't the same among the various cell types (Nyabi, Naessens et al. 2009). Additionally, a recent study testing several ubiquitous promoters in the *Rosa26* locus revealed that inserted genes displayed differences in expression level and pattern with different ubiquitous promoters (Tchorz, Suply et al. 2012). The authors showed that when EGFP gene driven by CAG or CMV promoters is inserted into the

Rosa26 locus, the transgene was expressed in ES cells. However, *in vivo* gene expression in the brain was only successful with the CAG promoter. Epigenetic mechanisms, which can silence the CMV promoter (Mehta, Majumdar et al. 2009), may also be a reason for mosaic SORLA expression in the brain of my mouse model. The sensitivity of the CAG promoter towards positional effects and inhibition from *Rosa26* anti-sense promoter (Zambrowicz, Imamoto et al. 1997) are the other factors potentially affecting the activity of the transgene promoter.

While, restricted expression of SORLA in my mice might simply be due to positional effects of the *Rosa26* locus, physiological mechanisms controlling expression of SORLA may also likely to explain the restricted expression profile of the receptor. In support of this idea, expression of endogenous SORLA is tightly regulated as the receptor is expressed only in the neurons. In line with absence of SORLA expression in astrocytes of *Rosa26*$^{Tg/+}$ mice, it was recently shown that expression of SORLA in rat glioma cells was significantly decreased when the cells were differentiated under low-serum conditions into GFAP expressing astrocytes (Salgado, Serrano et al. 2012). Conceptually, there may be certain mechanisms silencing protein expression in the non-neuronal cell types. Absence of specific transcription factors or proteins required for folding and trafficking of SORLA in the glial cells may be one of the reasons preventing the receptor expression. Another explanation may be that SORLA is transcribed in the glial cells but the mRNA is subjected to non-sense mediated RNA decay and cannot be translated into the protein. It is also possible that SORLA overexpression might be detrimental for the cells that normally don't express the receptor.

Nevertheless, expression of SORLA transgene in the neurons provided a specific neuronal overexpression in the brain (Figure 24) in my mouse model. Hence, this new line represented an ideal model to study the effects of SORLA overexpression on amyloidogenic processing in the neurons.

5.5. Impaired viability of *Rosa26*$^{Tg/Tg}$ newborns

At the beginning of my study, I used *Rosa26*$^{Tg/+}$ animals, which were viable and fertile despite strong overexpression of the receptor. High promoter activity of CAG from *Rosa26* locus was previously shown in a study where the mouse ES cells were stably or transiently transfected with constructs carrying different promoters (Chen, Krohn et al. 2011). It was shown that CAG promoter yields highest expression (9-10-fold in stably transfected ES cells) compared to the endogenous *Rosa26* promoter. Similar to this induction, quantifications of SORLA levels in the newborn brains, which might be comparable to primary cells, showed that single copy of the transgene in *Rosa26*$^{Tg/+}$ animals increases the receptor levels 8-10-fold compared to *Rosa26*$^{+/+}$ animals (Figure 26).

When I crossed *Rosa26*$^{Tg/+}$ animals to obtain mice carrying two transgene copies, I observed that *Rosa26*$^{Tg/Tg}$ mice displayed impaired viability at the perinatal stage (Figure 25). I found that the homozygous transgenic newborns (*Rosa26*$^{Tg/Tg}$) had 12-15-fold SORLA expression in their brains compared to *Rosa26*$^{+/+}$ animals. Possibly, high concentration of exogenous protein expression (as for SORLA) is toxic providing a molecular explanation for the impaired viability of *Rosa26*$^{Tg/Tg}$ mice (Madisen, Zwingman et al. 2010). In support of this assumption, overexpression of SORLA in restricted cell types seen in my model also suggests that very high receptor levels might be detrimental to non-neuronal cells. However, I failed to see any significant differences in SORLA concentrations in the brain of the *Rosa26*$^{Tg/Tg}$ animals that died or that survive (Figure 26). Also, histological examination of the newborn animal brains didn't reveal any discernable differences. Although these findings do not exclude a possible effect of too much SORLA activity on brain integrity and function, overexpression of SORLA in other organs such as kidney or liver may also exert toxic effect on *Rosa26*$^{Tg/Tg}$ animals. In spite of the above concerns, surviving *Rosa26*$^{Tg/Tg}$ mice lived a normal life span without any obvious phenotypes. Additionally, already the *Rosa26*$^{Tg/+}$ animals presented with a 4-fold overexpression of SORLA in the brain

without any obvious problems of viability suggesting that the *Rosa26*$^{Tg/}$ line was a valid and useful model.

5.6. Overexpression of SORLA doesn't alter levels of APP processing products

Analysis of amyloid processing products in the brain of newborn *Rosa26*$^{Tg/+}$ or *Rosa26*$^{Tg/Tg}$ mice revealed a significant decrease in Aβ concentrations compared to *Rosa26*$^{+/+}$ mice (Figure 27). A similar decrease was seen in human Aβ levels in PDAPP newborn mice overexpressing the reecptor (Figure 28). I confirmed these findings in the brain of adult PDAPP animals as well (Figure 29). Surprisingly, levels of other APP processing products including sAPPα, sAPPβ (Figures 27- 29) as well as CTF (Figure 30) remained unaltered in the *Rosa26*$^{Tg/+}$ or *Rosa26*$^{Tg/Tg}$ animals as compared to *Rosa26*$^{+/+}$ mice. These results suggested that processing of APP wasn't affected by high SORLA expression, an observation rather surprising given prior data from our lab and that of others documenting inverse an correlation of receptor levels with APP processing rates.

The relevance of SORLA for regulation of APP trafficking and processing was substantiated by several studies. Thus, SORLA interacts with APP to form a 1:1 stoichiometric complex as shown by analytical ultracentifugation experiments (Andersen, Reiche et al. 2005). Later, it was shown that the ligand-binding complement type repeats of the receptor and the carbohydrate-linked domain of APP mediate this interaction (Andersen, Schmidt et al. 2006). Deficiency of SORLA in the mice caused accumulation of Aβ along with sAPPα and sAPPβ in the brain (Dodson, Andersen et al. 2008; Rohe, Carlo et al. 2008). Moreover, overexpression of the receptor in neuronal cell lines decreased the concentration of the processing products secreted into the medium (Andersen, Reiche et al. 2005).

Taken together all published results strongly supported the concept that SORLA represents an APP receptor that prevents its proteolytic processing in neurons. More detailed cell biology data suggested that SORLA prevents

processing of APP in two different stages. Typically, newly synthesized APP is directed to secretory pathway to the cell surface (Figure 35). At the cell surface, it is cleaved by α-secretase or internalized into the endosomal compartments where amyloidogenic processing takes place. At the first level of regulation, SORLA acts as a retention factor for APP in the TGN. SORLA co-localizes with APP in the perinuclear compartments of the cells (Andersen, Reiche et al. 2005; Spoelgen, von Arnim et al. 2006), and prevents APP to exit the Golgi and reach the cell surface, a prerequisite for any subsequent processing steps (Schmidt, Sporbert et al. 2007). Additionally, SORLA interferes with β-secretase cleavage of APP by binding to the precursor protein and blocking its dimerization in the TGN (Schmidt, Baum et al. 2012).

Considering these convincing data from cell biological studies, it was surprising to observe decreased Aβ concentration in *Rosa26*$^{Tg/+}$ or *Rosa26*$^{Tg/Tg}$ animals as compared to *Rosa26*$^{+/+}$ mice without accompanying changes in other APP processing products (Figures 27-29). One reason why overexpression of SORLA in the *Rosa26*$^{Tg/+}$ and *Rosa26*$^{Tg/Tg}$ animals may not result in decreased amounts of sAPPα and sAPPβ levels may be that endogenous APP molecules in the neurons may already be saturated with the endogenous SORLA molecules. That might be the reason why even subtle changes in SORLA levels, as seen in humans, might affect processing of APP. However, I obtained a dramatic increase of SORLA expression in *Rosa26*$^{Tg/+}$ mice. *Rosa26*$^{Tg/+}$ newborn animals have 8-10 fold increased SORLA concentration compared to *Rosa26*$^{+/+}$ newborns (Figure 26), and SORLA levels are 4-5-fold increased in adult *Rosa26*$^{Tg/+}$ mice compared to *Rosa26*$^{+/+}$ animals (Figure 23). Accordingly, excessive amounts of SORLA molecules in my model may not be able to find any free APP molecules, and therefore have no effect on APP processing (Figure 35).

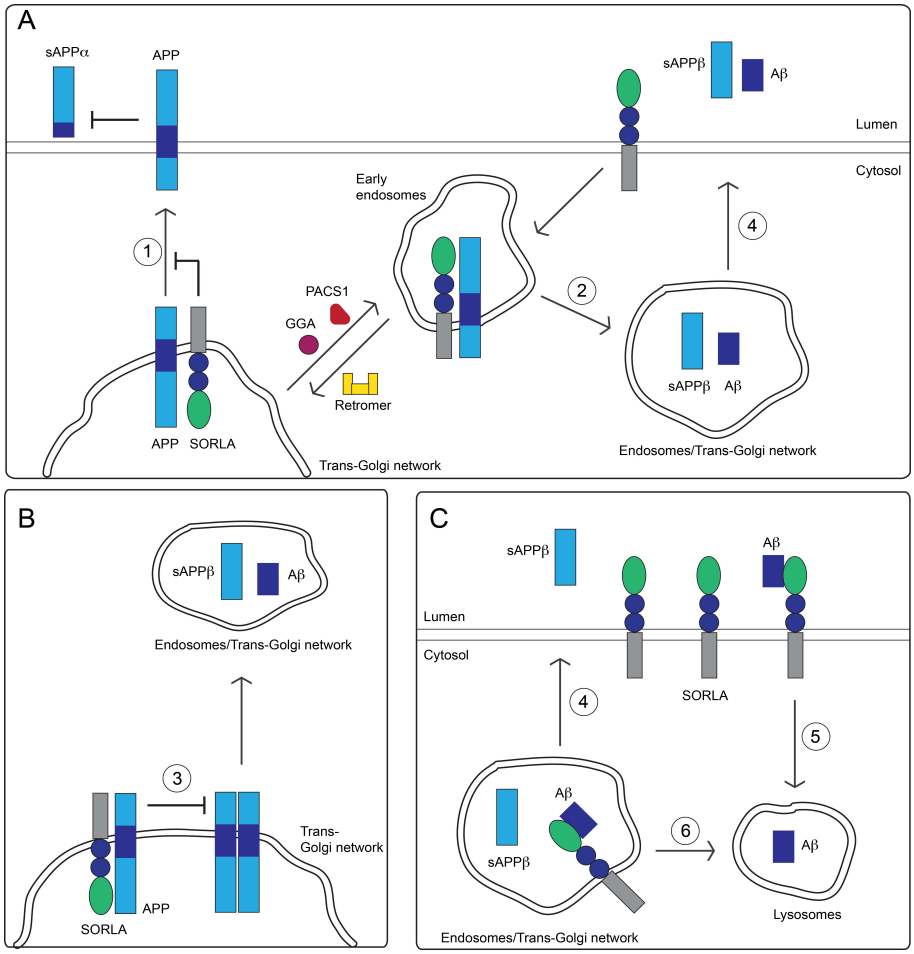

Figure 35. Overexpression of SORLA didn't affect the rate of APP processing and revealed a novel function for the receptor. (A) SORLA interferes with processing of APP by blocking exit of APP to the plasma membrane (1) or by preventing transport of the endocytosed precursor proteins into the late endosomes (2). Aβ peptides produced in the endosomal/recycling compartments or in the TGN are secreted into the extracellular space (4). (B) By binding to APP and preventing its dimerization, SORLA might also block access of the secretase complexes to the APP molecules in the TGN (3). (C) APP processing efficiency did not change in *Rosa26*$^{Tg/+}$ animals compared to *Rosa26*$^{+/+}$ animals, and some scenarios might explain this phenotype. One of the possibilities is that when APP molecules are saturated with endogenous SORLA (as in A), excess amount of the receptor (as in C) doesn't change the trafficking paths and hence processing of the precursor protein. Additionally, shortage of enough trafficking adaptors (GGA, PACS1 and the retromer) to sort SORLA between TGN and endosomes might result in excess amounts of the receptor trapped at the cell surface or in the endosomes/TGN, where it can interact with Aβ. Thus, SORLA might internalize the peptide from the extracellular space (5) or sort the intracellular peptide (6) to the lysosomes.

As a second regulatory step of APP processing, SORLA sorts the precursor proteins between the cellular compartments. Intracellular trafficking of SORLA, which is regulated by several adaptor proteins, in turn might be important to regulate the processing path of the APP molecules (Figure 35). These adaptors include GGAs, which direct the receptor from the TGN to the endosomes, the retromer complex that relocates the cargo from the endosomes to the TGN, and PACS1, which regulates transport of the receptor in either way. Disruption of binding sites on SORLA or knockdown of these proteins alters localization of SORLA as well as processing fate of APP molecules, showing the significance of these adaptor molecules in regulating SORLA's function (Schmidt, Sporbert et al. 2007; Fjorback, Seaman et al. 2012; Herskowitz, Offe et al. 2012). As the expression of SORLA is highly elevated in the brain of *Rosa26*$^{Tg/+}$ mice, the adaptor proteins might not be sufficient to sort SORLA into the compartments where APP is processed. Excess SORLA molecules in the *Rosa26*$^{Tg/+}$ cells might be localized to the plasma membrane or other cellular compartments where it might interact with Aβ and gain another function as Aβ sorting and clearance receptor (Figure 35).

5.7. SORLA as a sorting and clearance receptor for Aβ

Three-fold-decrease in murine and human Aβ concentrations in the brain of *Rosa26*$^{Tg/+}$ animals as compared to *Rosa26*$^{+/+}$ mice suggested a novel function for SORLA in clearane of Aβ. Aβ is continuously produced in the brain and circulates in the CSF, in the brain interstitial fluid (ISF), and in plasma. In extracellular fluids, Aβ may stay as a free peptide or may be coupled to different carrier proteins such as apolipoprotein (APO) E (Yang, Smith et al. 1997). Impairment of Aβ clearance pathways from ISF or CSF results in accumulation of Aβ in the brain.

Brain clearance studies in mice showed that one of the main pathways for Aβ clearance is transport across the blood-brain-barrier (BBB) into the vascular system (Shibata, Yamada et al. 2000). There are several cell-surface receptors such as the receptor for advanced glycation end products (RAGE),

low-density lipoprotein receptor-related protein 1 (LRP1), and LRP2 expressed in endothelial cells of the brain vasculature (Shibata, Yamada et al. 2000). RAGE can bind free Aβ and is involved in transport of Aβ from the luminal side of the BBB (Yan, Chen et al. 1996; Mackic, Stins et al. 1998). In contrast, LRP1 and LRP2, which bind Aβ when complexed with APOE or APOJ respectively, clear the peptide from the brain ISF (Zlokovic, Martel et al. 1996). This clearance mechanism by the BBB was shown to be more efficient in younger animals and was depending on the concentration of Aβ implying that accumulation of Aβ in older animals creates a positive feedback by impairing clearance of the peptide across the BBB (Shibata, Yamada et al. 2000). Among the cell-surface receptors, LRP1 has particular importance, as LRP1-dependent efflux of injected Aβ was shown across the BBB *in vivo* (Deane, Wu et al. 2004). Moreover, the clearance capability of LRP1 was blocked when mutant Aβ was injected suggesting impaired clearance of Aβ as an underlying cause of some AD cases (Deane, Wu et al. 2004). In contrast to LRP1, SORLA is not expressed in the BBB capillaries. Additionally, measurements of Aβ levels in plasma samples didn't show any significant differences in *Rosa26*$^{Tg/+}$ animals compared to *Rosa26*$^{+/+}$ mice (unpublished observations, Dr. Anne-Sophie Carlo). Therefore, contribution of the vascular SORLA expression to Aβ clearance through the brain capillaries in the *Rosa26*$^{Tg/+}$ animals is unlikely.

Another receptor that alters brain efflux of Aβ across the BBB is the low-density lipoprotein receptor (LDLR). Free Aβ can interact with LDLR, however the receptor is not expressed in the endothelial cells of the BBB (Castellano, Deane et al. 2012). So, LDLR doesn't directly transport the peptide, but it rather internalizes APOE. Since APOE slows down clearance rate of Aβ at the mouse brain capillaries (Deane, Sagare et al. 2008), clearance of APOE promotes interaction and efflux of free Aβ with LRP1 (Castellano, Deane et al. 2012). In line with these findings, overexpression of LDLR in AD transgenic mouse models resulted in a decrease of APOE, soluble Aβ, and plaque deposits (Kim, Castellano et al. 2009). The clearance

of Aβ in this mouse model is primarily mediated by efflux across the BBB. Additionally, decrease of Aβ in LDLR overexpressor mice is partially due to the astrocytic internalization of the peptide by LDLR (Basak, Verghese et al. 2012). Different to LDLR expression pattern, I didn't find significant SORLA expression in the glial cells of the *Rosa26*$^{Tg/+}$ brain (Figure 24) suggesting that SORLA doesn't act as clearance receptor in the glial cells.

Metabolism of Aβ in the brain is also mediated by degrading enzymes. Zinc metallopeptidases are the major Aβ degrading enzymes. Neprilysin is one of the best characterized of these peptidases. It breaks down extracellular oligopeptides with a particular preference for hydrophobic residues (Carson and Turner 2002). Deficiency of neprilysin elevates Aβ levels in the brain of mice in a dose-dependent manner (Iwata, Tsubuki et al. 2001). Another major Aβ degrading peptidase is insulin-degrading enzyme (IDE), which hydrolyses extracellular Aβ (Kurochkin and Goto 1994; Qiu, Walsh et al. 1998). Expression levels of these degrading enzymes weren't changed in *Rosa26*$^{Tg/+}$ animals compared to *Rosa26*$^{+/+}$ mice at mRNA as well as at protein level (Figure 31). These results suggested SORLA overexpression doesn't affect the major clearance or degrading pathways that are involved in metabolism of Aβ. Therefore I hypothesized a novel and direct role for SORLA in clearance of Aβ neurons. In consistent with such a role, I showed that when neurons were incubated with recombinant Aβ peptide, *Rosa26*$^{Tg/+}$ neurons internalized more Aβ compared to *Rosa26*$^{+/+}$ or *Sorl1*$^{-/-}$ cells (Figure 34). Until now, different members of the LDLR and VPS10P-domain family were shown to clear Aβ from the brain. One of these proteins is LRP1, which acts as a neuronal clearance receptor for soluble Aβ as discussed above (Kanekiyo, Zhang et al. 2011). Surface plasma resonance experiments showed that LRP1 can bind Aβ with high affinity and this interaction doesn't require any binding molecules (Deane, Wu et al. 2004), although direct Aβ binding to LRP1 couldn't be shown in another study (Yamada, Hashimoto et al. 2008). Aβ uptake studies using neuronal cell lines expressing LRP1 showed that this receptor, together with heparan sulphate proteoglycan, mediates

internalization of Aβ and its subsequent degradation in lysosomes (Kanekiyo, Zhang et al. 2011). Similar to the LRP1 expression pattern, SORLA is particularly localized to the neurons (Figures 24 & 33). This expression pattern together with the data from Aβ uptake assays, which showed increased internalized of Aβ by the cells overexpressing SORLA, suggest that neuronal SORLA also mediates clearance of Aβ in the brain. In the study evaluating clearance of Aβ by LRP1 (Kanekiyo, Zhang et al. 2011), incubation of primary neuronal cultures with anti-LRP1 antibody decreased internalized Aβ peptides by 25%. Similar to the contribution by LRP1, I observed that Aβ uptake is reduced by 25% in SORLA deficient neurons compared to wild-type neurons (Figure 34). On the other hand, Aβ internalization occurred in the *Sorl1*$^{-/-}$ neurons, which lack SORLA but still express endogenous LRP1 or other presumed Aβ receptors. Moreover, accumulation of internalized Aβ in the SORLA deficient neurons that were pre-treated with chloroquine confirms presence of other neuronal pathways for Aβ clearance as well. These results indicate that Aβ can be cleared both by SORLA and LRP1 with a similar efficiency, and there might be even other receptors internalizing Aβ as well. Additionally, the presence of mediator molecules such as APOE or α2-macroglobulin might affect clearance of the peptide from the extracellular space.

Most likely, decreased levels of Aβ in the brain of *Rosa26*$^{Tg/+}$ animals compared to *Rosa26*$^{+/+}$ mice might be explained by clearance of extracellular Aβ by SORLA, which sorts the peptide to lysosomal compartments for degradation. However, another possibility may be sorting of intracellular Aβ into the lysosomal degradation pathways by SORLA. Intracellular localization of Aβ production is not known precisely. Using electron microscopy to detect localization of Aβ, it was suggested that in the hippocampal neurons Aβ is produced in the TGN and to lesser extent in the ER, whereas in non-neuronal cells Aβ is predominantly found close to the plasma membrane (Hartmann, Bieger et al. 1997; Kamenetz, Tomita et al. 2003). Since SORLA is mainly localized to the TGN and perinuclear compartments in the neurons (Figure

33), it would be intriguing to analyze whether SORLA might be involved in intracellular trafficking and sorting of Aβ peptides as well.

5.8. Sortilin and SORLA as clearance receptors

Sortilin, another VPS10P domain receptor was recently identified as Aβ clearance receptor by our lab (Carlo, Gustafsen et al. 2013). Deficiency of the receptor was found to cause accumulation of soluble Aβ as well as amyloid plaques in the brain of mice. Although sortilin cannot bind to free Aβ with high affinity, it binds to APOE as shown by surface plasma resonance binding assays. Accumulation of APOE in sortilin knockout mice and uptake of Aβ with lipidated APOE particles by cultured cells expressing sortilin indicated that sortilin acts as a major APOE clearance receptor in the neurons, and that it mediates uptake of APOE-bound Aβ (Carlo, Gustafsen et al. 2013). In contrast to this mechanism, APOE is not required by SORLA in metabolism of Aβ. It was shown that SORLA mediates the internalization of APOE-rich lipoproteins by the cells (Taira, Bujo et al. 2001). However, in my uptake assays the cells expressing SORLA successfully internalized free Aβ without externally added APOE (Figure 34), although I cannot exclude APOE produced in the neuronal culture. Additionally, *Rosa26*$^{Tg/+}$ animals have similar levels of APOE compared to *Rosa26*$^{+/+}$ mice excluding an impact of SORLA on APOE catabolism per se (Figure 31).

Differences in Aβ clearance mechanism by sortilin and SORLA might be explained by their different binding affinities for this ligand. It was shown with fluorescence polarization assays that VPS10P domain of SORLA, but not that of sortilin, binds to the free Aβ (unpublished observations, Prof. Junichi Takagi's group, Osaka University, Japan). Binding of SORLA VPS10P domain to Aβ was shown to be sensitive to pH with abolished interaction at acidic conditions. These *in-vitro* binding assays suggested a role for SORLA in delivery of soluble Aβ to endosomal compartments wherein low pH results in release of the ligand from the receptor. Increased Aβ uptake in *Rosa26*$^{Tg/+}$ primary neurons compared to *Rosa26*$^{+/+}$ neurons is supporting this

hypothesis. I also found that internalized Aβ is partially localized to the Lamp-1 positive vesicles (Figure 34). These data altogether indicate that SORLA mediates clearance of free Aβ and its transport to the lysosomal compartments (Figure 36).

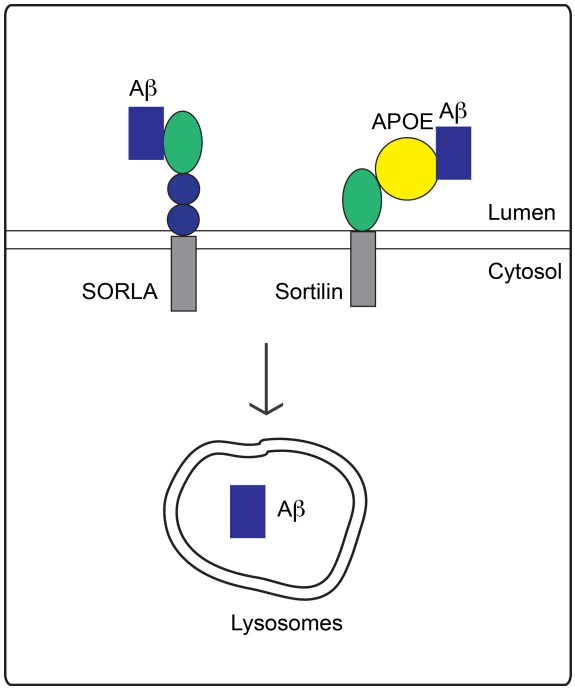

Figure 36. SORLA and sortilin are involved in clearance of Aβ. SORLA and sortilin mediate clearance and lysosomal degradation of soluble Aβ. However the clearance mechanisms are different. The VPS10P domain of SORLA interacts with free Aβ and transports it to the lysosomes for catabolism. In contrast, sortilin acts as a receptor for APOE and clears APOE-bound Aβ molecules.

The differences in ligand binding properties emphasize the structural differences of the VPS10P domains of SORLA and sortilin. In line with such difference, alignment of the amino acid sequences of the VPS10P domains of the two receptors using UniProt website (www.uniprot.org) (2012), documented only 27% homology. It was already shown that the VPS10P domain of sortilin consists of ten-bladed β-propeller structure followed by the 10CC module, and sortilin's well-established ligand neurotensin binds inside this tunnel (Quistgaard, Madsen et al. 2009). As a complementary study, it will be interesting to elucidate the structure of the VPS10P domain of SORLA

and its interaction sites with Aβ that weren't seen for the VPS10P domain of sortilin.

Taken together, my studies confirmed the association of high receptor levels with protection from Aβ production and accumulation. Surprisingly, my studies uncovered a novel molecular mechanism how SORLA might be protective. Apart from controlling the intracellular transport and processing of APP as a sorting receptor at the TGN, SORLA also seems to mediate cellular catabolism of Aβ.

6. Outlook: FAD mutations in ligand binding domains of SORLA

In a recent study, several familial mutations causing AD were identified in *SORL1* (Pottier, Hannequin et al. 2012). For instance two of the mutations (Tyr141Cys; Gly511Arg) are in the VPS10P domain of SORLA, and another one (Ans1358Ser) is in the APP binding domain of the receptor (Pottier, Hannequin et al. 2012). *In silico* pathogenicity analysis of the mutations in the same study showed that VPS10P mutations are deleterious whereas Asn1358Ser might be tolerated. The presence of different mutations in different functional sites of the receptor also supports possible divergent functions for SORLA. Nevertheless, the molecular effects of these mutations on SORLA's function in the brain are not yet known. It would be very interesting to analyze whether the VPS10P domain mutations influence possible binding capacity of SORLA to Aβ and thereby affecting trafficking or clearance of Aβ. If that holds true, decreased Aβ metabolism may explain the accumulation of Aβ in these patients carrying the mutations in SORLA VPSP10 domain.

7. Appendix

Table 6. Genotypes of the individuals in the sample set.

SNPs 1-4

	1	2	3	4
ID	**rs668387**	**rs689021**	**rs641120**	**rs11218313**
1	CT	AG	AG	AG
2	TT	AA	AA	AA
3	CT	AG	AG	AA
4	CT	AG	AG	AG
5	CC	GG	GG	AA
6	CT	AG	AG	AA
7	TT	AA	AA	AA
8	CT	AG	AG	AA
9	CT	AG	AG	AA
10	CT	AG	AG	AA
11	CT	AA	AG	AA
12	CT	AG	AG	AA
13	CT	AG	AG	AA
14	TT	AA	AA	AA
15	TT	AA	AA	AA
16	CT	AG	AG	AA
17	CT	AG	AG	AA
18	CC	GG	GG	AA
19	CC	GG	GG	AG
20	CT	AG	AG	AA
21	CC	GG	GG	AA
22	CC	GG	GG	AA
23	CC	GG	GG	GG
24	CT	AG	AG	AA
25	TT	AA	AA	AA
26	CT	AG	AG	AG
27	TT	AA	AA	AA
28	CC	GG	GG	AA
29	CT	AG	AG	AA
30	CC	GG	GG	AA
31	CT	AG	AG	AA
32	CT	AG	AG	AG
33	CT	AG	AG	AA
34	CT	AG	AG	AA
35	CC	GG	GG	AA
36	CT	AG	AG	AA
37	CC	GG	GG	AG
38	CT	AG	AG	AA
39	CC	GG	GG	AG
40	CC	GG	GG	AA
41	TT	AA	AA	AA
42	CT	AG	AG	AA

	1	2	3	4
ID	**rs668387**	**rs689021**	**rs641120**	**rs11218313**
43	CT	AG	AG	AA
44	CT	AG	AG	AA
45	CT	AG	AG	AA
46	TT	AA	AA	AA
47	CC	GG	GG	AA
48	CT	AG	AG	AA
49	TT	AA	AA	AA
50	CC	GG	GG	AA
51	CT	AG	AG	AA
52	CT	AG	AG	AA
53	TT	AA	AA	AA
54	CT	AG	AG	AA
55	CC	GG	GG	AA
56	CT	AG	AG	AA
57	CC	GG	GG	AA
58	CC	GG	GG	AG
59	TT	AA	AA	AA
60	CC	GG	GG	AA
61	CT	AG	AG	AA
62	CT	AG	AG	AA
63	CC	GG	GG	AG
64	CT	AA	AG	AA
65	CT	AG	AG	AA
66	CT	AG	AG	AA
67	CT	AG	AG	AA
68	CC	GG	GG	AA
69	CT	AG	AG	AA
70	CT	AG	AG	AA
71	CC	GG	GG	AA
72	CC	GG	GG	AG
73	CC	GG	GG	AA
74	CC	GG	GG	AG
75	CC	GG	GG	AA
76	CT	AG	AG	AA
77	CT	AG	AG	AA
78	CC	GG	GG	AA
79	CC	GG	GG	AA
80	CT	AG	AG	AA
81	CT	AG	AG	AG
82	CC	GG	GG	AG
83	CC	GG	GG	AG
84	CT	AG	AG	AA
85	TT	AA	AA	AA
86	CC	GG	GG	AA
87	TT	AA	AA	AA
88	CC	GG	GG	AA

SNPs 5-8

	5	6	7	8
ID	**rs2276346**	**rs7131432**	**rs2070045**	**rs1699102**
1	GG	TT	GT	CC
2	GT	TT	GT	CC
3	GG	TT	GT	CC
4	GG	TT	TT	TT
5	GT	TT	GT	CT
6	GT	TT	TT	CT
7	GG	TT	GT	CT
8	GT	TT	GG	CC
9	GG	TT	TT	TT
10	GT	TT	GT	CT
11	GG	TT	TT	TT
12	GG	TT	TT	TT
13	GT	TT	TT	TT
14	GG	TT	TT	TT
15	GG	TT	GT	CT
16	GT	AT	TT	CT
17	GT	TT	GT	CT
18	TT	TT	GT	CT
19	GT	TT	TT	TT
20	GG	TT	GT	CT
21	GT	TT	GT	CT
22	GT	TT	GT	CT
23	GG	TT	GT	CT
24	GT	TT	TT	TT
25	GG	TT	TT	TT
26	GG	TT	TT	CT
27	GG	TT	TT	TT
28	TT	TT	TT	TT
29	GT	TT	TT	TT
30	TT	TT	TT	CT
31	GG	TT	GT	CT
32	GG	TT	TT	TT
33	GT	TT	TT	TT
34	GT	TT	GT	CT
35	TT	TT	GT	CT
36	GT	TT	GT	CT
37	GT	TT	GT	CT
38	GT	TT	GT	CT
39	GT	TT	TT	TT
40	TT	TT	GT	CT
41	GG	TT	TT	CT
42	GT	TT	GG	CC
43	GT	TT	GT	CT
44	GT	TT	TT	TT
45	GT	TT	GT	CT

	5	6	7	8
ID	**rs2276346**	**rs7131432**	**rs2070045**	**rs1699102**
46	GG	TT	GT	CC
47	TT	TT	TT	TT
48	GG	TT	TT	TT
49	GG	TT	GT	CT
50	TT	TT	TT	TT
51	GT	TT	GG	CC
52	GG	TT	GT	CT
53	GG	TT	TT	CT
54	GT	TT	GT	CT
55	GG	TT	TT	CT
56	GT	TT	GT	CT
57	TT	TT	GT	CT
58	GT	TT	TT	CT
59	GG	TT	TT	TT
60	TT	TT	TT	CT
61	GT	TT	TT	TT
62	GG	TT	GT	CT
63	GG	TT	GT	CT
64	GG	TT	TT	TT
65	GG	TT	GT	CT
66	GT	TT	TT	TT
67	GT	TT	TT	TT
68	GG	TT	TT	TT
69	GT	TT	TT	TT
70	GT	TT	GG	CC
71	GT	TT	GG	CC
72	GG	TT	TT	TT
73	TT	TT	TT	TT
74	GT	TT	TT	TT
75	GG	TT	GT	CC
76	GT	TT	GT	CT
77	GT	TT	GT	CT
78	TT	TT	TT	CT
79	GG	TT	TT	CT
80	GT	TT	GT	TT
81	GG	TT	TT	TT
82	GG	TT	GT	CC
83	GT	TT	TT	CC
84	TT	TT	GG	CT
85	GG	TT	GT	CT
86	GT	TT	TT	TT
87	GG	TT	GT	CT
88	GT	TT	TT	TT

SNPs 9-12

	9	10	11	12
ID	**rs2282649**	**rs726601**	**rs1784931**	**rs1010159**
1	TT	TT	CC	CC
2	TT	TT	CC	CC
3	CT	CT	CC	CT
4	CC	CC	AA	TT
5	CT	CT	AC	CT
6	CC	CC	AC	TT
7	CT	CT	AC	CT
8	TT	TT	CC	CC
9	CC	CC	AA	TT
10	CT	CT	AC	CT
11	CC	CC	AA	TT
12	CC	CC	AA	TT
13	CC	CC	AA	TT
14	CC	CC	AA	TT
15	CT	CT	CC	CC
16	CT	CT	CC	CT
17	CT	CT	AC	CT
18	CT	CT	AC	CT
19	CC	CC	AA	TT
20	CT	CT	AC	CT
21	CT	CT	AC	CT
22	CT	CT	AC	CT
23	CT	CT	AC	CT
24	CC	CC	AC	CT
25	CC	CC	AA	TT
26	CC	CT	AC	CT
27	CC	CC	AA	TT
28	CT	CT	AC	CT
29	CC	CC	AA	TT
30	CT	CT	AC	CT
31	CT	CT	AC	CT
32	CC	CC	AA	TT
33	CC	CC	AA	TT
34	CT	CT	AC	CT
35	CT	CT	AC	CT
36	CT	CT	AC	CT
37	TT	TT	CC	CC
38	CT	CT	AC	CT
39	CC	CC	AA	TT
40	CT	CT	AC	CT
41	CC	CC	AC	TT
42	TT	TT	CC	CC
43	CT	CT	AC	CT
44	CC	CC	AA	TT
45	CT	CT	AC	CT

	9	10	11	12
ID	**rs2282649**	**rs726601**	**rs1784931**	**rs1010159**
46	CT	CT	AC	CT
47	CC	CC	AA	TT
48	CC	CC	AA	TT
49	CT	CT	AC	CT
50	CC	CC	AA	TT
51	TT	TT	CC	CC
52	CT	CT	AC	CT
53	CT	CT	AC	CT
54	CT	CT	AC	CT
55	CC	CC	AC	CT
56	CT	CT	AC	CT
57	CT	CT	AC	CT
58	CC	CT	AC	CT
59	CC	CC	AA	TT
60	CC	CC	AA	TT
61	CC	CC	AA	TT
62	CT	CT	AC	CT
63	CT	CT	AC	CT
64	CC	CC	AA	TT
65	CT	CT	AC	CT
66	CC	CC	AA	TT
67	CC	CC	AA	TT
68	CC	CC	AA	TT
69	CC	CC	AA	TT
70	TT	TT	CC	CC
71	TT	TT	CC	CC
72	CC	CC	AA	TT
73	CC	CC	AA	TT
74	CC	CC	AA	TT
75	TT	TT	CC	CC
76	CT	CT	AC	CT
77	CT	CT	AC	CT
78	CT	CT	CC	CC
79	CC	CT	AC	CT
80	CC	CC	AA	TT
81	CC	CC	AA	TT
82	TT	TT	CC	CC
83	CT	TT	CC	CC
84	CC	CT	AC	CT
85	CT	CT	AC	CT
86	CC	CC	AA	TT
87	CT	CT	AC	CT
88	CC	CC	AA	TT

Table 7. SORLA concentrations of the individuals in the sample set.

ID	SORLA (ng/mg)
1	14.23
2	27.78
3	8.21
4	152.01
5	151.67
6	222.11
7	11.65
8	13.11
9	6.32
10	43.04
11	125.66
12	74.64
13	62.59
14	44.96
15	53.60
16	100.84
17	147.20
18	144.78
19	66.61
20	87.66
21	105.57
22	54.73
23	99.18
24	123.73
25	141.64
26	98.17
27	48.93
28	113.12
29	121.66
30	22.43
31	35.53
32	65.11
33	57.36
34	56.93
35	80.53
36	49.15
37	91.10
38	100.76
39	83.01
40	45.45
41	38.71
42	44.16
43	45.57
44	89.56

ID	SORLA (ng/mg)
45	58.97
46	51.94
47	57.84
48	65.74
49	78.37
50	76.44
51	45.63
52	47.29
53	45.25
54	30.42
55	16.96
56	33.37
57	22.75
58	100.17
59	17.58
60	22.26
61	178.91
62	98.67
63	114.52
64	118.04
65	115.80
66	89.00
67	65.15
68	54.86
69	63.48
70	69.02
71	36.78
72	104.21
73	48.37
74	72.85
75	64.34
76	56.34
77	41.18
78	83.74
79	65.85
80	64.61
81	99.22
82	94.76
83	70.78
84	43.92
85	77.29
86	137.75
87	51.50
88	23.68

8. Bibliography

(2012). "Reorganizing the protein space at the Universal Protein Resource (UniProt)." Nucleic Acids Res **40**(Database issue): D71-75.

Andersen, O. M., J. Reiche, et al. (2005). "Neuronal sorting protein-related receptor sorLA/LR11 regulates processing of the amyloid precursor protein." Proc Natl Acad Sci U S A **102**(38): 13461-13466.

Andersen, O. M., V. Schmidt, et al. (2006). "Molecular dissection of the interaction between amyloid precursor protein and its neuronal trafficking receptor SorLA/LR11." Biochemistry **45**(8): 2618-2628.

Bales, K. R., T. Verina, et al. (1997). "Lack of apolipoprotein E dramatically reduces amyloid beta-peptide deposition." Nat Genet **17**(3): 263-264.

Ballard, C., S. Gauthier, et al. (2011). "Alzheimer's disease." Lancet **377**(9770): 1019-1031.

Barrett, J. C., B. Fry, et al. (2005). "Haploview: analysis and visualization of LD and haplotype maps." Bioinformatics **21**(2): 263-265.

Basak, J. M., P. B. Verghese, et al. (2012). "Low-density lipoprotein receptor represents an apolipoprotein E-independent pathway of Abeta uptake and degradation by astrocytes." J Biol Chem **287**(17): 13959-13971.

Bell, R. D., A. P. Sagare, et al. (2007). "Transport pathways for clearance of human Alzheimer's amyloid beta-peptide and apolipoproteins E and J in the mouse central nervous system." J Cereb Blood Flow Metab **27**(5): 909-918.

Benilova, I., E. Karran, et al. (2012). "The toxic Abeta oligomer and Alzheimer's disease: an emperor in need of clothes." Nat Neurosci **15**(3): 349-357.

Bertram, L., D. Blacker, et al. (2000). "Evidence for genetic linkage of Alzheimer's disease to chromosome 10q." Science **290**(5500): 2302-2303.

Bertram, L., M. B. McQueen, et al. (2007). "Systematic meta-analyses of Alzheimer disease genetic association studies: the AlzGene database." Nat Genet **39**(1): 17-23.

Bettens, K., N. Brouwers, et al. (2008). "SORL1 is genetically associated with increased risk for late-onset Alzheimer disease in the Belgian population." Hum Mutat **29**(5): 769-770.

Blennow, K., M. J. de Leon, et al. (2006). "Alzheimer's disease." Lancet **368**(9533): 387-403.

Bonifacino, J. S. (2004). "The GGA proteins: adaptors on the move." Nat Rev Mol Cell Biol **5**(1): 23-32.

Bonifacino, J. S. and J. H. Hurley (2008). "Retromer." Curr Opin Cell Biol **20**(4): 427-436.

Bonifacino, J. S. and L. M. Traub (2003). "Signals for sorting of transmembrane proteins to endosomes and lysosomes." Annu Rev Biochem **72**: 395-447.

Campioni, S., B. Mannini, et al. (2010). "A causative link between the structure of aberrant protein oligomers and their toxicity." Nat Chem Biol **6**(2): 140-147.

Capon, F., M. H. Allen, et al. (2004). "A synonymous SNP of the corneodesmosin gene leads to increased mRNA stability and demonstrates association with psoriasis across diverse ethnic groups." Hum Mol Genet **13**(20): 2361-2368.

Carlo, A. S., C. Gustafsen, et al. (2013). "The Pro-Neurotrophin Receptor Sortilin Is a Major Neuronal Apolipoprotein E Receptor for Catabolism of Amyloid-beta Peptide in the Brain." J Neurosci **33**(1): 358-370.

Carson, J. A. and A. J. Turner (2002). "Beta-amyloid catabolism: roles for neprilysin (NEP) and other metallopeptidases?" J Neurochem **81**(1): 1-8.

Castellano, J. M., R. Deane, et al. (2012). "Low-density lipoprotein receptor overexpression enhances the rate of brain-to-blood Abeta clearance in a mouse model of beta-amyloidosis." Proc Natl Acad Sci U S A **109**(38): 15502-15507.

Chen, C. M., J. Krohn, et al. (2011). "A comparison of exogenous promoter activity at the ROSA26 locus using a PhiiC31 integrase mediated cassette exchange approach in mouse ES cells." PLoS One **6**(8): e23376.

Churchill, G. A. and R. W. Doerge (1994). "Empirical threshold values for quantitative trait mapping." Genetics **138**(3): 963-971.

Corder, E. H., A. M. Saunders, et al. (1993). "Gene dose of apolipoprotein E type 4 allele and the risk of Alzheimer's disease in late onset families." Science **261**(5123): 921-923.

Crump, C. M., Y. Xiang, et al. (2001). "PACS-1 binding to adaptors is required for acidic cluster motif-mediated protein traffic." EMBO J **20**(9): 2191-2201.

Crystal, H., D. Dickson, et al. (1988). "Clinico-pathologic studies in dementia: nondemented subjects with pathologically confirmed Alzheimer's disease." Neurology **38**(11): 1682-1687.

Damasio, A. R. (1992). "Aphasia." N Engl J Med **326**(8): 531-539.

De Jager, P. L., J. M. Shulman, et al. (2012). "A genome-wide scan for common variants affecting the rate of age-related cognitive decline." Neurobiol Aging **33**(5): 1017 e1011-1015.

De Strooper, B. (2010). "Proteases and proteolysis in Alzheimer disease: a multifactorial view on the disease process." Physiol Rev **90**(2): 465-494.

Deane, R., A. Sagare, et al. (2008). "apoE isoform-specific disruption of amyloid beta peptide clearance from mouse brain." J Clin Invest **118**(12): 4002-4013.

Deane, R., Z. Wu, et al. (2004). "LRP/amyloid beta-peptide interaction mediates differential brain efflux of Abeta isoforms." Neuron **43**(3): 333-344.

Dineley, K. T., M. Westerman, et al. (2001). "Beta-amyloid activates the mitogen-activated protein kinase cascade via hippocampal alpha7 nicotinic acetylcholine receptors: In vitro and in vivo mechanisms related to Alzheimer's disease." J Neurosci **21**(12): 4125-4133.

Dodson, S. E., O. M. Andersen, et al. (2008). "Loss of LR11/SORLA enhances early pathology in a mouse model of amyloidosis: evidence for a proximal role in Alzheimer's disease." J Neurosci **28**(48): 12877-12886.

Dodson, S. E., M. Gearing, et al. (2006). "LR11/SorLA expression is reduced in sporadic Alzheimer disease but not in familial Alzheimer disease." J Neuropathol Exp Neurol **65**(9): 866-872.

Farrer, L. A., L. A. Cupples, et al. (1997). "Effects of age, sex, and ethnicity on the association between apolipoprotein E genotype and Alzheimer disease. A meta-analysis. APOE and Alzheimer Disease Meta Analysis Consortium." JAMA **278**(16): 1349-1356.

Ferri, C. P., M. Prince, et al. (2005). "Global prevalence of dementia: a Delphi consensus study." Lancet **366**(9503): 2112-2117.

Fiete, D., Y. Mi, et al. (2007). "N-linked oligosaccharides on the low density lipoprotein receptor homolog SorLA/LR11 are modified with terminal GalNAc-4-SO4 in kidney and brain." J Biol Chem **282**(3): 1873-1881.

Fjorback, A. W., M. Seaman, et al. (2012). "Retromer binds the FANSHY sorting motif in SorLA to regulate amyloid precursor protein sorting and processing." J Neurosci **32**(4): 1467-1480.

Frisoni, G. B., N. C. Fox, et al. (2010). "The clinical use of structural MRI in Alzheimer disease." Nat Rev Neurol **6**(2): 67-77.

Games, D., D. Adams, et al. (1995). "Alzheimer-type neuropathology in transgenic mice overexpressing V717F beta-amyloid precursor protein." Nature **373**(6514): 523-527.

Gatz, M., C. A. Reynolds, et al. (2006). "Role of genes and environments for explaining Alzheimer disease." Arch Gen Psychiatry **63**(2): 168-174.

Goate, A., M. C. Chartier-Harlin, et al. (1991). "Segregation of a missense mutation in the amyloid precursor protein gene with familial Alzheimer's disease." Nature **349**(6311): 704-706.

Goedert, M., C. M. Wischik, et al. (1988). "Cloning and sequencing of the cDNA encoding a core protein of the paired helical filament of Alzheimer disease: identification as the microtubule-associated protein tau." Proc Natl Acad Sci U S A **85**(11): 4051-4055.

Grear, K. E., I. F. Ling, et al. (2009). "Expression of SORL1 and a novel SORL1 splice variant in normal and Alzheimers disease brain." Mol Neurodegener **4**: 46.

Greene, J. D. (2005). "Apraxia, agnosias, and higher visual function abnormalities." J Neurol Neurosurg Psychiatry **76 Suppl 5**: v25-34.

Gross, R. G. and M. Grossman (2008). "Update on apraxia." Curr Neurol Neurosci Rep **8**(6): 490-496.

Guo, L. H., C. Westerteicher, et al. (2012). "SORL1 genetic variants and cerebrospinal fluid biomarkers of Alzheimer's disease." Eur Arch Psychiatry Clin Neurosci **262**(6): 529-534.

Haass, C., C. Kaether, et al. (2012). "Trafficking and Proteolytic Processing of APP." Cold Spring Harb Perspect Med **2**(5): a006270.

Haass, C., M. G. Schlossmacher, et al. (1992). "Amyloid beta-peptide is produced by cultured cells during normal metabolism." Nature **359**(6393): 322-325.

Hampe, W., M. Rezgaoui, et al. (2001). "The genes for the human VPS10 domain-containing receptors are large and contain many small exons." Hum Genet **108**(6): 529-536.

Hardy, J., A. Myers, et al. (2004). "Problems and solutions in the genetic analysis of late-onset Alzheimer's disease." Neurodegener Dis **1**(4-5): 213-217.

Hardy, J. and D. J. Selkoe (2002). "The amyloid hypothesis of Alzheimer's disease: progress and problems on the road to therapeutics." Science **297**(5580): 353-356.

Hartmann, T., S. C. Bieger, et al. (1997). "Distinct sites of intracellular production for Alzheimer's disease A beta40/42 amyloid peptides." Nat Med **3**(9): 1016-1020.

Hebert, L. E., P. A. Scherr, et al. (2003). "Alzheimer disease in the US population: prevalence estimates using the 2000 census." Arch Neurol **60**(8): 1119-1122.

Hermey, G., I. B. Riedel, et al. (1999). "Identification and characterization of SorCS, a third member of a novel receptor family." Biochem Biophys Res Commun **266**(2): 347-351.

Herskowitz, J. H., K. Offe, et al. (2012). "GGA1-mediated endocytic traffic of LR11/SorLA alters APP intracellular distribution and amyloid-beta production." Mol Biol Cell **23**(14): 2645-2657.

Holtzman, D. M., J. C. Morris, et al. (2011). "Alzheimer's disease: the challenge of the second century." Sci Transl Med **3**(77): 77sr71.

Huang, Y. and L. Mucke (2012). "Alzheimer mechanisms and therapeutic strategies." Cell **148**(6): 1204-1222.

Ikemura, T. (1985). "Codon usage and tRNA content in unicellular and multicellular organisms." Mol Biol Evol **2**(1): 13-34.

Ikeuchi, T., S. Hirayama, et al. (2010). "Increased levels of soluble LR11 in cerebrospinal fluid of patients with Alzheimer disease." Dement Geriatr Cogn Disord **30**(1): 28-32.

Ingelsson, M., Y. Shin, et al. (2003). "Genotyping of apolipoprotein E: comparative evaluation of different protocols." Curr Protoc Hum Genet **Chapter 9**: Unit9 14.

Irion, S., H. Luche, et al. (2007). "Identification and targeting of the ROSA26 locus in human embryonic stem cells." Nat Biotechnol **25**(12): 1477-1482.

Iwata, N., S. Tsubuki, et al. (2001). "Metabolic regulation of brain Abeta by neprilysin." Science **292**(5521): 1550-1552.

Jack, C. R., Jr., D. S. Knopman, et al. (2010). "Hypothetical model of dynamic biomarkers of the Alzheimer's pathological cascade." Lancet Neurol **9**(1): 119-128.

Jacobsen, L., P. Madsen, et al. (2001). "Activation and functional characterization of the mosaic receptor SorLA/LR11." J Biol Chem **276**(25): 22788-22796.

Jacobsen, L., P. Madsen, et al. (1996). "Molecular characterization of a novel human hybrid-type receptor that binds the alpha2-macroglobulin receptor-associated protein." J Biol Chem **271**(49): 31379-31383.

Jacobsen, L., P. Madsen, et al. (2002). "The sorLA cytoplasmic domain interacts with GGA1 and -2 and defines minimum requirements for GGA binding." FEBS Lett **511**(1-3): 155-158.

Jin, M., N. Shepardson, et al. (2011). "Soluble amyloid beta-protein dimers isolated from Alzheimer cortex directly induce Tau hyperphosphorylation and neuritic degeneration." Proc Natl Acad Sci U S A **108**(14): 5819-5824.

K, T. C., K. L. Lunetta, et al. (2008). "Association of distinct variants in SORL1 with cerebrovascular and neurodegenerative changes related to Alzheimer disease." Arch Neurol **65**(12): 1640-1648.

Kamenetz, F., T. Tomita, et al. (2003). "APP processing and synaptic function." Neuron **37**(6): 925-937.

Kanaki, T., H. Bujo, et al. (1998). "Developmental regulation of LR11 expression in murine brain." DNA Cell Biol **17**(8): 647-657.

Kanekiyo, T., J. Zhang, et al. (2011). "Heparan sulphate proteoglycan and the low-density lipoprotein receptor-related protein 1 constitute major pathways for neuronal amyloid-beta uptake." J Neurosci **31**(5): 1644-1651.

Kayed, R., E. Head, et al. (2003). "Common structure of soluble amyloid oligomers implies common mechanism of pathogenesis." Science **300**(5618): 486-489.

Kim, J., J. M. Basak, et al. (2009). "The role of apolipoprotein E in Alzheimer's disease." Neuron **63**(3): 287-303.

Kim, J., J. M. Castellano, et al. (2009). "Overexpression of low-density lipoprotein receptor in the brain markedly inhibits amyloid deposition and increases extracellular A beta clearance." Neuron **64**(5): 632-644.

Kirchhausen, T. (2002). "Single-handed recognition of a sorting traffic motif by the GGA proteins." Nat Struct Biol **9**(4): 241-244.

Kolsch, H., F. Jessen, et al. (2008). "Influence of SORL1 gene variants: association with CSF amyloid-beta products in probable Alzheimer's disease." Neurosci Lett **440**(1): 68-71.

Kolsch, H., F. Jessen, et al. (2009). "Association of SORL1 gene variants with Alzheimer's disease." Brain Res **1264**: 1-6.

Kurochkin, I. V. and S. Goto (1994). "Alzheimer's beta-amyloid peptide specifically interacts with and is degraded by insulin degrading enzyme." FEBS Lett **345**(1): 33-37.

Levy-Lahad, E., W. Wasco, et al. (1995). "Candidate gene for the chromosome 1 familial Alzheimer's disease locus." Science **269**(5226): 973-977.

Li, Y., C. Rowland, et al. (2008). "SORL1 variants and risk of late-onset Alzheimer's disease." Neurobiol Dis **29**(2): 293-296.

Li, Y., C. J. Willer, et al. (2010). "MaCH: using sequence and genotype data to estimate haplotypes and unobserved genotypes." Genet Epidemiol **34**(8): 816-834.

Lucin, K. M. and T. Wyss-Coray (2009). "Immune activation in brain aging and neurodegeneration: too much or too little?" Neuron **64**(1): 110-122.

Ma, Q. L., D. R. Galasko, et al. (2009). "Reduction of SorLA/LR11, a sorting protein limiting beta-amyloid production, in Alzheimer disease cerebrospinal fluid." Arch Neurol **66**(4): 448-457.

Mackic, J. B., M. Stins, et al. (1998). "Human blood-brain barrier receptors for Alzheimer's amyloid-beta 1- 40. Asymmetrical binding, endocytosis, and transcytosis at the apical side of brain microvascular endothelial cell monolayer." J Clin Invest **102**(4): 734-743.

Madisen, L., T. A. Zwingman, et al. (2010). "A robust and high-throughput Cre reporting and characterization system for the whole mouse brain." Nat Neurosci **13**(1): 133-140.

Marcusson, E. G., B. F. Horazdovsky, et al. (1994). "The sorting receptor for yeast vacuolar carboxypeptidase Y is encoded by the VPS10 gene." Cell **77**(4): 579-586.

Matsuo, M., H. Ebinuma, et al. (2009). "Development of an immunoassay for the quantification of soluble LR11, a circulating marker of atherosclerosis." Clin Chem **55**(10): 1801-1808.

Mattsson, N., K. Blennow, et al. (2010). "Inter-laboratory variation in cerebrospinal fluid biomarkers for Alzheimer's disease: united we stand, divided we fall." Clin Chem Lab Med **48**(5): 603-607.

Mawuenyega, K. G., W. Sigurdson, et al. (2010). "Decreased clearance of CNS beta-amyloid in Alzheimer's disease." Science **330**(6012): 1774.

Mayeux, R. and Y. Stern (2012). "Epidemiology of Alzheimer disease." Cold Spring Harb Perspect Med **2**(8).

Mc Donald, J. M., G. M. Savva, et al. (2010). "The presence of sodium dodecyl sulphate-stable Abeta dimers is strongly associated with Alzheimer-type dementia." Brain **133**(Pt 5): 1328-1341.

McCarthy, J. J., S. Saith, et al. (2012). "The Alzheimer's associated 5' region of the SORL1 gene cis regulates SORL1 transcripts expression." Neurobiol Aging **33**(7): 1485 e1481-1488.

McLean, C. A., R. A. Cherny, et al. (1999). "Soluble pool of Abeta amyloid as a determinant of severity of neurodegeneration in Alzheimer's disease." Ann Neurol **46**(6): 860-866.

Mehta, A. K., S. S. Majumdar, et al. (2009). "Epigenetic regulation of cytomegalovirus major immediate-early promoter activity in transgenic mice." Gene **428**(1-2): 20-24.

Meng, Y., J. H. Lee, et al. (2007). "Association between SORL1 and Alzheimer's disease in a genome-wide study." Neuroreport **18**(17): 1761-1764.

Morris, J. C., C. M. Roe, et al. (2010). "APOE predicts amyloid-beta but not tau Alzheimer pathology in cognitively normal aging." Ann Neurol **67**(1): 122-131.

Motoi, Y., T. Aizawa, et al. (1999). "Neuronal localization of a novel mosaic apolipoprotein E receptor, LR11, in rat and human brain." Brain Res **833**(2): 209-215.

Muhammad, A., I. Flores, et al. (2008). "Retromer deficiency observed in Alzheimer's disease causes hippocampal dysfunction, neurodegeneration, and Abeta accumulation." Proc Natl Acad Sci U S A **105**(20): 7327-7332.

Nackley, A. G., S. A. Shabalina, et al. (2006). "Human catechol-O-methyltransferase haplotypes modulate protein expression by altering mRNA secondary structure." Science **314**(5807): 1930-1933.

Naj, A. C., G. Jun, et al. (2011). "Common variants at MS4A4/MS4A6E, CD2AP, CD33 and EPHA1 are associated with late-onset Alzheimer's disease." Nat Genet **43**(5): 436-441.

Nilsberth, C., A. Westlind-Danielsson, et al. (2001). "The 'Arctic' APP mutation (E693G) causes Alzheimer's disease by enhanced Abeta protofibril formation." Nat Neurosci **4**(9): 887-893.

Nyabi, O., M. Naessens, et al. (2009). "Efficient mouse transgenesis using Gateway-compatible ROSA26 locus targeting vectors and F1 hybrid ES cells." Nucleic Acids Res **37**(7): e55.

Offe, K., S. E. Dodson, et al. (2006). "The lipoprotein receptor LR11 regulates amyloid beta production and amyloid precursor protein traffic in endosomal compartments." J Neurosci **26**(5): 1596-1603.

Otto, C., I. Fuchs, et al. (2009). "GPR30 does not mediate estrogenic responses in reproductive organs in mice." Biol Reprod **80**(1): 34-41.

Palop, J. J., J. Chin, et al. (2006). "A network dysfunction perspective on neurodegenerative diseases." Nature **443**(7113): 768-773.

Palop, J. J. and L. Mucke (2010). "Amyloid-beta-induced neuronal dysfunction in Alzheimer's disease: from synapses toward neural networks." Nat Neurosci **13**(7): 812-818.

Perrin, R. J., A. M. Fagan, et al. (2009). "Multimodal techniques for diagnosis and prognosis of Alzheimer's disease." Nature **461**(7266): 916-922.

Petersen, C. M., M. S. Nielsen, et al. (1997). "Molecular identification of a novel candidate sorting receptor purified from human brain by receptor-associated protein affinity chromatography." J Biol Chem **272**(6): 3599-3605.

Pfaffl, M. W. (2001). "A new mathematical model for relative quantification in real-time RT-PCR." Nucleic Acids Res **29**(9): e45.

Pottier, C., D. Hannequin, et al. (2012). "High frequency of potentially pathogenic SORL1 mutations in autosomal dominant early-onset Alzheimer disease." Mol Psychiatry **17**(9): 875-879.

Putcha, D., M. Brickhouse, et al. (2011). "Hippocampal hyperactivation associated with cortical thinning in Alzheimer's disease signature regions in non-demented elderly adults." J Neurosci **31**(48): 17680-17688.

Qiu, W. Q., D. M. Walsh, et al. (1998). "Insulin-degrading enzyme regulates extracellular levels of amyloid beta-protein by degradation." J Biol Chem **273**(49): 32730-32738.

Quistgaard, E. M., P. Madsen, et al. (2009). "Ligands bind to Sortilin in the tunnel of a ten-bladed beta-propeller domain." Nat Struct Mol Biol **16**(1): 96-98.

Reitz, C., R. Cheng, et al. (2011). "Meta-analysis of the association between variants in SORL1 and Alzheimer disease." Arch Neurol **68**(1): 99-106.

Reynolds, C. A., M. G. Hong, et al. (2010). "Sequence variation in SORL1 and dementia risk in Swedes." Neurogenetics **11**(1): 139-142.

Reynolds, C. A., C. Zavala, et al. (2013). "Sortilin receptor 1 predicts longitudinal cognitive change." Neurobiol Aging **34**(6): 1710 e1711-1718.

Rezgaoui, M., G. Hermey, et al. (2001). "Identification of SorCS2, a novel member of the VPS10 domain containing receptor family, prominently expressed in the developing mouse brain." Mech Dev **100**(2): 335-338.

Rogaev, E. I., R. Sherrington, et al. (1995). "Familial Alzheimer's disease in kindreds with missense mutations in a gene on chromosome 1 related to the Alzheimer's disease type 3 gene." Nature **376**(6543): 775-778.

Rogaeva, E., Y. Meng, et al. (2007). "The neuronal sortilin-related receptor SORL1 is genetically associated with Alzheimer disease." Nat Genet **39**(2): 168-177.

Rohe, M., A. S. Carlo, et al. (2008). "Sortilin-related receptor with A-type repeats (SORLA) affects the amyloid precursor protein-dependent stimulation of ERK signaling and adult neurogenesis." J Biol Chem **283**(21): 14826-14834.

Rovelet-Lecrux, A., D. Hannequin, et al. (2006). "APP locus duplication causes autosomal dominant early-onset Alzheimer disease with cerebral amyloid angiopathy." Nat Genet **38**(1): 24-26.

Sagare, A., R. Deane, et al. (2007). "Clearance of amyloid-beta by circulating lipoprotein receptors." Nat Med **13**(9): 1029-1031.

Salgado, I. K., M. Serrano, et al. (2012). "SorLA in glia: shared subcellular distribution patterns with caveolin-1." Cell Mol Neurobiol **32**(3): 409-421.

Sauna, Z. E. and C. Kimchi-Sarfaty (2011). "Understanding the contribution of synonymous mutations to human disease." Nat Rev Genet **12**(10): 683-691.

Schellenberg, G. D., T. D. Bird, et al. (1992). "Genetic linkage evidence for a familial Alzheimer's disease locus on chromosome 14." Science **258**(5082): 668-671.

Scherzer, C. R., K. Offe, et al. (2004). "Loss of apolipoprotein E receptor LR11 in Alzheimer disease." Arch Neurol **61**(8): 1200-1205.

Scheuner, D., C. Eckman, et al. (1996). "Secreted amyloid beta-protein similar to that in the senile plaques of Alzheimer's disease is increased

in vivo by the presenilin 1 and 2 and APP mutations linked to familial Alzheimer's disease." Nat Med **2**(8): 864-870.

Schmidt, V., K. Baum, et al. (2012). "Quantitative modelling of amyloidogenic processing and its influence by SORLA in Alzheimer's disease." EMBO J **31**(1): 187-200.

Schmidt, V., A. Sporbert, et al. (2007). "SorLA/LR11 regulates processing of amyloid precursor protein via interaction with adaptors GGA and PACS-1." J Biol Chem **282**(45): 32956-32964.

Scott, P. M., P. S. Bilodeau, et al. (2004). "GGA proteins bind ubiquitin to facilitate sorting at the trans-Golgi network." Nat Cell Biol **6**(3): 252-259.

Seaman, M. N. (2012). "The retromer complex - endosomal protein recycling and beyond." J Cell Sci **125**(Pt 20): 4693-4702.

Seaman, M. N., E. G. Marcusson, et al. (1997). "Endosome to Golgi retrieval of the vacuolar protein sorting receptor, Vps10p, requires the function of the VPS29, VPS30, and VPS35 gene products." J Cell Biol **137**(1): 79-92.

Selkoe, D. J. and M. B. Podlisny (2002). "Deciphering the genetic basis of Alzheimer's disease." Annu Rev Genomics Hum Genet **3**: 67-99.

Sherrington, R., E. I. Rogaev, et al. (1995). "Cloning of a gene bearing missense mutations in early-onset familial Alzheimer's disease." Nature **375**(6534): 754-760.

Shibata, M., S. Yamada, et al. (2000). "Clearance of Alzheimer's amyloid-ss(1-40) peptide from brain by LDL receptor-related protein-1 at the blood-brain barrier." J Clin Invest **106**(12): 1489-1499.

Soriano, P. (1999). "Generalized lacZ expression with the ROSA26 Cre reporter strain." Nat Genet **21**(1): 70-71.

Spoelgen, R., C. A. von Arnim, et al. (2006). "Interaction of the cytosolic domains of sorLA/LR11 with the amyloid precursor protein (APP) and beta-secretase beta-site APP-cleaving enzyme." J Neurosci **26**(2): 418-428.

St Clair, D., J. Norrman, et al. (1994). "Apolipoprotein E epsilon 4 allele frequency in patients with Lewy body dementia, Alzheimer's disease and age-matched controls." Neurosci Lett **176**(1): 45-46.

Strittmatter, W. J., A. M. Saunders, et al. (1993). "Apolipoprotein E: high-avidity binding to beta-amyloid and increased frequency of type 4 allele in late-onset familial Alzheimer disease." Proc Natl Acad Sci U S A **90**(5): 1977-1981.

Taira, K., H. Bujo, et al. (2001). "LR11, a mosaic LDL receptor family member, mediates the uptake of ApoE-rich lipoproteins in vitro." Arterioscler Thromb Vasc Biol **21**(9): 1501-1506.

Tchorz, J. S., T. Suply, et al. (2012). "A modified RMCE-compatible Rosa26 locus for the expression of transgenes from exogenous promoters." PLoS One **7**(1): e30011.

Tesco, G., Y. H. Koh, et al. (2007). "Depletion of GGA3 stabilizes BACE and enhances beta-secretase activity." Neuron **54**(5): 721-737.

Walsh, D. M., I. Klyubin, et al. (2002). "Naturally secreted oligomers of amyloid beta protein potently inhibit hippocampal long-term potentiation in vivo." Nature **416**(6880): 535-539.

Walter, J., A. Capell, et al. (1997). "Ectodomain phosphorylation of beta-amyloid precursor protein at two distinct cellular locations." J Biol Chem **272**(3): 1896-1903.

Walter, J. and C. Haass (2000). "Posttranslational modifications of amyloid precursor protein : ectodomain phosphorylation and sulfation." Methods Mol Med **32**: 149-168.

Wan, L., S. S. Molloy, et al. (1998). "PACS-1 defines a novel gene family of cytosolic sorting proteins required for trans-Golgi network localization." Cell **94**(2): 205-216.

Webster, J. A., A. J. Myers, et al. (2008). "Sorl1 as an Alzheimer's disease predisposition gene?" Neurodegener Dis **5**(2): 60-64.

Willnow, T. E., A. S. Carlo, et al. (2010). "SORLA/SORL1, a neuronal sorting receptor implicated in Alzheimer's disease." Rev Neurosci **21**(4): 315-329.

Willnow, T. E., C. M. Petersen, et al. (2008). "VPS10P-domain receptors - regulators of neuronal viability and function." Nat Rev Neurosci **9**(12): 899-909.

Yamada, K., T. Hashimoto, et al. (2008). "The low density lipoprotein receptor-related protein 1 mediates uptake of amyloid beta peptides in

an in vitro model of the blood-brain barrier cells." J Biol Chem **283**(50): 34554-34562.

Yamazaki, H., H. Bujo, et al. (1996). "Elements of neural adhesion molecules and a yeast vacuolar protein sorting receptor are present in a novel mammalian low density lipoprotein receptor family member." J Biol Chem **271**(40): 24761-24768.

Yan, S. D., X. Chen, et al. (1996). "RAGE and amyloid-beta peptide neurotoxicity in Alzheimer's disease." Nature **382**(6593): 685-691.

Yang, D. S., J. D. Smith, et al. (1997). "Characterization of the binding of amyloid-beta peptide to cell culture-derived native apolipoprotein E2, E3, and E4 isoforms and to isoforms from human plasma." J Neurochem **68**(2): 721-725.

Zambrowicz, B. P., A. Imamoto, et al. (1997). "Disruption of overlapping transcripts in the ROSA beta geo 26 gene trap strain leads to widespread expression of beta-galactosidase in mouse embryos and hematopoietic cells." Proc Natl Acad Sci U S A **94**(8): 3789-3794.

Zeeberg, B. (2002). "Shannon information theoretic computation of synonymous codon usage biases in coding regions of human and mouse genomes." Genome Res **12**(6): 944-955.

Zlokovic, B. V., C. L. Martel, et al. (1996). "Glycoprotein 330/megalin: probable role in receptor-mediated transport of apolipoprotein J alone and in a complex with Alzheimer disease amyloid beta at the blood-brain and blood-cerebrospinal fluid barriers." Proc Natl Acad Sci U S A **93**(9): 4229-4234.

Selbständigkeitserklärung

Hiermit erkläre ich, dass ich die vorliegende Arbeit mit dem Titel “SORLA/SORL1 as Genetic Risk Factor in Alzheimer Disease” selbstständig und ohne Hilfe Dritter angefertigt habe. Sämtliche Hilfsmittel, Hilfen sowie Literaturquellen sind als solche kenntlich gemacht. Ausserdem erkläre ich hiermit, dass ich mich nicht anderweitig um einen entsprechenden Doktorgrad beworben habe. Die Promotionsordnung des Fachbereichs Biologie, Chemie, Pharmazie der Freien Universität Berlin habe ich gelesen und akzeptiert.

Berlin, April 2013

Safak Caglayan

Acknowledgements

I would like to express my sincerest gratitude to my supervisor
Prof. Dr. Thomas E. Willnow for his encouragement, motivation, and support throughout my thesis work. I very much benefited from his mentorship and scientific perspective.

I am grateful to Prof. Dr. Fritz G. Rathjen for becoming my university supervisor.

I am indebted to Dr. Anne-Sophie Carlo for her help in mouse work.

I would like to thank Dr. Vanessa Schmidt for her help in SORLA ELISA and expression constructs.

I want to thank Dr. Anja Bauerfeind for her help in statistical analyses of human genetics data.

Thanks to Verona Kuhle and Sylvia Sibilak. They helped a lot to me in administrative issues and bureaucratic paperworks.

I would like to thank all people in the lab for providing a supportive environment throughout the whole work. I have been very happy to be a member of the AG Willnow.

Loving thanks to my friends for whom I need a chapter to mention all. Each of them is very valuable for me and I will always remember them.

Lastly, I would like to thank my family. It is impossible to express my endless love to them. I just love them.